Hydration of C_3S and Al-doped C_3S in the presence of gypsum

José da Silva Andrade Neto[1,a*], Erich D. Rodríguez[2,b], Paulo J. M. Monteiro[3,c], Angeles G. De la Torre[4,d], and Ana Paula Kirchheim[1,e]

[1] Núcleo Orientado para a Inovação da Edificação (NORIE) – Programa de Pós-Graduação em Engenharia Civil: Construção e Infraestrutura / Universidade Federal do Rio Grande do Sul – Av. Osvaldo Aranha 99, Centro Histórico, 90035-190, Porto Alegre/RS, Brazil

[2] Universidade Federal de Santa Maria - Av Roraima 1000. Prédio 10A (Centro de Tecnologia; CT), Camobi, Santa Maria/RS, Brasil, CEP 97105-900.

[3] Department of Civil and Environmental Engineering, University of California, Berkeley, CA 94720, USA

[4] Departamento de Química Inorgánica, Cristalografía y Mineralogía, Universidad de Malaga, Campus Teatinos s/n., 29071 Málaga, Spain

[a]jose.andrade@ufrgs.br, [b]erich.rodriguez@ufsm.br, [c]monteiro@ce.berkeley.edu, [d]mgd@uma.es, [e]anapaula.k@ufrgs.br

*Corresponding author.

ABSTRACT

A full understanding of how gypsum accelerates the C_3S hydration, and the role of aluminum has not been achieved. The effects of gypsum (at 2.5 wt.% and 5.0 wt.%) on the hydration of tricalcium silicate (C_3S) and aluminum-doped C_3S (Al-C_3S) hydration are assessed. Isothermal calorimetry, thermodynamic modeling, XRD, TGA, and ^{27}Al and ^{29}Si MAS-NMR were performed to analyze gypsum's influence on the hydration of C_3S and Al-C_3S. The inclusion of gypsum retarded the initial hydration (first 3 h) for both C_3S and Al-C_3S, due to the interaction between the sulfate ions and C_3S. In contrast, gypsum enhanced the hydration of both C_3S and Al-C_3S afterward. This acceleration effect occurred earlier for the Al-C_3S due to the removal of aluminum from the solution. However, this is not the main mechanism behind the acceleration of C_3S by gypsum, which mainly results from changes in C-S-H morphology and increases in the ionic strength.

Keywords: C_3S; Sulfate; Gypsum; Aluminum; Hydration.

1 INTRODUCTION

Calcium sulfate, like gypsum, hemihydrate, and/or anhydrite, is added in Portland cement (PC) to control the C_3A hydration and subsequently improve its industrial application feasibility [1,2]. However, despite the much fewer studies, when compared to C_3A-calcium sulfate systems, calcium sulfate also modifies the C_3S/alite hydration and the morphology of its hydration products [3–12]. Also, as observed by Zunino and Scrivener [13], the C-S-H precipitation rate and, consequently, the alite reaction influences the sulfate demand of PC and, mainly, of blended cements. Therefore, the interactions between gypsum and alite may have an essential role in sulfate optimization of Portland cements, influencing the setting, workability, mechanical performance, and shrinkage of these cementitious materials [2]. This is particularly important for blended cements, which present different sulfate demands compared to PC [2,13]. Thus, the effects of calcium sulfate on alite reaction might influence the sulfate balance of a more complex system.

In clinker, C_3S usually forms solid solutions, containing several foreign elements as Mg^{2+}, Al^{3+}, Fe^{3+}, S^{6+}, Na^{+}, K^{+}, and P^{5+} [14,15]. The presence of these elements changes the C_3S structure and might influence its reactivity [14]. Therefore, it is important to differentiate C_3S as a single phase from the C_3S present in industrial clinkers. Because of this, the C_3S-solid solution present in the clinker is usually referred to as alite. In this study, the term alite is used when referred to the C_3S present in industrial clinker. Furthermore, the term "C_3S" is used to referred stoichiometric C_3S or C_3S with some incorporation of Mg^{2+}. Finally, the term "Al-C_3S" refers to the C_3S that contains Al^{3+} (and also Mg^{2+}).

The initial C_3S dissolution is delayed in the presence of gypsum, prolonging the induction period -the period where the initial rapid rate of hydration decreases within the first few minutes and remains at a low rate until the nucleation and growth period [16]. According to Nicoleau *et al.* [3] and Juilland *et al.* [4] this behavior occurs due to electrostatic interactions between the sulfate ions and the C_3S surface. The authors postulated that neutral $CaSO_4^0$ species are formed at the surface, reducing the charge screening created by calcium cations and resulting in a more negative surface charge, slowing the C_3S dissolution rate. However, after the induction period, during the nucleation and growth period – the period in which the hydration rate increases again [16]-, the presence of

calcium sulfate enhances C_3S hydration rate, resulting in higher main hydration peaks [2,5–12].

Some authors [6–8] state that this enhancement is due to ettringite- $[Ca_3Al(OH)_2 \cdot 12H_2O]_2 \cdot (SO_4)_3 \cdot 2H_2O$ -formation (Eqs. 1-3 [17]), which occurs when C_3A is presented or when the C_3S contains aluminum (such as Al-doped laboratory prepared C_3S and alite of industrial clinker-which typically contains 1.0 wt.% of Al_2O_3 [14]). According to Quennoz and Scrivener [6], the ettringite formation decreases the aluminum concentration on the solution, which is known to retard the Al-C_3S/alite hydration [3,18,19], and therefore increasing the hydration rate. Bergold *et al.* [8] suggested that the acceleration on alite hydration (by the inclusion of gypsum is due to the seeding effect of very fine (nano-)ettringite, which might provide a suitable surface for heterogeneous nucleation of C-S-H and thus to a faster dissolution of alite.

$$AlO_2^- + 2OH^- + 2H_2O = [Al(OH)_6]^{3-} \quad (1)$$

$$2[Al(OH)_6]^{3-} + 6Ca^{2+} + 24H_2O = \{Ca_6[Al(OH)_6]_2 \cdot 24H_2O\}^{6+} \quad (2)$$

$$\{Ca_6[Al(OH)_6]_2 \cdot 24H_2O\}^{6+} + 3SO_4^{2-} + 2H_2O = \{Ca_6[Al(OH)_6]_2 \cdot 24H_2O\} \cdot [3SO_4^{2-} \cdot 2H_2O] \quad (3)$$

However, other authors report that gypsum also accelerates the aluminum-free C_3S hydration [9–12], where no ettringite formation is observed. These hypotheses would not be enough to explain the effect of gypsum on C_3S hydration without consensus on the mechanism by which calcium sulfate accelerates the C_3S hydration and whether aluminum ions have any influence or not. Therefore, the reason for that is not yet clearly understood.

The presence of gypsum also changes the C-S-H morphology [2,7,20,21]. According to Mota *et al.* [7], a cloud of sulfate ions is physically adsorbed in the positively charged C-S-H surface, which results in the electrical repulsion of C-S-H needles. This leads to a more divergent needle structure instead of the convergent morphology formed in C_3S pastes without sulfates.

In summary, there is no consensus on the mechanism by which calcium sulfate accelerates the C_3S/alite hydration and whether aluminum ions have any influence or not. Therefore,

this study aims to verify if the aluminum presented in aluminum-doped C_3S plays a crucial role in enhancing C_3S hydration due to gypsum and quantitatively compare the effects of gypsum on C_3S and Al-C_3S hydration. The results obtained here are expected to advance in understanding the mechanism by which gypsum influences C_3S hydration and, therefore, in the sulfate optimization of Portland cement.

In this study, we assessed the hydration of C_3S and aluminum-doped C_3S (Al-C_3S) in the presence and absence of gypsum. Isothermal calorimetry (IC), thermodynamic modeling, X-ray diffractometry (XRD), thermogravimetry analysis (TGA), and ^{27}Aluminum and ^{29}Silicon magic angle spinning nuclear magnetic resonance spectroscopy (^{27}Al and ^{29}Si MAS-NMR) were performed to follow the C_3S and Al-C_3S hydration up to 7 days of curing.

2 MATERIALS AND METHODS

2.1 Materials

Powder samples of C_3S and aluminum-doped C_3S (Al-C_3S) were obtained from Mineral Research Processing (M.R.PRO, France). Both phases were synthesized in a laboratory by heating at 1450 °C, a stoichiometric mixture of reagent grade $CaCO_3$ and SiO_2. Approximately 0.8 wt.% of Al_2O_3 was used in the synthesis of Al-C_3S. In order to stabilize the intended polymorphs, ~0.5 and 1.0 wt.% of MgO were added to synthesize C_3S and Al-C_3S, respectively. Besides, high purity natural gypsum (> 96 wt.%) was used.

The samples were characterized by X-ray diffractometry (XRD), using an X´Pert MPD PRO diffractometer from PANalytical (Almelo, Netherlands). Monochromatic Cu-Kα_1 radiation, λ = 1.54059 Å obtained by a Ge (111) monochromator and an X'Celerator detector were used. The X-ray tube operated at 45 kV and 40 mA, and the samples were measured between 5º to 70º (2θ) with a step size of 0.016º, using a spinning sample-holder (16 rpm) to enhance particle statistics. The crystalline phases were identified using the X'Pert Highscore software (PANalytical) and quantified by the Rietveld method using the GSAS II software. The fitting process was adjusted to obtain an R_{WP} lower than 12% and a goodness-of-fit (GOF) lower than 5.

Figure 1 presents the X-ray patterns for the anhydrous materials. The C_3S sample presented 95.7 wt.% of triclinic C_3S (T1, Ca_3SiO_5, Inorganic Crystal Database - ICSD#

4331), 1.5 wt.% of magnesite ($MgCO_3$, ICSD# 40117), 1.5 wt.% of calcite ($CaCO_3$, ICSD# 73446), and 1.3 wt.% of portlandite ($Ca(OH)_2$, ICSD# 202220) (final agreement factor R_{WP} of 10.7% and GOF of 3.8 were obtained). The Al-C_3S consist of 98.7 wt.% of monoclinic C_3S (M1, Ca_3SiO_5, de Noirfontaine *et al.* [22]), 0.9 wt.% of magnesite ($MgCO_3$, ICSD# 40117), 0.4 wt.% of calcite ($CaCO_3$, ICSD# 73446) and 0.1 wt.% of portlandite ($Ca(OH)_2$, ICSD# 202220) (final agreement factor R_{WP} of 11.4% and GOF of 4.1 were obtained). The natural gypsum contains 96.1 wt.% of gypsum ($CaSO_4 \cdot 2H_2O$, ICSD# 151692), 3.4% of dolomite ($CaMg(CO_3)_2$, ICSD# 66333), and 0.5% of quartz (SiO_2, ICSD# 200721) (final agreement factor R_{WP} of 11.7% and GOF of 3.1).

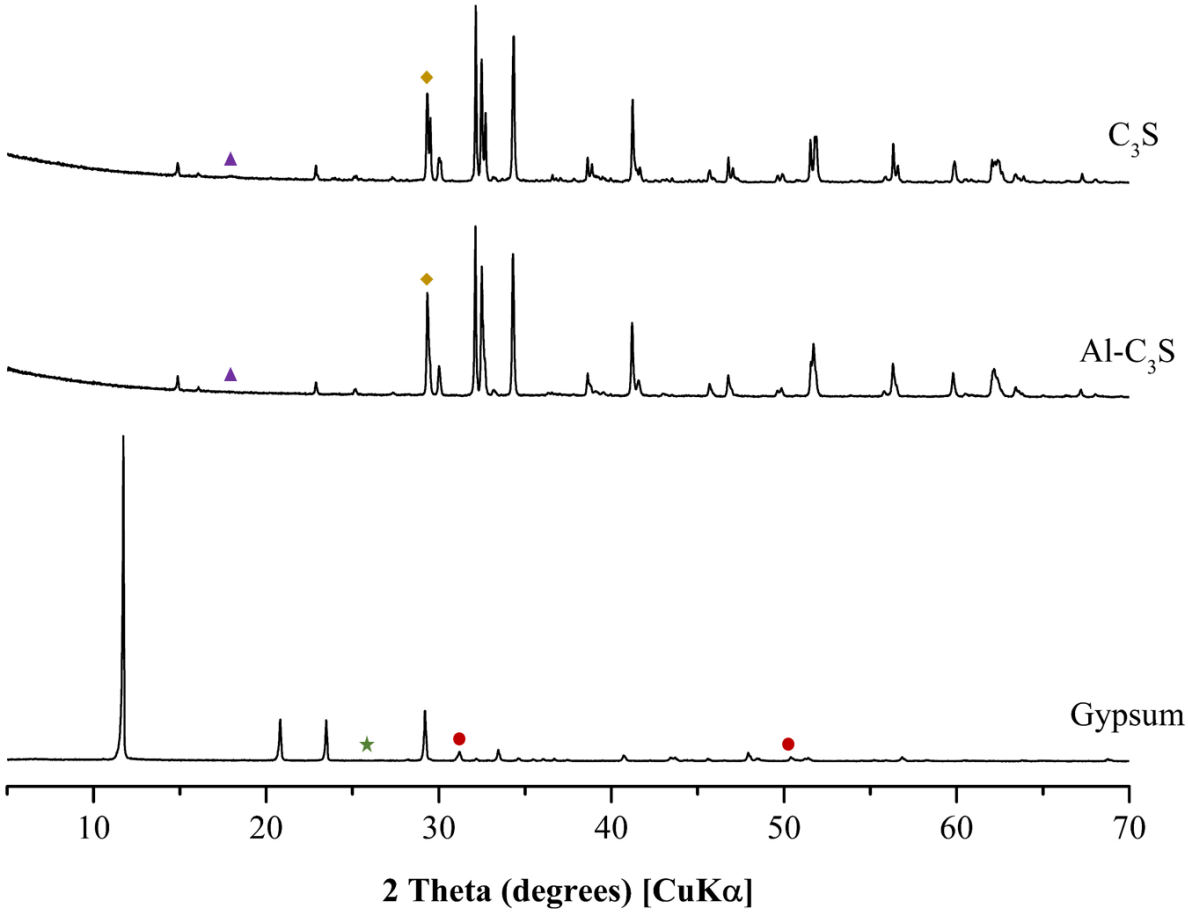

Figure 1 – X-ray diffractograms for the anhydrous materials. Symbols indicate the main reflections of the minor phases. Triangle: Portlandite; Rhombus: Calcite; Star: Quartz; Circle: Dolomite. Note that in some cases – such as calcite – the peaks overlap with the peak of the main phases.

The raw materials' BET surface area was obtained using an ASAP 2420 equipment from Micromeritics (Georgia, USA), according to the guidelines presented in Palacios et al. [23]. The particle size distribution was determined by laser diffraction, using PSA 1090

equipment from Anton Paar (Graz, Austria), isopropanol as dispersant, and considering Mie theory [23]. Finally, the raw materials' density was determined through gas helium pycnometry, using an AccuPyc II 1340 pycnometer from Micromeritics (Georgia, USA). The physical characterization results are presented in Table 1, and Figure 2 shows the particle size distribution of the raw materials. The Al-C_3S has a larger particle size and a slightly lower BET surface area (5.3% lower than C_3S).

Table 1 – Physical characterization of the raw materials.

Property	**C_3S**	**Al-C_3S**	**Gypsum**
BET surface area* (m^2/g)	1.14	1.08	1.33
D_v 90 (µm)	16.9	32.4	51.8
D_v 50 (µm)	6.7	11.6	16.9
D_v 10 (µm)	1.5	1.7	3.6
Density (kg/m^3)	3130	3150	2350

*Brunauer-Emmett-Teller theory surface area

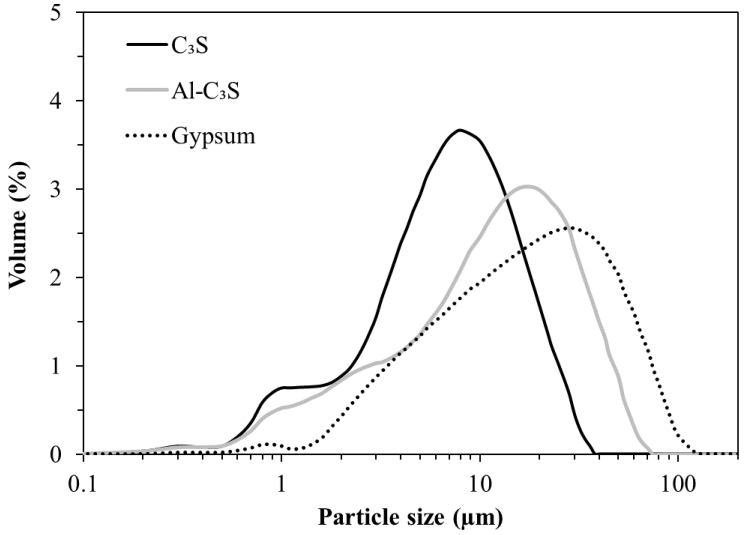

Figure 2 – Particle size distribution of the raw materials.

The raw materials' chemical composition was determined by X-ray fluorescence (XRF), using an ADVANT'XP+ spectrometer from Thermo Fisher Scientific (Waltham, USA). In terms of oxides, the chemical composition of C_3S, Al-C_3S, and gypsum is shown in Table 2.

Table 2 – Chemical composition, obtained by XRF, of the raw materials expressed as a weight percentage of oxides.

Constituent	C_3S	Al-C_3S	Gypsum
CaO	72.8	72.9	32.7
SiO_2	25.3	25.5	0.9
Al_2O_3	-	0.8	0.1
MgO	1.0	0.5	0.8
SO_3	-	-	44.3
*LOI	0.9	0.3	21.2

Loss on ignition (LOI) at 1000 ºC.

2.2 Methods

2.2.1 Formulations and paste preparation

Table 3 shows the different formulations studied. Mixtures containing 0.00 wt.%, 2.50 wt.%, and 5.00 wt.% of gypsum (in relation to C_3S wt.%) with both tricalcium silicates were analyzed. The water/solid ratio was adjusted to 0.50. Table 3 also presents the tests conducted for each formulation: isothermal calorimetry (IC), thermogravimetric analysis (TGA), X-ray diffraction (XRD), and ^{27}Al and ^{29}Si nuclear magnetic resonance (^{27}Al and ^{29}Si MAS-NMR), which will be described in Section 2.2.2.

Table 3 – Formulations studied.

Mixture	C_3S (wt.%)	Gypsum (wt.%)	Test conducted
C_3S	100.00	0.00	IC, TGA, XRD, ^{29}Si NMR
C_3S_2.5%G	97.56	2.44	IC, TGA, XRD, ^{29}Si NMR
C_3S_5.0%G	95.24	4.76	IC
Al-C_3S	100.00	0.00	IC, TGA, XRD, ^{29}Si NMR, ^{27}Al NMR
Al-C_3S _2.5%G	97.56	2.44	IC, TGA, XRD, ^{29}Si NMR, ^{27}Al NMR
Al-C_3S _5.0%G	95.24	4.76	IC

The anhydrous materials (C_3S in the absence and the presence of gypsum) were manually mixed in an agate mortar for 10 minutes.

For the calorimetry analysis, 8 g of anhydrous materials were manually mixed with 4 g of distilled water for 1 min. Then, the paste was mixed in a vortex mixer for 1 extra min. Finally, ~ 6 g of paste were placed in a 20 mL glass ampoule used for the calorimetry analysis (see section 2.2.2).

For the TGA, XRD, and ^{27}Al and ^{29}Si MAS-NMR analysis, cylindrical specimens were molded using a hermetically closed PTFE cylindric recipient (as shown in Figure 3) that has eight cylinders (10 mm diameter). For this, 10 g of anhydrous materials were mixed with 5 g of distilled water in a vertical mixer (IKA model RW 20 digital). The pastes were mechanically mixed during 180 s at 800 rpm, where 30 s of stabilization time was performed. Our lab's previous results showed a good correlation between this procedure and the procedure adopted for the calorimetry analysis.

The PTFE recipient was sealed and kept rotating at 15 rpm in a benchtop roller (Wheaton) for the first 10 h to obtain homogeneous samples [24]. Then, one cylinder of each sample was demolded, and the hydration was stopped. The PTFE recipient was sealed again and kept rotating at 15 rpm for 14 h more (totaling 24 h). After this initial period, the pastes were not hard enough to demold. Thus, the device was introduced in a humidity chamber at 99% RH at 20 ± 1 °C. After each curing time (1, 3, and 7 days), one cylinder was demolded, and the hydration was stopped.

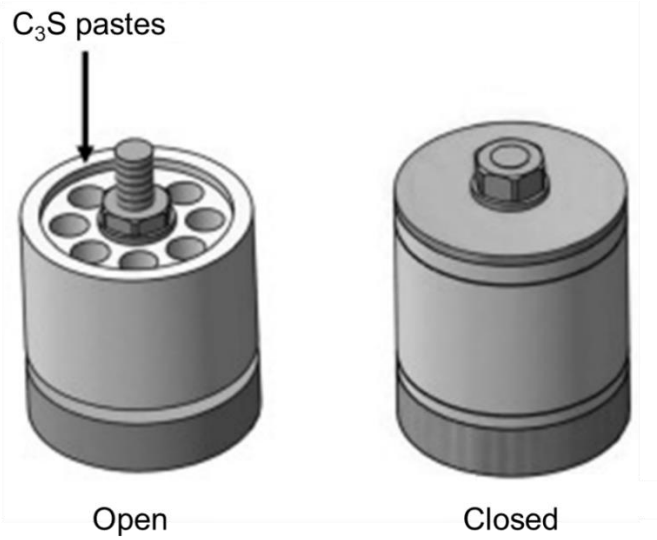

Figure 3 – PTFE cylinder shape recipient to prepare the C_3S pastes. Adapted from García-Maté *et al.* [24]

At 10 h, 1, 3, and 7 days, one fraction of the pastes was milled to fine powder in an agate mortar and the hydration was stopped by solvent exchange with isopropanol and ether, according to the procedure described by García-Maté *et al.* [24]. The stopping procedure consisted of filtration in a Whatman system (90 mm diameter Whatman filter with a pore size of 2.5 μm and Teflon support) with isopropanol (VWR Chemicals) twice and finally with diethyl ether (Prolabo S.A.). Then, thermogravimetric analysis (TGA) and X-ray diffraction (XRD) were performed in these pastes. ^{27}Al and ^{29}Si MAS-NMR of the pastes at 7 days were also assessed on them.

2.2.2 Tests conducted

The isothermal calorimetric study was performed in an eight-channel Thermal Activity Monitor of Tam Air, TA Instruments (New Castle, DE, USA) using glass ampoules of 20 mL. Distilled water was used as reference material. The amount of water used as reference was calculated according to Wadsö [25] to obtain the same heat capacity of the C_3S paste. The heat flow (thermal power, mW/g of solids) and the cumulative heat (integral of thermal power, J/g of solids) were collected for up to 3 days at 20 °C. Only the heat released after the first 45 minutes was considered for the cumulative heat, as the first peak has low reproducibility. These first 45 minutes were used as a stabilization period after the disturbance in calorimeter temperature after introducing the reference and the sample.

TGA measurement of C_3S pastes was done in an SDT-Q600 analyzer from TA Instruments (New Castle, DE, USA). The temperature varied from room temperature (RT) to 1000 °C at a heating rate of 10 °C/min. The samples were placed in open platinum crucibles under airflow. From the TGA results, the bound water and the portlandite content were determined. After stopping hydration, the bound water of the pastes was assigned to be the weighed loss from RT to 550°C. Due to this, the actual bounded water has to be calculated by Eq. 4 and the free water by Eq. 5 [26]:

$$\mathrm{BW} = \frac{\mathrm{BW_{ATD}} \cdot \mathrm{CM}}{100 - \mathrm{BW_{ATD}}} \tag{4}$$

$$\mathrm{FW} = \mathrm{TW} - \mathrm{BW} \tag{5}$$

Where BW corresponds to actual chemically bound water content, BW_{ATD} is the loss of mass measured up to 550 ºC from TGA curves, and CM is the cement content, and TW is the total water content added (all the numbers in weight percentage).

The portlandite content was obtained by Eq. 6 [27].

$$Ca(OH)_{2,measured} = WL_{Ca(OH)_2} \cdot \frac{m_{Ca(OH)_2}}{m_{H_2O}} \quad (6)$$

where $WL_{Ca(OH)_2}$ is the weight loss due to the decomposition of crystalline portlandite obtained by the integration of DTG peak located in the temperature range from ~450 and ~550 ºC, using the tangential method [27], the $m_{Ca(OH)_2}$ is the molecular mass of portlandite (74 g/mol) and m_{H_2O} is the molecular mass of water (18 g/mol).

For the XRD analysis, the C_3S pastes, after the hydration stoppage, were manually ground and mixed with 20 wt.% of crystalline quartz (99.5%, AlfaAesar) used as an internal standard in an agate mortar for 10 minutes. The XRD with internal standard data was collected on a D8 ADVANCE diffractometer from Bruker AXS (Massachusetts, USA) equipped with a Molybdenum X-ray tube and a Johansson Ge (111) monochromator, using strictly monochromatic Mo-Kα_1 radiation, $\lambda = 0.7093$ Å, in transmission geometry (θ/θ). The X-ray tube operated at 50 kV and 50 mA, and the data were collected between 2.5 and 35° (2θ) with a step size of 0.01° and 2.5 s/step. A spinning sample-holder (10 rpm) was used to enhance particle statistics.

The crystalline phases were identified using the X´Pert High Score software (PANalytical). Rietveld analysis was performed using GSAS II software, with the cif files of the Inorganic Crystal Structures Database (ICSD). The structural models used for the Rietveld analysis are shown in Table 4. The phase fractions, background coefficients, zero-shift error and cell parameters were refined. The peak shapes were fitted by using a pseudo-Voigt function. The preferred orientation coefficient of C_3S T1, C_3S M1 and portlandite was refined by the March-Dollase ratio. Finally, the non-crystalline content (amorphous and nanocrystalline) was determined by the internal standard method [28]. The degree of hydration (DoH_{XRD}) of C_3S was calculated from the XRD results according to Eq. 7.

$$\mathrm{DoH}_{C_3S\,(t)} = \frac{\mathrm{W}_{C_3S,i} - \mathrm{W}_{C_3S,t}}{\mathrm{W}_{C_3S,i}} \cdot 100 \quad (7)$$

where $\mathrm{DoH}_{C_3S\,(t)}$ is the degree of hydration of C_3S at a specific time (t), $\mathrm{W}_{C_3S,i}$ is the amount of C_3S in the anhydrous mixture obtained by XRD-Rietveld, $\mathrm{W}_{C_3S,t}$ is the amount of C_3S in the paste at a specific time (t) obtained by XRD-Rietveld.

As the total mass of solids increases with the progress of the C_3S hydration, as free water is bound into hydration products, phase contents determined by XRD-Rietveld and the portlandite content obtained by TGA need to be normalized. For this purpose, Eq. 8 was used to normalize the contents obtained per 100 g of paste [26]

$$\mathrm{W_{j,rescaled}} = \mathrm{W_{i,measured}} \cdot \frac{(100 - \mathrm{FW})}{100} \quad (8)$$

Where $\mathrm{W_{j,rescaled}}$ is the weight of phase per 100 g of paste, $\mathrm{W_{i,measured}}$ is the phase content obtained by TGA or XRD-Rietveld, and FW is the free water content determined by TGA according to Eq. 5.

Table 4 – Structural models used for the Rietveld analysis of C_3S and Al-C_3S pastes.

Phase	ICSD code	References
C_3S triclinic (T1)	4331	Golovastikov et al. [29]
C_3S monoclinic (M1)	-	de Noirfontaine et al. [22]
Lime	52783	Smith and Leider [30]
Gypsum	151692	De la Torre et al. [31]
Quartz	200721	Jorgensen [32]
Ettringite	155395	Goetz-Neunhoeffer and Neubauer [33]
Portlandite	15471	Petch [34]
Calcite	79673	Wartchow [35]

Solid-state single pulse ^{27}Aluminum and ^{29}Si magic angle spinning nuclear magnetic resonance spectroscopy (^{27}Al MAS-NMR and ^{29}Si MAS-NMR) of the pastes, at 7 days, were performed in an AVANCEII HD 600 spectrometer from Bruker AXS. A MAS probe of 2.5 mm was used at a spinning rate of 15 kHz. The magnetic field was 14.1 T for the

^{27}Al MAS-NMR, which corresponds to a ^{27}Al resonance frequency of 156.37 MHz. ^{27}Al MAS NMR spectra were collected with a 1 μs (corresponding to π/2 flip angle) excitation pulse with ^{1}H decoupling and summing up 200 scans. The ^{29}Si MAS-NMR spectra were recorded at 79.49 MHz and were collected with a 6 μs (corresponding to π/2 flip angle) excitation pulse with ^{1}H decoupling and summing up 800 scans.

^{29}Si MAS-NMR and ^{27}Al MAS-NMR results were normalized for 0 to 1 (0 corresponding to the minimum value and 1 the maximum value obtained) and then peak deconvolutions were computed using Excel software. The ^{29}Si MAS-NMR, distinct peaks centered in different Si sites, denoted as Q^0, Q^1, $Q^2(1Al)$, and Q^2, were fitted varying their intensity and width, assuming Gaussian line-shaped. The DoH_{NMR} of C_3S was obtained through Eq. 9 [36]. The mean silicate chain length (MCL)-which stands for the average polymerization degree of silicate chains in C-S-H, and the fraction of tetrahedrally coordinated Al in the C-S-H phase (molar Al(IV)/Si ratio) were calculated using Eqs. 10 and 11 [36].

$$DoH_{NMR} = 1 - Q^0 \tag{9}$$

$$MCL = \frac{2 \cdot \left[Q^1 + Q^2 + \frac{3}{2} \cdot Q^2(1Al)\right]}{Q^1} \tag{10}$$

$$Al(IV)/Si = \frac{Q^2(1Al)}{2 \cdot [Q^1 + Q^2 + Q^2(1Al)]} \tag{11}$$

The quantitative analyses of ^{27}Al MAS-NMR are less straightforward than ^{29}Si MAS-NMR, as there are non-symmetric line shapes caused by a second order quadrupolar broadening of the central transition for the ^{27}Al quadrupole. However, the octahedral Al sites of ettringite, monosulfoaluminates-type phases (AFm) and the so-called third aluminate hydrate (TAH) – from octahedral Al sites associated with C-(A)-S-H phase, have small ^{27}Al quadrupole coupling those results in Gaussian-like line shapes for the center band at 14.1 T. The ettringite, AFm, and TAH contents were estimated by dividing the areas of their respective gaussian peaks by the spectrum's total area.

2.2.3 Thermodynamic modeling

Thermodynamic modeling of C_3S and Al-C_3S pastes with different amounts of gypsum was carried out using the CemGEMS web application [37], coupled with the CEMDATA18 database [38]. For this, the chemical characterization of C_3S, Al-C_3S, and gypsum was used as input data. A four-parameter logistic (4PL) fit (Eq. 12) [37,39] of the Degree of Hydration (DoH) of C_3S obtained by XRD was used to describe the DoH of C_3S over time. All fits have good correlations (with an R^2 between 0.97 and 0.98), as presented in the supplementary data (Figure S1). For the pastes with 5 wt.% of gypsum, the fits of the corresponding pastes with 2.5 wt.% of gypsum were used for the thermodynamic modeling due to the lack of the DoH obtained by XRD for these pastes. This seems plausible as the C_3S in the pastes with 5 wt.% of gypsum presents a very similar DoH of the C_3S compared to the pastes with 2.5 wt.% of gypsum, as observed by isothermal calorimetry (see Section 3.1). The phase assemblage (in mass, g/100g of paste), the pore solution composition (in mM), and the ionic strength (in molal) of the pore solution were analyzed by thermodynamic modeling.

$$DoH_{C_3S} = d + \frac{(a-d)}{1 + \left({}^{t}/_{c}\right)^{b}} \quad (12)$$

where *t* is the hydration time in days, *a* is the asymptote minimum DoH value (considered here equal to 0%), *d* is the asymptote maximum DoH value (considered here equal to 97%), *b* is the maximum steepness, and *c* is the time position of the inflection point [37].

3 RESULTS

3.1 Isothermal calorimetry (IC) study

Figures 4 A and B show the heat flow and cumulative heat curves of C_3S and Al-C_3S pastes, respectively, without gypsum, and the systems with 2.5 wt.% and 5.0 wt.% of gypsum (in relation to C_3S wt.%) during the first 72 hours of hydration. Table 5 presents the main parameters obtained from the heat flow and cumulative heat curves.

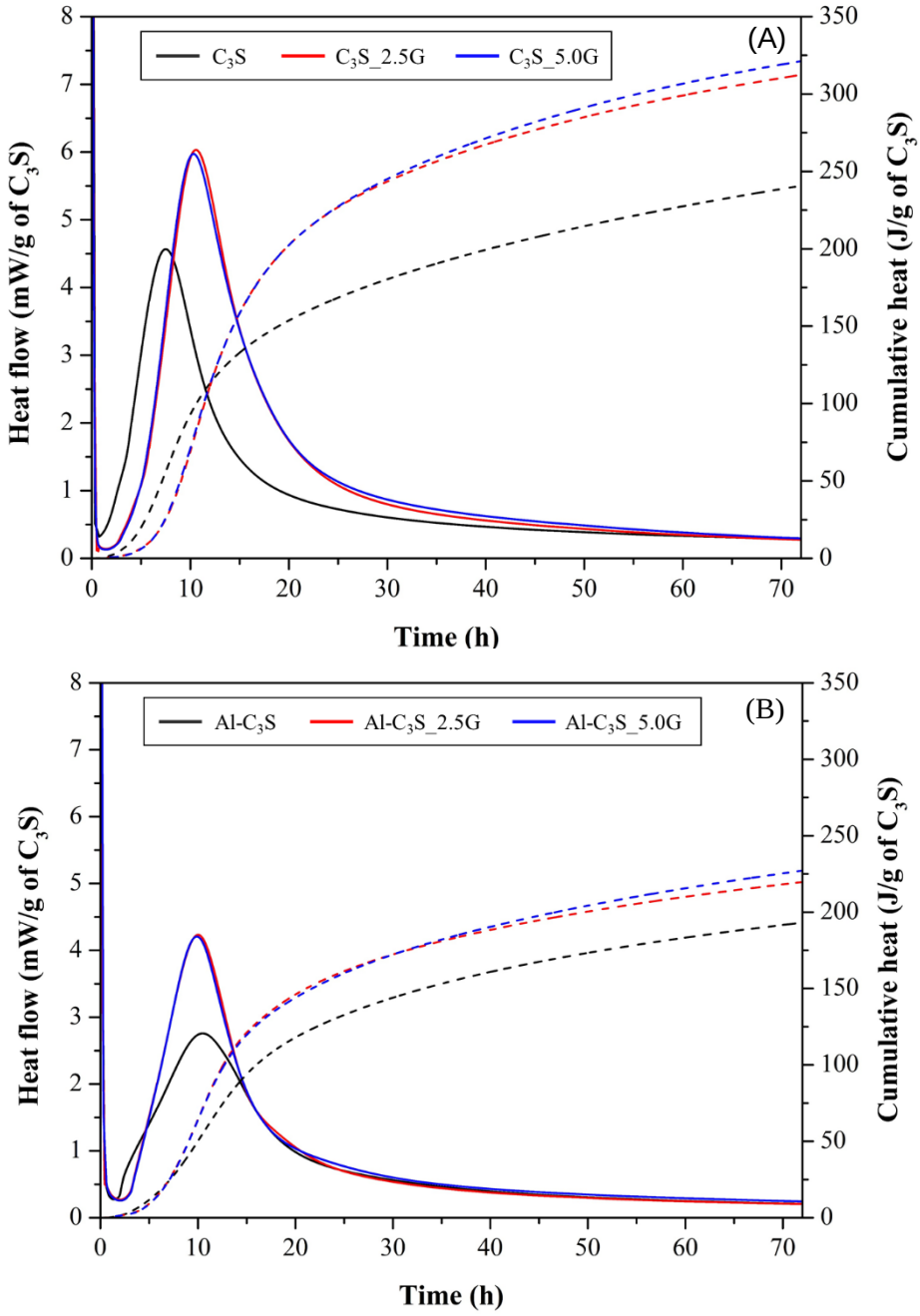

Figure 4 – Heat flow curves (solid lines and primary/left "y" axis) and cumulative heat curves (dashed lines and secondary/right "y" axis) of the (A) C_3S and (B) Al-C_3S pastes with different amounts of gypsum during the first 72 hours of hydration.

Table 5 – Parameters determined from the calorimetry results.

Parameter	C_3S	C_3S_2.5G	C_3S_5.0G	Al-C_3S	Al-C_3S_2.5G	Al-C_3S_5.0G
Induction period length (min)*	40.3	165.8	174.4	81.7	137.9	146.5
Heat flow rate at the acceleration period (mW/g of C_3S □ h)*	0.89	1.01	1.13	0.29	0.64	0.65
Maximum heat flow of the main hydration peak (mW/g of C_3S)	4.57	6.03	5.97	2.76	4.23	4.21
Heat of hydration at 24 h (J/g of C_3S)	165.77	222.90	223.16	129.79	158.77	157.21
Heat of hydration at 48 h (J/g of C_3S)	211.77	281.87	287.61	171.10	198.15	201.68
Heat of hydration at 72 h (J/g of C_3S)	240.73	312.35	321.21	193.16	219.69	227.15

* calculated as indicated in Figure S2;

Comparing both C_3S pastes without gypsum, the Al-C_3S paste presents a more extended induction period (103% longer) and a broader and lower hydration peak (40% lower), with a lower hydration rate at the acceleration period (67% lower). Besides, the cumulative heat released by the Al-C_3S paste during the first 72 hours of hydration is lower than the heat released by the C_3S paste (22%, 19%, and 20% lower at 24 h, 48 h, and 72 h, respectively). These results indicate that the Al-C_3S has a lower hydration rate when compared to the C_3S, which agrees with the results obtained by Stephan *et al.* [40], Begarin *et al* [41], and Wagner *et al*. [42]. Moreover, these results were also expected since the particle size of Al-C_3S was coarser than the C_3S without Al doping. To decouple the role of aluminum, the heat flow and cumulative heat curves were also normalized by the specific surface area (SSA) of C_3S and Al-C_3S, as shown in the supplementary information (Figure S3). The difference between the samples reduced, but the Al-C_3S pastes still present lower hydration peak (36% lower) and lower heat release (17%, 15%, and 15% lower at 24 h, 48 h, and 72 h, respectively), evidencing the retard effect of aluminum on C_3S hydration.

The effect of gypsum on hydration was similar for both samples. The addition of 2.5 wt.% of gypsum prolonged the induction period (311% and 69% longer for the C_3S and Al-C_3S pastes, respectively) but increased the hydration rate at the acceleration period (increases

of 13% and 121% for the C_3S and Al-C_3S pastes, respectively) and the main hydration peak (increases of 32% and 53% for the C_3S and Al-C_3S pastes, respectively). Thus, the cumulative heat released for the C_3S pastes without gypsum was higher than the C_3S pastes with gypsum until ~ 12 hours but lower afterward (34%, 33%, and 30% lower at 24 h, 48 h, and 72 h, respectively). The Al-C_3S pastes without gypsum presented a similar cumulative heat until ~ 7 hours, but lower after this period than the Al-C_3S pastes with gypsum (22%, 16%, and 14% lower at 24 h, 48 h, and 72 h, respectively). This indicates that gypsum delays the initial hydration of C_3S (induction period) but accelerates afterward, which agrees with several previous studies [2,6,7,9,11].

The increase in the gypsum content added to 5.0 wt.% slightly prolonged the induction period (5% and 6% longer than the C_3S_2.5G and Al-C_3S_2.5G pastes, respectively) and slightly decreased the main C_3S hydration peak (decrease of 1% for the C_3S_5.0G and Al-C_3S_5.0G pastes). This indicates that further increases in the gypsum content will not increase more the C_3S hydration rate. Similar behaviors were observed in previous studies [5,9,10].

The inclusion of gypsum on the C_3S pastes, the amount of C_3S present in the mixture decreases, and therefore, the heat released by C_3S dissolution and C-S-H and portlandite precipitation decreases. Thus, the heat flow and cumulative curves were normalized per gram of C_3S. The heat released by gypsum dissolution in the C_3S and Al-C_3S pastes with gypsum, and the heat released by ettringite formation in the Al-C_3S_2.5G and Al-C_3S_5.0G pastes, contributes to the increase in the heat release with gypsum addition. However, due to the low amount of gypsum dissolved and ettringite formed (see Sections 3.2 and 3.3 for more details), this cannot account for the great increases in the heat released observed.

3.2 Thermodynamic Analysis

Figure 5 presents the phase assemblage (in g/100g) of the C_3S and Al-C_3S pastes with different amounts of gypsum (0, 2.5, and 5.0 wt.% in relation to C_3S wt.%) obtained by thermodynamic modeling. The addition of gypsum is not expected to result in any different hydrated phases in C_3S pastes. However, in Al-C_3S, gypsum addition led to the formation of ettringite instead of monocarboaluminate (MC, CO_2-AFm) and hydrotalcite (HT, $Mg_6Al_2CO_3(OH)_{16}\cdot 4H_2O$), as expected. For the Al-C_3S_2.5G, gypsum depletion is predicted to happen at ~ 280 hours of hydration, leading to the formation of

hydrotalcite. In turn, for the Al-C_3S_5.0G, the gypsum depletion is not expected to happen up to 10000 hours of hydration. Finally, in Al-C_3S pastes, the addition of gypsum results in a decrease of portlandite (4% and 8% of reduction at 10000 hours for the pastes with 2.5 and 5.0 wt.% of gypsum, respectively). This occurs as calcium ions are consumed for the ettringite formation. For the C_3S pastes this does not occur as the addition of gypsum does not result in ettringite formation.

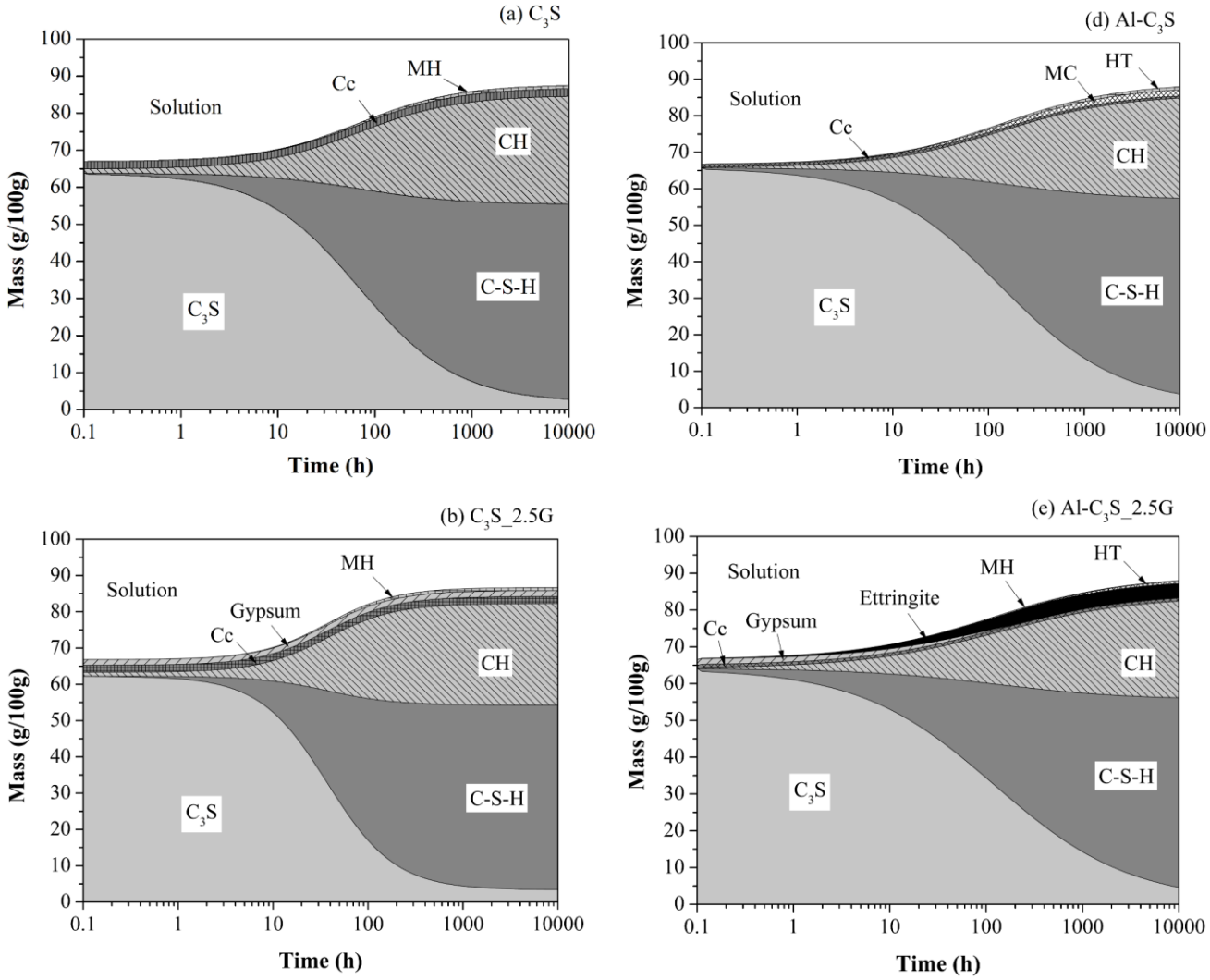

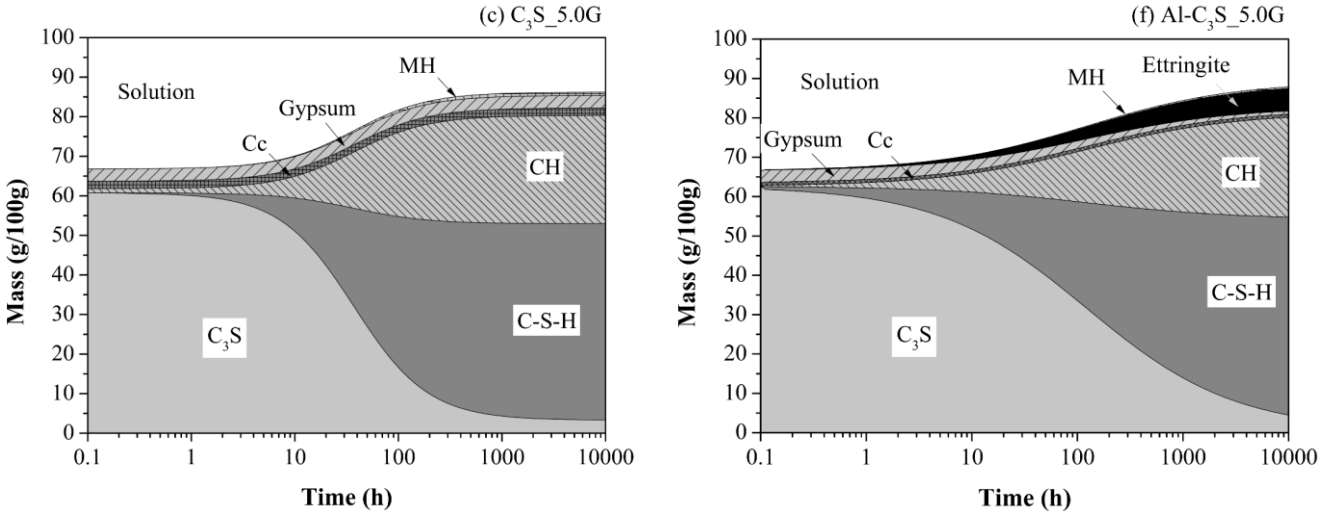

Figure 5 – Phase assemblage (in g/100 g of paste) of the C_3S and Al-C_3S pastes with different amounts of gypsum as predicted by cemGEMS. Where CH is Portlandite, Cc is calcium carbonate, MH is magnesium hydroxide (brucite), and HT is hydrotalcite.

The pore solution compositions of the C_3S and Al-C_3S pastes with different gypsum amounts, obtained by thermodynamic modeling, are shown in the supplementary information (Figure S4). For all pastes, the concentrations of the ions are not expected to change with the progress of the hydration, except for the Al-C_3S_2.5G which shows a decrease in Ca (from 32.9 to 21.3 mM), S (from 12.8 to 0.4 mM), and Mg (from 0.14 μM to 0.11 μM) concentrations at ~ 280 hours (when occurs gypsum depletion), leading to the formation of hydrotalcite.

The addition of 2.5 wt.% gypsum in both C_3S and Al-C_3S resulted in an S concentration of 12.8 mM and increased the Ca concentration from 21.0 to 32.9 mM (an increase of 56.7%). Further additions of gypsum (*i.e.*, for the pastes with 5.0 wt.% of gypsum) did not result in any change of the composition of the pore solutions of the C_3S pastes in the first 10000 hours of hydration, as this further amount of gypsum is expected to not dissolve. In turn, for the Al-C_3S paste, the further addition of gypsum also did not change the initial composition of the pore solution but prevented gypsum depletion (which is expected to occur around 280 hours for the Al-C_3S_2.5G paste). Therefore, the pore solution composition of the Al-C_3S_5.0G pastes is expected to remain constant up to 10000 hours of hydration.

As shown by the thermodynamic modeling, the concentration of Al in the pore solution reduces from 0.005 mM in Al-C_3S pastes to 0 mM in Al-C_3S_2.5G and Al-C_3S_5G pastes. This result means that all the aluminum coming from the dissolution of Al-C_3S is

expected to be immediately consumed by the formation of ettringite in the pastes with gypsum.

The ionic strength of the pore solution of the pastes was calculated using cemGEMS. During the first 48 h, the average ionic strength of the pore solution of C_3S and Al-C_3S pastes are very similar (0.055 molal). The addition of 2.5% of gypsum is predicted to increase the ionic of both C_3S and Al-C_3S up to 0.083 molal (an increase of 51%). Further additions of gypsum are not predicted to increase more the ionic strength, and the C_3S_5.0G and Al-C_3S_5.0G presented the same ionic strength as the pastes with 2.5% of gypsum (0.083 molal).

The increase in the ionic strength due to the addition of gypsum occurs due to the release of SO_4^{2-} ions into the pore solution, which is a divalent ion and greatly contributes to the increase of the ionic strength. The increase of the amount of gypsum added (from 2.5 to 5.0 wt.%) did not result in further increases, as the additional amount of gypsum is not expected to dissolve, and therefore the S concentration into the pore solution remains the same during the first days of hydration, as discussed before.

3.3 X-ray diffraction (XRD)

Figures 6 A-D present the normalized results of crystalline and non-crystalline phases quantification by the Rietveld method over time. Tables S1-S4 gives the normalized phase assemblage with time for the samples without and with 2.5 wt.% of gypsum. All Rietveld quantifications presented an R_{WP} lower than 12.0 and GOF lower than 5, indicating good refinements. Figures S5 and S6 in the supplementary information show as representative example the Rietveld plots of C_3S_2.5G and Al-C_3S_2,5G at 1 day Figure 7 presents the degree of hydration of C_3S (DoH_{XRD}) over the first 7 days, determined from the XRD-Rietveld results.

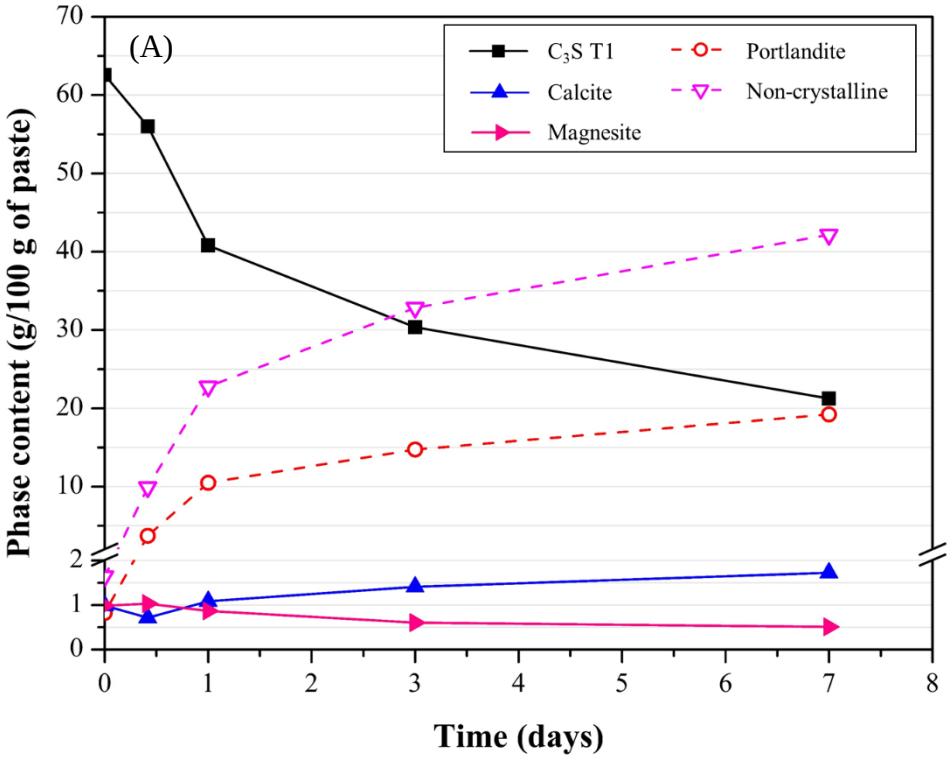
(A)
C3S T1
Portlandite
Calcite
Non-crystalline
Magnesite
Phase content (g/100 g of paste)
Time (days)
70
60
50
40
30
20
10
2
1
0
0
1
2
3
4
5
6
7
8

1

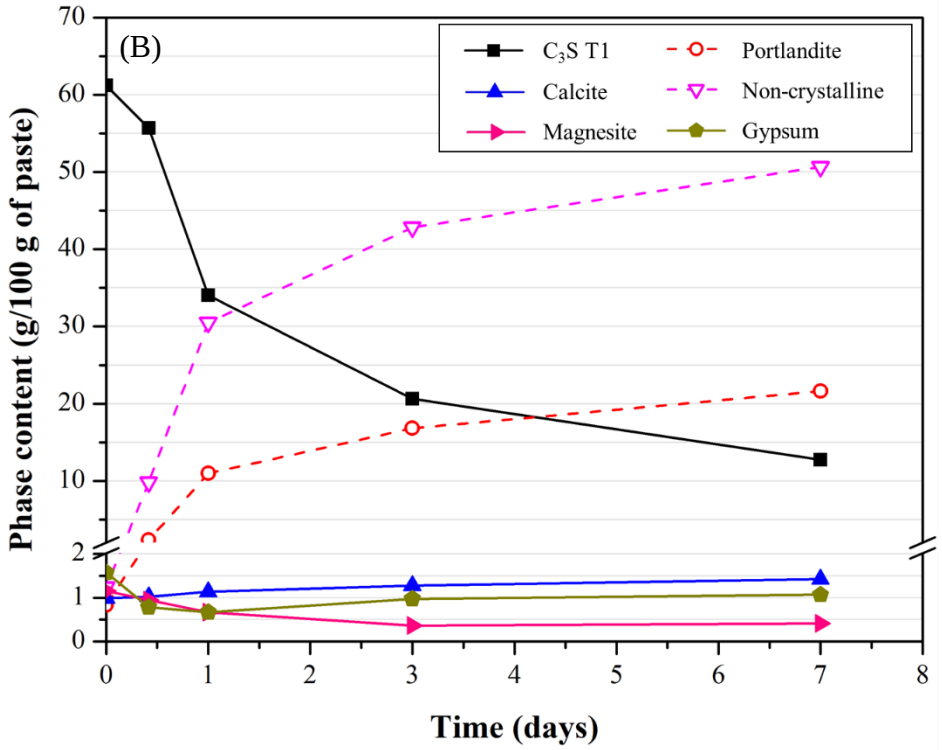
(B)
C3S T1
Portlandite
Calcite
Non-crystalline
Magnesite
Gypsum
Phase content (g/100 g of paste)
Time (days)

1

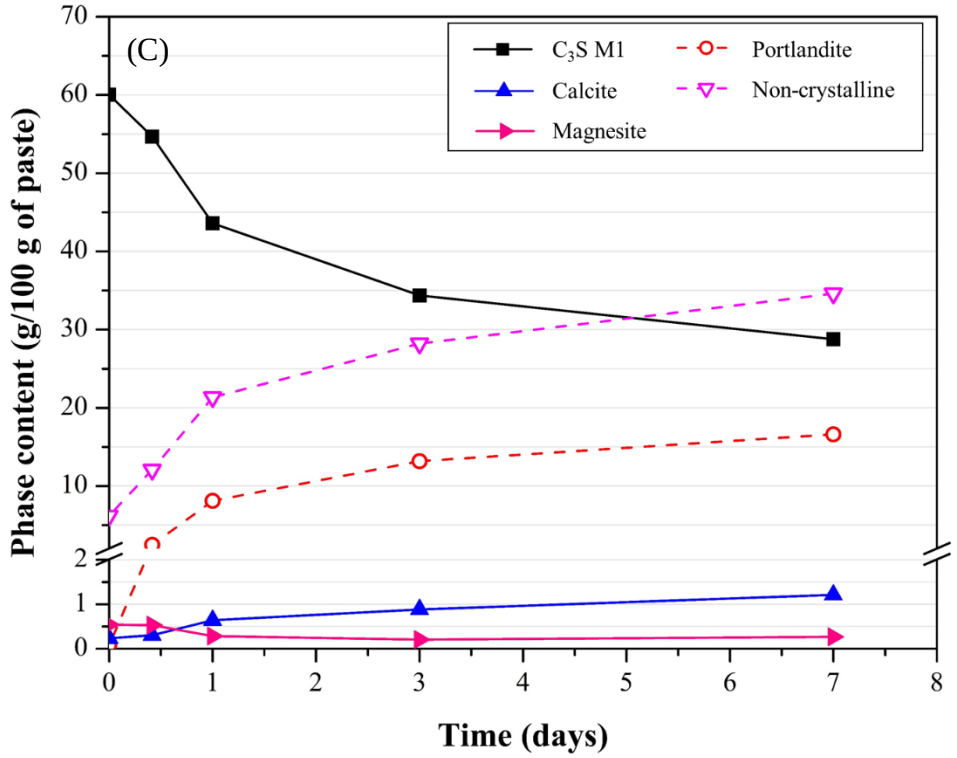
(C)
C3S M1
Portlandite
Calcite
Non-crystalline
Magnesite
Phase content (g/100 g of paste)
Time (days)

2

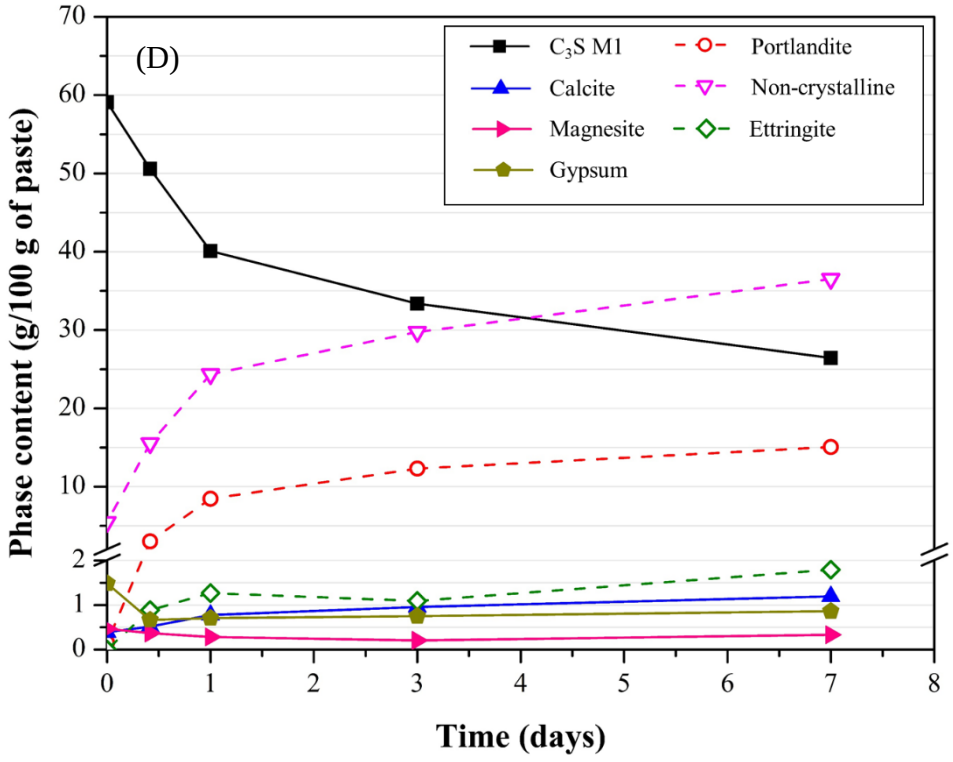

Figure 6 – Crystalline and non-crystalline phases content (g/100 g of paste) obtained by XRD-Rietveld: (A) C_3S; (B) C_3S_2.5%G; (C) Al-C_3S; (D) Al-C_3S_2.5%G.

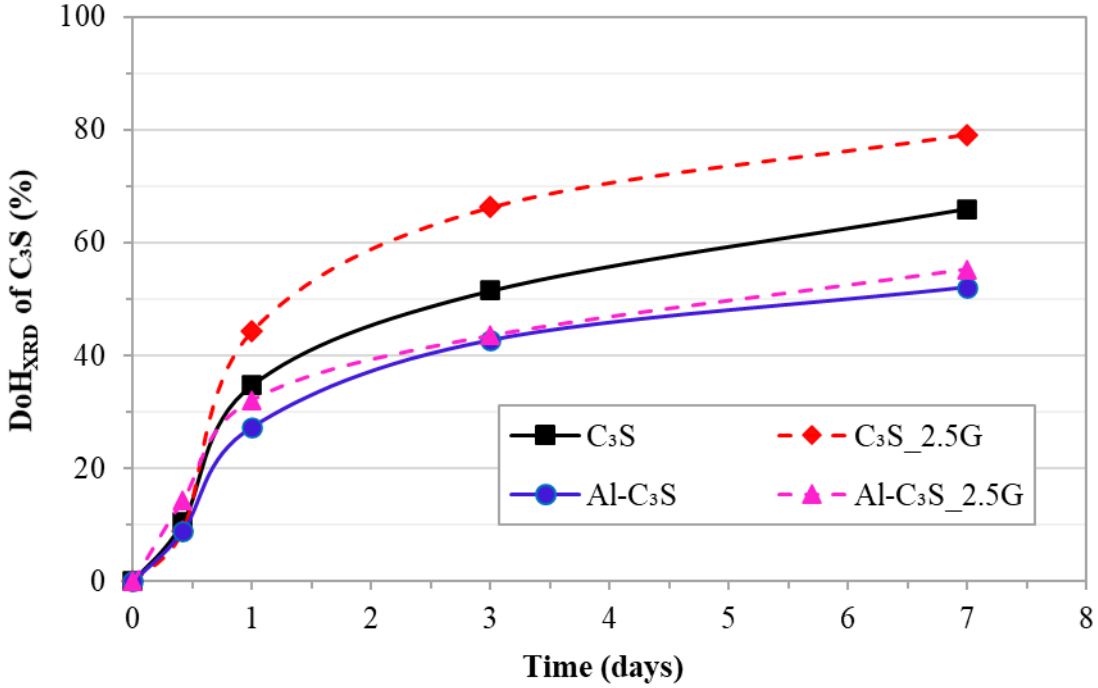

Figure 7 – Degree of hydration of C_3S (%) obtained by XRD-Rietveld.

As expected, the anhydrous phases (C_3S T1, C_3S M1, magnesite, and gypsum) were still remaining samples in all pastes and times of hydration. Concerning the hydration

products, portlandite was identified for all pastes, while ettringite (2.3 wt.% at 7 d) was only identified for Al-C_3S_2.5%G paste, as this mixture was the only one with aluminum (from Al-C_3S) and sulfate (from gypsum). Calcite was presented for all hydrated pastes as C_3S and Al-C_3S have 1.5 wt.% and 0.4 wt.% of calcite. Calcite content increased as a function of the time for all the samples due to slight carbonation effect of samples due to reactions with the atmospheric CO_2 during sample preparation and the tests. The non-crystalline phases of all pastes are mainly related to C-S-H [43].

Comparing C_3S and Al-C_3S pastes without gypsum, the dissolution of anhydrous phases and formation of hydration products are faster in the aluminum-free paste. At 3 and 7 d, the DoH_{XRD} of C_3S is 51.5% and 66.0% for the C_3S paste and 42.7% and 52.1% for the Al-C_3S paste, respectively. The amount of portlandite formed follows the same tendency, and the C_3S pastes present 14.7 wt.% and 19.2 wt.% while the Al-C_3S shows 13.2 wt.% and 16.6 wt.% of portlandite at 3 and 7 d, respectively. This behavior is coherent with the calorimetry results, indicating that the C_3S reacts faster than the Al-C_3S.

The addition of gypsum in the C_3S (T1) pastes did not affect the crystalline hydration products coming from C_3S, but it changed the dissolution rate of anhydrous phases and the rate of formation of portlandite and non-crystalline phases. On the one hand, at 10 h, the gypsum addition slightly decreased the DoH_{XRD} of C_3S (which was 10.5% for the C_3S paste and 9.0% for the C_3S_2.5G paste) and decreased the portlandite content formed by 36.8%. On the other hand, at 1, 3, and 7 d, the presence of sulfate increased the DoH_{XRD} of C_3S by 27.6%, 28.7%, and 20.0%, and increased the portlandite content by 4.8%, 14.1%, and 12.6%, respectively. These results indicate that the addition of gypsum in the C_3S (T1) pastes delays the initial C_3S hydration (until ~ 10 h) but accelerates afterward, as also observed by calorimetry.

For the Al-C_3S (M1) pastes, the delay in the dissolution of C_3S at 10 h, due to gypsum addition, was not observed. On the contrary, the DoH_{XRD} of Al-C_3S increases 61.9%, 17.5%, 1.9%, and 6.2% at 10 h, 1, 3, and 7 d, respectively. This was expected as the gypsum enhanced the Al-C_3S hydration rate after ~ 7 hours, as observed by IC. On the other hand, the portlandite content at 3 and 7 d was reduced by 6.6% and 9.2%. This agreed with thermodynamic modeling (See Section 3.2) and was also observed by He *et al.* [44] and is probably related to the consumption of calcium ions to ettringite formation.

3.4 Thermal analysis (TG/DTG)

Figures 8 A-D shows the DTG curves of the C_3S and Al-C_3S pastes, without and with 2.5 wt.% of gypsum, at 10 h, 1, 3, and 7 d. One peak between 400 and 500 °C, corresponding to the decomposition of portlandite [27], and one peak between 600 and 700 °C, related to the decomposition of calcium carbonates [27], were observed for all pastes, which corroborates with the XRD results. Furthermore, all samples also presented a peak of weight loss between 50 and 300 °C, which is related to the decomposition of C-S-H and C-(A)-S-H [27], and a peak between 800 and 900 °C that corresponds to the transformation of C-S-H in wollastonite ($CaSiO_3$) [27]. Finally, as also observed by XRD, the sample Al-C_3S_2.5%G was the only one that presents the signal due to the loss of water of ettringite, which is associated with a signal around 100 °C [27]. Regarding the samples with gypsum, a peak around 130°C is observed in C_3S_2.5G, while it is not observed in Al-C_3S_2.5G, indicating that gypsum dissolution is faster in the latter, which is expected due to the consumption of sulfate ions to ettringite formation.

With the increase of the hydration time, the peaks related to the hydrated phases' decomposition increased, indicating a higher amount of hydration products and a higher degree of hydration.

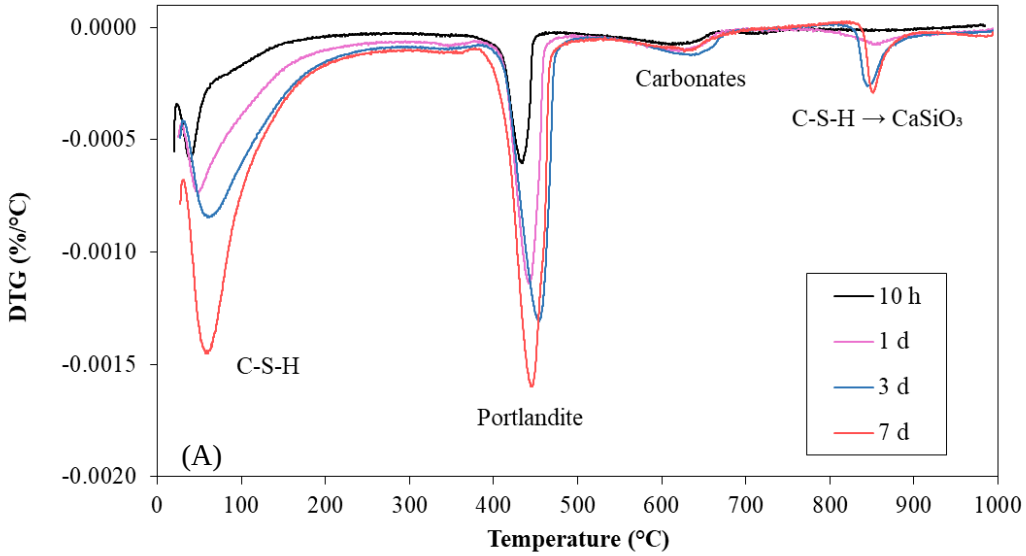

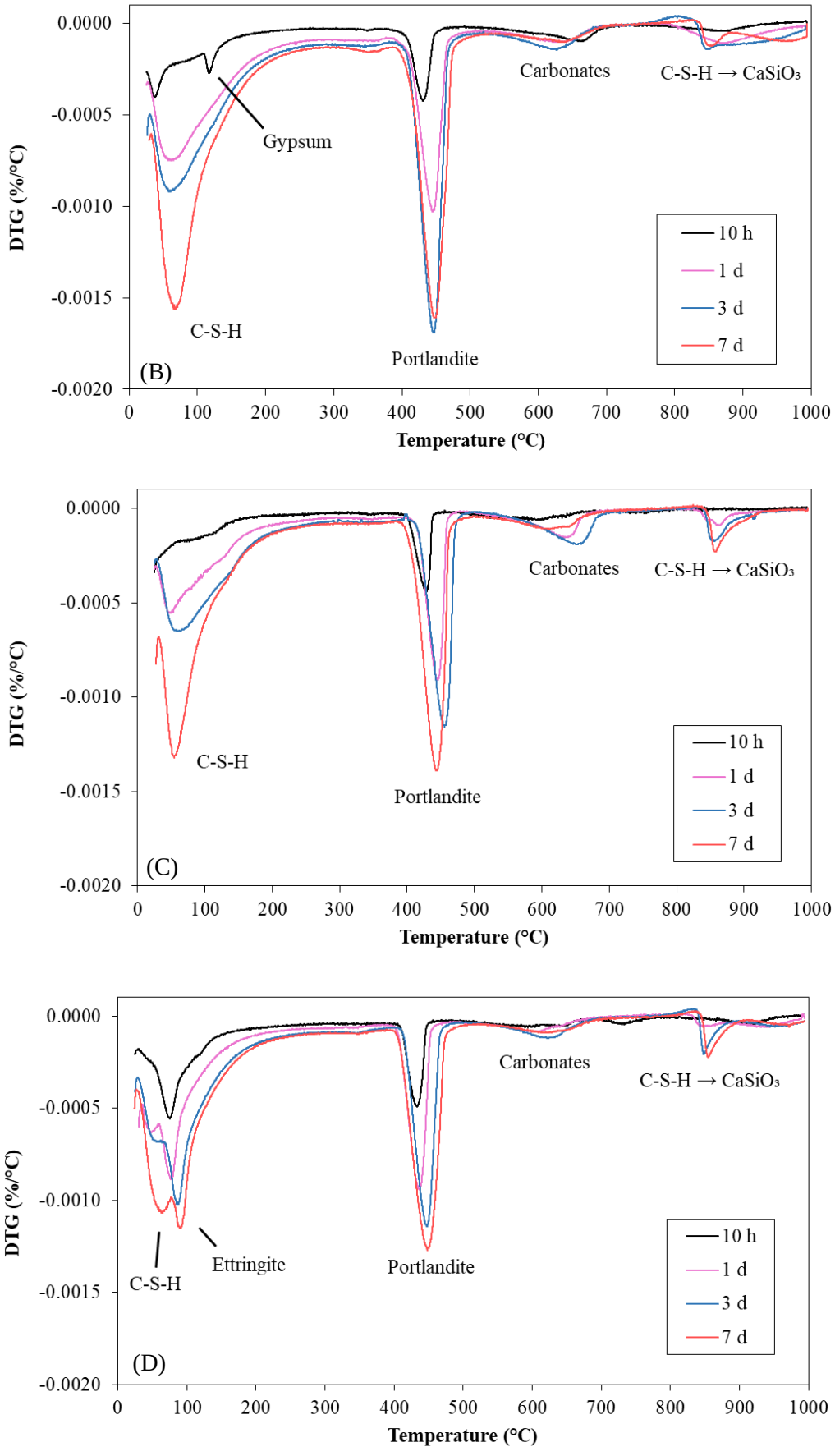

Figure 8 – DTG of: (A) C_3S; (B) C_3S_2.5%G; (C) Al-C_3S; (D) Al-C_3S_2.5%G pastes.

From the TGA results, the bound water content was calculated and is presented in Figure 9. The bound water content indicates the DoH and has an excellent linear correlation (R^2 = 0.99) with the IC's cumulative heat, as presented in Figure 10. As observed for the cumulative heat, in the gypsum free pastes, the C_3S paste has a higher DoH when compared to the Al-C_3S one, resulting in higher bound water content for all ages evaluated. Furthermore, for both C_3S and Al-C_3S, gypsum's addition increased the bound water content, indicating higher C_3S hydration, as also observed by IC and XRD.

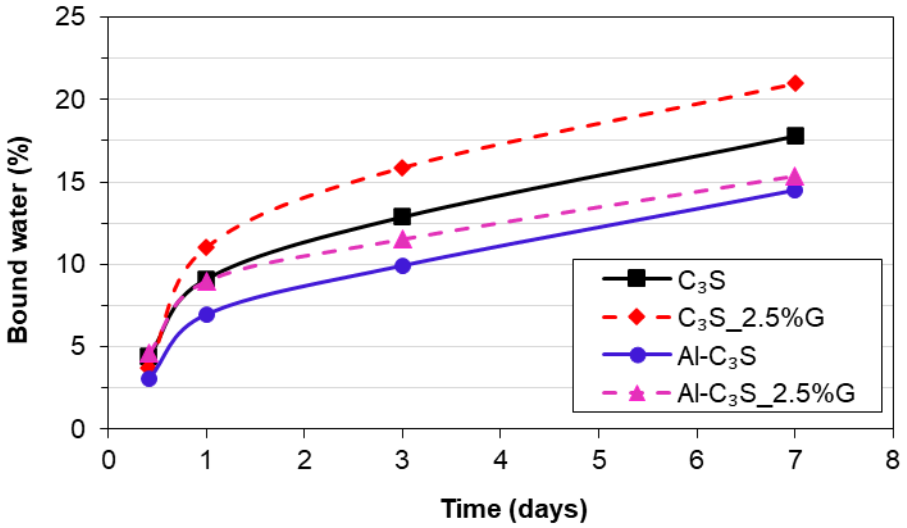

Figure 9 – Bound water content (wt.%) of the various pastes evaluated, obtained by TGA.

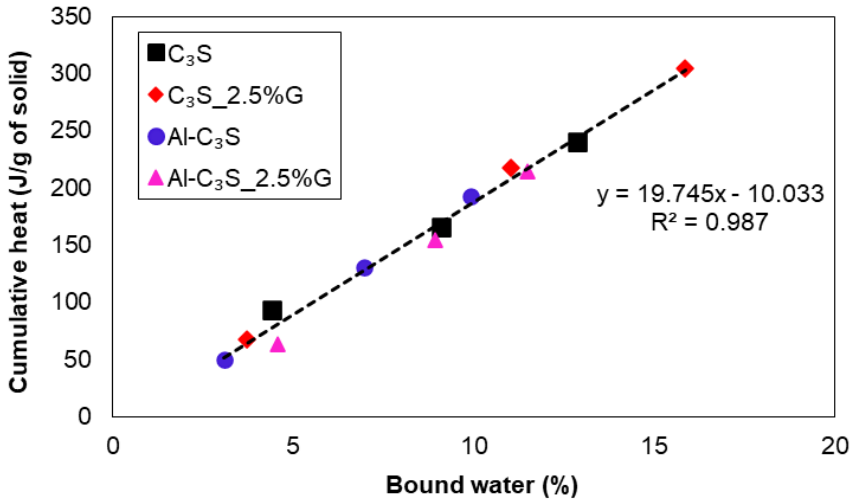

Figure 10 – Correlation between the cumulative heat obtained in the IC and the bond water (wt.%) determined by TGA at 10 h, 1 and 3 days.

The portlandite content was also determined from the TGA results, and the results are shown in Figure 11. As shown in Figure 12, the portlandite content determined by TGA has an excellent correlation (R^2 = 0.97) with the content obtained by XRD-Rietveld, as expected.

The C_3S pastes have a higher portlandite content for all ages tested compared to the Al-C_3S pastes. This results from the higher hydration degree, as observed by IC, XRD, and the bound water content.

The addition of gypsum in the C_3S paste decreased the portlandite content at 10 h but increased after 1 d. These data agree with the IC and XRD results, which indicate that the gypsum delays the initial C_3S hydration (until ~ 12 h) but accelerates after that. On the other hand, the gypsum slightly decreased the portlandite content of the Al-C_3S paste. As mentioned before, in item 4.3.2, this results from the consumption of calcium ions during the ettringite formation.

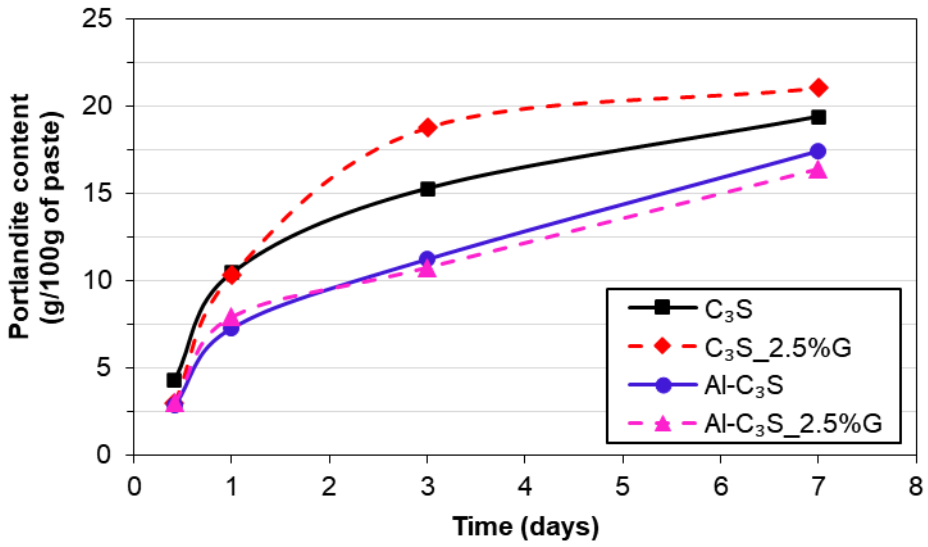

Figure 11 – Portlandite content (wt.%) of the various pastes evaluated, obtained by TGA.

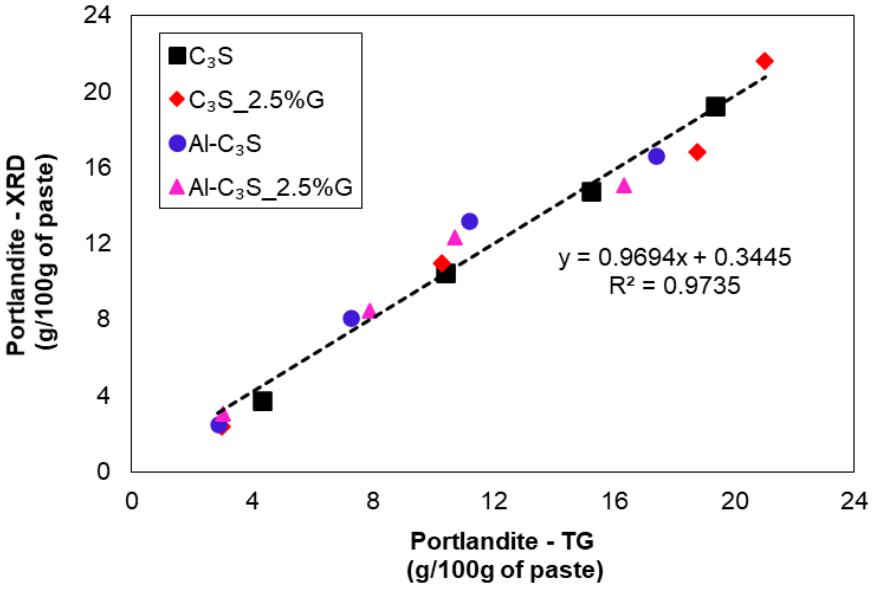

Figure 12 – Correlation between the portlandite content (wt.%) determined by XRD and TGA, at 10 h, 1, 3, and 7 days.

3.5 ^{29}Si and ^{27}Al Nuclear Magnetic Resonance (^{29}Si and ^{27}Al MAS-NMR)

Figure 13 presents the ^{29}Si MAS-NMR spectra of the C_3S and Al-C_3S pastes at 7 days of hydration with peak deconvolution. In the region of Q^0, five resonances at -68.4, -69.5, -71.6, -73.0, and -74.5 ppm are observed for all samples evaluated. This region corresponds to the anhydrous C_3S and Al-C_3S that is remaining in the first 7 d of hydration [45,46].

For all samples, two resonances at -76.9 and -79.1 ppm-in the Q^1 region-, and three resonances at -82.0, -84.1, and -85.5 ppm-in the Q^2 region- are observed. These resonances are related to the C-S-H type phases. The resonances at the Q^1 region correspond to the silica present at the end of the "dreierketten" chain of C-S-H. The resonances at the Q^2 region correspond to the silica within the "dreierketten" chain as bridging (Q^2_b)–at -82.0 ppm- and as pairing (Q^2_p)- at -84.1 and -85.5 ppm [46,47].

For the Al-C_3S and Al-C_3S_2.5G pastes, a resonance at -81.3 ppm that corresponds to the Q^2(1Al) is also observed. This is evidence of the incorporation of aluminum into C-S-H and corresponds to a pairing silica tetrahedron neighboring aluminum in the bridging position [46,47].

Table 6 presents the average chain length of aluminosilicate tetrahedra (MCL), the DoH_{NMR} of C_3S, and the molar ratio of tetrahedral Al incorporated in the C-(A)-S-H, obtained from the deconvolution of peaks of the ^{29}Si MAS-NMR spectra, according to the procedure described in Section 2.2.2.

All sample's MCL values were within the usual range of C-(A)-S-H [48]. The Al-C_3S paste presented a higher MCL than the C_3S paste, which was not expected, as the Al incorporated in C-S-H usually increases the MCL [49]. This discrepancy might be the result of the difference in C_3S polymorphism. The gypsum effect in MCL was not straightforward, as it decreased the MCL in the C_3S pastes but increased it in the Al-C_3S paste. More investigation on the impact of sulfates in the C-S-H MCL is needed.

As shown in Table 6, the addition of gypsum increased the DoH_{NMR} of C_3S by 12.6%, while did not significantly change the DoH_{NMR} of Al-C_3S (a slight increase of 0.4%). These results are very similar to the results of DoH_{XRD} ($R^2 = 0.96$) that showed that, at 7 d, gypsum increases the DoH_{XRD} of C_3S by 20.0%, while only increased the DoH_{XRD} of Al-C_3S by 6.2%.

The presence of gypsum decreased by 17.3% the Al(IV)/Si molar ratio, see Table 6. This was expected as in the Al-C_3S_2.5G paste, a part of the aluminum released with the Al-C_3S dissolution is consumed through the ettringite formation, as observed by XRD and TGA.

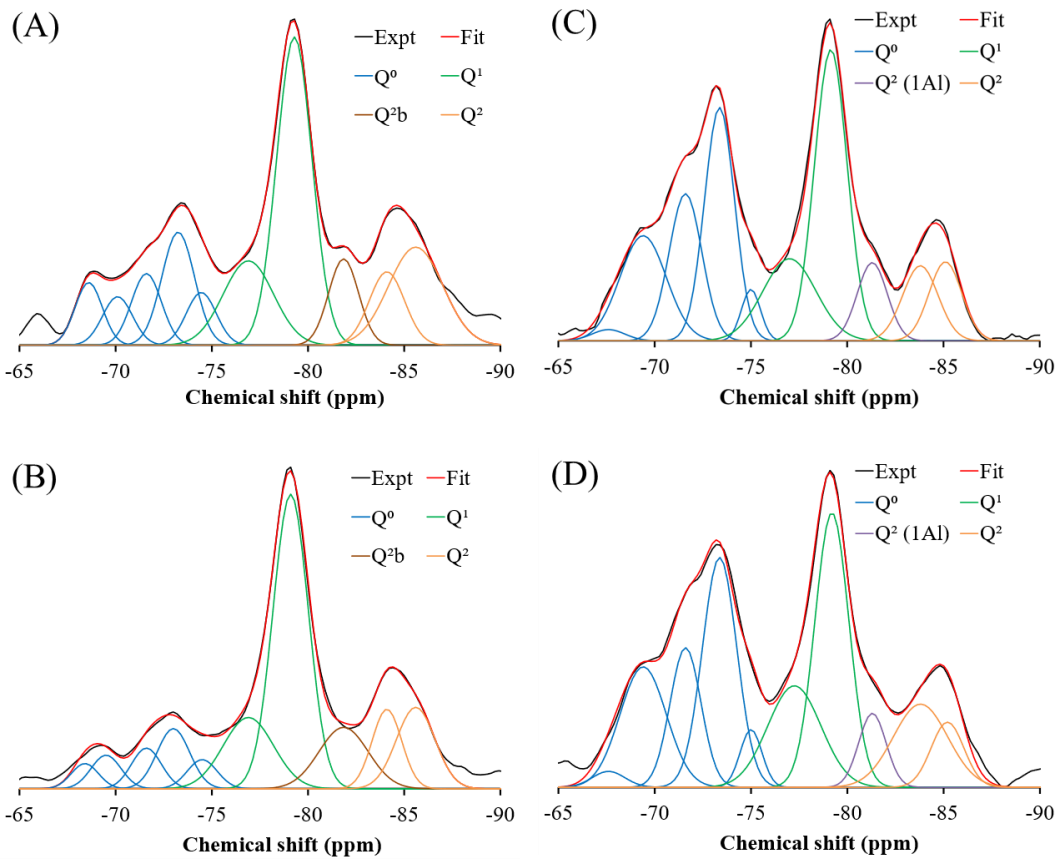

Figure 13 – ^{29}Si MAS-NMR spectra of the (A) C_3S, (B) C_3S_2.5G, (C) Al-C_3S, and (D) Al-C_3S_2.5G pastes at 7 days.

Figure 14 shows the ^{27}Al MAS-NMR spectra of the Al-C_3S and the Al-C_3S_2.5G pastes at 7 days. At the spectral region of the octahedrally coordinated aluminum Al(VI), 20 to -10 ppm, three narrow resonances centered at δ_{obs} = 5, 10 and 13 ppm are observed for the Al-C_3S_2.5G paste, which corresponds to the third aluminum hydrate (TAH)-a nanostructured amorphous aluminum hydroxide or a calcium aluminate hydrate produced in a less ordered form as a surface precipitate on the C-S-H phase [50]-, OH-AFm, and ettringite, respectively [45,46,51]. For the Al-C_3S paste, the resonance corresponding to ettringite is not observed, as this sample does not have gypsum. For both samples, a broad and low-intensity resonance are observed at the spectral region of tetrahedrally coordinated aluminum Al(IV), 80 to 50 ppm, which correspond to the aluminum incorporated in the C_3S and/or in C-S-H [45–47,51], not being possible to differentiate them with the resolution obtained in the present study.

The peaks due to OH-AFm and TAH (in both samples) are slightly broader than ettringite. This means that the degree of crystallinity of these phases is low, and consequently, they are not observed in XRD.

Table 6 presents the molar fractions of TAH, AFm and ettringite phases, obtained by integrating their respectively corresponding peaks. The formation of ettringite by the addition of gypsum resulted in a decrease of 58.2% in the AFm molar fraction, as expected, and resulted in a decrease of 41.1% in the TAH molar fraction. This indicates that when gypsum is present and the ettringite is formed, less aluminum is incorporated in the C-(A)-S-H -as TAH can be considered a part of C-S-H [49]- corroborating the ^{29}Si MAS-NMR results. This result agrees with previous studies [50,52], which observed that an increase in gypsum content decreases TAH. This is due to the percentage of the Al^{3+} ions released with Al-C_3S dissolution forms ettringite when gypsum is present, decreasing the Al^{3+} ions available for the formation of AFm and TAH.

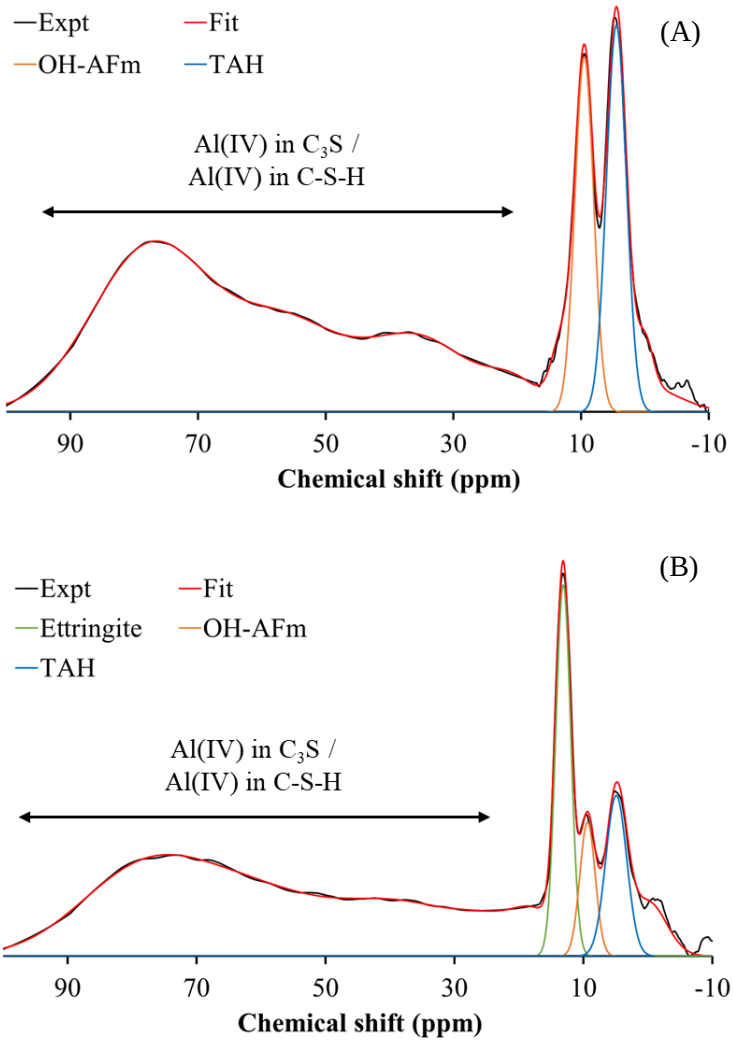

Figure 14 – ^{27}Al MAS-NMR spectra of the (A) Al-C_3S and (B) Al-C_3S_2.5G pastes at 7 days.

Table 6 – Results from spectral analysis of the ^{29}Si and ^{27}Al MAS-NMR spectra for the pastes hydrated for seven days.

Sample	^{29}Si MAS-NMR			^{27}Al MAS-NMR		
	MCL	**DoH (C_3S)**	**Al(IV)/Si**	**AF_t**	**AF_m**	**TAH**
C_3S	3.56	70.8%	-	-	-	-
C_3S_2.5G	3.43	79.7%	-	-	-	-
Al-C_3S	3.26	54.3%	0.052	-	12.2%	14.1%
Al-C_3S_2.5G	3.31	54.5%	0.043	13.7%	5.1%	8.3%

4 DISCUSSION

As observed by IC, XRD, TGA and ^{29}Si MAS-NMR, the C_3S reacts faster than the Al-C_3S, which was also observed by Stephan *et al.* [40] and Begarin *et al.* [41]. As observed in several studies, the C_3S hydration is delayed in aluminum-containing solutions [3,18,19,53]. However, the reason for that is not straight forward and some hypotheses found in the literature need to be discussed. According to Garrault *et al.* [18], Begarin *et al.* [41], and Wagner *et al*. [42], the C-(A)-S-H, formed in the Al-C_3S pastes as identified by ^{27}Al MAS-NMR (Figure 14), does not grow and is not as good seeding for C-S-H growth as C-S-H nuclei themselves. Therefore, the uptake of Al by C-S-H would reduce its reactive surface, leading to a lower hydration rate [42]. However, several other studies [54–56], including some in blended cements with higher Al uptake by C-S-H, show that C-(A)-S-H has a very similar morphology to C-S-H. Further research is necessary to verify if the uptake of aluminum by C-S-H indeed decreases its reactive surface or not. Another hypothesis is that the delay in C_3S dissolution in Al-containing solution is due to the condensation of aluminum-silicate species at C_3S surface [3,19].

Despite the initial delay on C_3S and Al-C_3S dissolution, the presence of gypsum accelerated the C_3S hydration after ~ 12 h and the Al-C_3S hydration after ~ 7 h, as observed by increases in cumulative heat (IC), in the amorphous content (XRD) and water-bound content (TG/DTG), as well as a decrease in the anhydrous content (XRD) in all the ages evaluated. Similar behaviors were observed by several authors [5–12]. However, the reason for that is not apparent yet.

As observed by IC, mixtures with 5.0 wt.% of gypsum had a similar hydration rate as those with 2.5 wt.% of gypsum. This indicates that the C_3S hydration is accelerated up to a certain gypsum content, without significant difference in higher contents, besides a slight decrease in the heat flow due to the lower amount of C_3S in the mixture, known as the dilution effect. Several authors made similar observations [5,9] with aluminum-free C_3S and are following the simulations performed by Gunay *et al.* [10] which shows that the gypsum increases the C-S-H growth rate up to plateau value at 1.0 wt.% of gypsum. As observed by IC, the Al-C_3S shows the same behavior, where the Al-C_3S_5.0G had a similar hydration rate as the Al-C_3S_2.5G, indicating that the aluminum doping of C_3S does not influences the existence of a plateau value of gypsum concerning the Al-C_3S' hydration rate.

As observed by thermodynamic modeling, the presence of gypsum in the Al-C_3S pastes reduces the Al concentration of the pore solution from 0.005 to 0 mM, indicating that all the aluminum released by Al-C_3S dissolution is expected to be immediately consumed by ettringite formation. Thus, as Al^{3+} ions in the pore solution retards C_3S, as previously discussed, their removal must contribute to the acceleration of Al-C_3S hydration, as suggested by Quennoz and Scrivener [6]. This is probably the reason for the much earlier acceleration in Al-C_3S hydration than in the C_3S hydration due to gypsum, resulting in great increases of the hydration rate at the acceleration period and a significant increase of the main heat flow peak (see Section 3.1). However, contrary to Quennoz and Scrivener's [6] conclusions, this cannot be the only or the main mechanism responsible for the acceleration of C_3S hydration due to gypsum, as gypsum also enhanced the C_3S hydration rate after ~ 12 h of hydration.

This behavior was also previously related to the seeding effect of very fine nano-ettringite [8]. However, in C_3S pastes, which do not contain aluminum, no ettringite is formed, as observed by XRD and TGA. Therefore, none of these hypotheses can fully explain the effect of calcium sulfate on the C_3S hydration. As suggested by Zunino and Scrivener [9], the enhancement in C_3S hydration rate is probably mainly related to interactions between the calcium sulfate and the silicates (C_3S and/or C-S-H) rather than interactions that involve the aluminates.

Based on the simulations performed by Gunay *et al.* [10], the presence of gypsum increases the perpendicular and parallel C-S-H growth rate. The reason for this is still not

understood. Three different hypotheses can be proposed to explain the enhancement in C_3S, and Al-C_3S hydration rate by gypsum: (*i*) The sulfate ions change the C-S-H needle morphology, reducing the lateral impingement and accelerating the growth of the C-S-H needles. (*ii*) The change in the C-S-H needle morphology would provide more sites for the precipitation of hydration products. (*iii*) Sulfate ions increase the ionic strength, increasing the nucleation and growth rate of C-S-H. The first two hypotheses relate the enhancement in C_3S hydration rate by gypsum with the change of C-S-H needles' morphology. Mota *et al.* [7] showed that a negatively charged cloud of sulfate ions is physically adsorbed in the positivity charged C-S-H needles. This yields to the C-S-H needles' repulsion, leading to a more divergent needle structure instead of the convergent morphology observed in plain C_3S pastes [7].

According to the first hypothesis, this divergent needle structure would reduce the lateral impingement between the C-S-H needles, accelerating their growth and final length, as exemplified in Figure 15. As suggested by Zhang et al. [57], the C-S-H needles may be described as ellipsoidal particles randomly distributed on the C_3S surface. Adjacent C-S-H needles may impinge on each other, which probably will reduce its growth rate [57,58]. The convergent structure of the C-S-H needles in sulfate-free solutions probably induces more and faster impingement between the adjacent C-S-H needles than the more divergent structure of C-S-H needles in solution with sulfate, which may explain the enhancement of C_3S hydration due to gypsum on the acceleration period – the moment which the nucleation and growth of C-S-H needles occur.

Furthermore, according to Ouzia and Scrivener [59] the C-S-H needles grow until a certain critical length, when the growth rate decreases abruptly, which results in the decrease of the hydration rate. The reasons for that are still unknown but increases in C-S-H needle length result in a higher hydration rate [59]. One possible reason could be the lateral impingement between C-S-H needles. If this is true, the more divergent morphology of C-S-H needles with the gypsum addition might decrease the lateral impingement, which may increase the length of C-S-H needles, as illustrated in Figure 15.

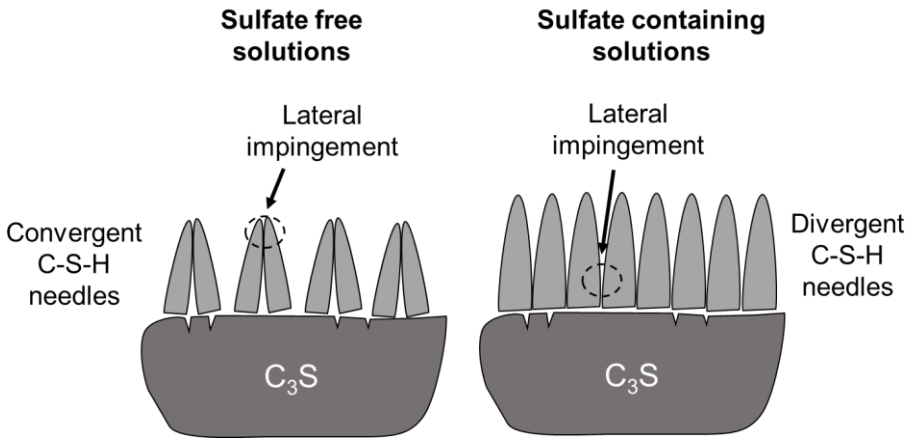

Figure 15 – Schematic representation of the impact of sulfate ions on C-S-H morphology (adapted from Mota et al. [7]

According to hypothesis (*ii*), the more divergent structure of the C-S-H needles would increase its surface area, resulting in more sites for the precipitation of hydration products. This hypothesis agrees with Huang and Yang's [60] results, who observed an increase in the specific surface area of the C-S-H by adding K_2SO_4 when compared to plain C_3S pastes. This might result from the divergent morphology of C-S-H needles when adding K_2SO_4 (a similar morphology as those observed by Mota *et al.* [7] when adding gypsum). However, the surface area of the hydrating C_3S is also highly influenced by the number of C-S-H needles. In addition, the experimental errors associated with this determination should be account for as it is extremely difficult to stop the C_3S hydration quickly and precisely enough to obtained different samples at equal DoH. Therefore, further studies on this topic are necessary to verify if the more divergent structure of C-S-H needles due to sulfates addition leads to a higher surface area or not.

Finally, the enhancement in C_3S hydration rate by gypsum could be due to the increase in the ionic strength (*iii*). As observed by thermodynamic modeling (Section 3.2), the addition of 2.5 wt.% of gypsum increases 51% in the ionic strength (0.055 to 0.083 molal). Increases in the ionic strength favor increases in the number of C-S-H nuclei per unit surface area of C_3S/alite, increasing the nucleation rate and growth of C-S-H [61,62]. This might be the reason or one of the reasons for the enhancement of C_3S hydration. On the other hand, the further addition of gypsum (*i.e.*, the mixes with 5.0 wt.% of gypsum) did not increase the ionic strength, which might explain the plateau in the enhancement effect of gypsum on C_3S hydration.

5 CONCLUSIONS

- Aluminum doped C_3S has a slower hydration rate when compared to aluminum-free C_3S, which probably result from the releasing of aluminum ions into the solution with the Al-C_3S dissolution. Note that the larger particle size of Al-C_3S may also contribute to this result.
- The presence of gypsum delayed the initial hydration of C_3S and Al-C_3S, prolonging the induction period. The initial delay seems to be related to the interaction between the sulfate ions and C_3S.
- The presence of gypsum accelerated the C_3S and the Al-C_3S hydration during the nucleation and growth period (after the induction period), increasing the main hydration peak, the cumulative heat, the dissolution of C_3S and Al-C_3S, and the amount of bound water. The acceleration on the hydration due to gypsum addition was higher for the C_3S samples -increases of 20.0% and 12.6% in DoH_{XRD} and DoH_{NMR} at 7 d - compared to the Al-C_3S samples -increases of 6.2% and 0.4% in DoH_{XRD} and DoH_{NMR} at 7 d.
- As observed by thermodynamic modeling, the addition of 2.5 wt.% of gypsum increased 51% in ionic strength of the pore solution of C_3S and Al-C_3S pastes. However, further addition of gypsum (5.0 wt.%) did not result in further increases.
- For the aluminum-free C_3S pastes, the addition of gypsum increased the portlandite content due to the increase in the hydration rate. However, for the Al-C_3S, a decrease in portlandite content was observed, probably due to the consumption of calcium ions for ettringite formation despite the higher degree of hydration.
- The addition of gypsum in Al-C_3S resulted in a decrease of AFm and TAH phases and a decrease in Al incorporated in C-S-H due to the ettringite formation, which decreases Al^{3+} available in the solution.
- The acceleration effect of gypsum on C_3S hydration occurred much earlier in Al-C_3S pastes than in the C_3S pastes, resulting in great increases of the hydration rate at the acceleration period and a significant increase of the main heat flow peak. As observed by thermodynamic modeling, the presence of gypsum in the Al-C_3S pastes reduces the Al^{3+} concentration of the pore solution. All the aluminum

released by Al-C_3S dissolution is expected to be immediately consumed by ettringite formation in the presence of 2.5 wt.% of gypsum. Thus, as Al^{3+} ions in the pore solution retards C_3S, their removal from the pore solution must contribute to the acceleration of Al-C_3S hydration.

- As gypsum also accelerated the aluminum-free C_3S hydration, where no ettringite is formed, the formation of ettringite cannot be the only neither the main mechanism responsible for the acceleration of C_3S hydration in the presence of calcium sulfate.

- The results indicate that the enhancement in C_3S and Al-C_3S hydration rate after the induction period due to gypsum is probably related to (*i*, *ii*) the more divergent needle-structure C-S-H morphology when sulfate is present (according to bibliography), which (*i*) may reduce the lateral impingement between adjacent C-S-H needles increasing their growth rate and (*ii*) may increase the site for the precipitation of hydration products. (*iii*) The increase in ionic strength when adding gypsum.

6 ACKNOWLEDGEMENTS

JSAN thanks the financial support of CAPES (Coordination for the Improvement of Higher Education Personnel) [88882.439908/2019-01]. JSAN also thanks the Spanish Junta de Andalucía [UMA18-FEDERJA-095 and P18-RT-720] research projects for the research stage at the University of Málaga (Spain) and the Graduate Program in Civil Engineering: Construction and Infrastructure (PPGCI) of the Federal University of Rio Grande do Sul (UFRGS). APK and EDR were sponsored by CNPq (Brazilian National Council for Scientific and Technological Development) through the research fellowships PQ2017 303753 / 2017-0 and 305530 / 2017-8. The authors thank Alejandro Morales Cantero for the help in the calorimetry and TG tests and Márlon Augusto Longhi for helping in the MAS-NMR analysis. The authors also thank the creators and developers of cemGEMS web application, who made it available for free, as well as several tutorials on how to use it.

7 REFERENCES

[1] K.L. Scrivener, A. Nonat, Hydration of cementitious materials, present and future, Cement and Concrete Research. 41 (2011) 651–665. https://doi.org/10.1016/j.cemconres.2011.03.026.

[2] J. da S. Andrade Neto, A.G. de la Torre, A.P. Kirchheim, Effects of sulfates on the hydration of Portland cement – A review, Construction and Building Materials. 279 (2021). https://doi.org/10.1016/j.conbuildmat.2021.122428.

[3] L. Nicoleau, E. Schreiner, A. Nonat, Ion-specific effects influencing the dissolution of tricalcium silicate, Cement and Concrete Research. 59 (2014) 118–138. https://doi.org/10.1016/j.cemconres.2014.02.006.

[4] P. Juilland, L. Nicoleau, R.S. Arvidson, E. Gallucci, Advances in dissolution understanding and their implications for cement hydration, RILEM Technical Letters. 2 (2017) 90. https://doi.org/10.21809/rilemtechlett.2017.47.

[5] A. Bentur, Effect of Gypsum on the Hydration and Strength of C3S Pastes, Journal of the American Ceramic Society. 59 (1976) 210–213. https://doi.org/10.1111/j.1151-2916.1976.tb10935.x.

[6] A. Quennoz, K.L. Scrivener, Interactions between alite and C3A-gypsum hydrations in model cements, Cement and Concrete Research. 44 (2013) 46–54. https://doi.org/10.1016/j.cemconres.2012.10.018.

[7] B. Mota, T. Matschei, K. Scrivener, The influence of sodium salts and gypsum on alite hydration, Cement and Concrete Research. 75 (2015) 53–65. https://doi.org/10.1016/j.cemconres.2015.04.015.

[8] S.T. Bergold, F. Goetz-Neunhoeffer, J. Neubauer, Interaction of silicate and aluminate reaction in a synthetic cement system: Implications for the process of alite hydration, Cement and Concrete Research. 93 (2017) 32–44. https://doi.org/10.1016/j.cemconres.2016.12.006.

[9] F. Zunino, K. Scrivener, Factors influencing the sulfate balance in pure phase C3S/C3A systems, Cement and Concrete Research. 133 (2020) 106085. https://doi.org/10.1016/j.cemconres.2020.106085.

[10] S. Gunay, S. Garrault, a Nonat, P. Termkhajornkit, Influence of calcium sulphate on hydration and mechanical strength of tricalcium silicate, 13th International Congress on the Chemistry of Cement. (2011) 1–7.

[11] P.W. Brown, C.L. Harner, E.J. Prosen, The effect of inorganic salts on tricalcium silicate hydration, Cement and Concrete Research. 16 (1986) 17–22. https://doi.org/10.1016/0008-8846(86)90063-3.

[12] Y. Zhang, X. Zhang, Research on effect of limestone and gypsum on C3A, C3S and PC clinker system, Construction and Building Materials. 22 (2008) 1634–1642. https://doi.org/10.1016/j.conbuildmat.2007.06.013.

[13] F. Zunino, K. Scrivener, The influence of the filler effect on the sulfate requirement of blended cements, Cement and Concrete Research. 126 (2019) 105918. https://doi.org/10.1016/j.cemconres.2019.105918.

[14] H.F.W. Taylor, Cement chemistry, 2nd ed., Thomas Telford, 1997. https://doi.org/10.1680/cc.25929.

[15] K. Schraut, B. Adamczyk, C. Adam, D. Stephan, B. Meng, S. Simon, J. von Werder, Synthesis and characterisation of alites from reduced basic oxygen furnace slags, Cement and Concrete Research. 147 (2021) 106518. https://doi.org/10.1016/j.cemconres.2021.106518.

[16] K.L. Scrivener, P. Juilland, P.J.M. Monteiro, Advances in understanding hydration of Portland cement, Cement and Concrete Research. 78 (2015) 38–56. https://doi.org/10.1016/j.cemconres.2015.05.025.

[17] J. Peng, J. Zhang, J. Qu, Mechanism of the formation and transformation of ettringite, Journal Wuhan University of Technology, Materials Science Edition. 21 (2006) 158–161. https://doi.org/10.1007/BF02840908.

[18] S. Garrault, A. Nonat, Y. Sallier, L. Nicolaeau, On the Origin of the Dormant Period of Cement Hydration, in: 13th International Congress on the Chemistry of Cement., Madrid, 2011: pp. 1–7.

[19] E. Pustovgar, R.K. Mishra, M. Palacios, J.B. d'Espinose de Lacaillerie, T. Matschei, A.S. Andreev, H. Heinz, R. Verel, R.J. Flatt, Influence of aluminates on the hydration kinetics of tricalcium silicate, Cement and Concrete Research. 100 (2017) 245–262. https://doi.org/10.1016/j.cemconres.2017.06.006.

[20] D. Ménétrier, I. Jawed, J. Skalny, Effect of gypsum on C3S hydration, Cement and Concrete Research. 10 (1980) 697–701.

[21] E.M.J. Bérodier, A.C.A. Muller, K.L. Scrivener, Effect of sulfate on C-S-H at early age, Cement and Concrete Research. 138 (2020) 106248. https://doi.org/10.1016/j.cemconres.2020.106248.
[22] M.N. de Noirfontaine, M. Courtial, F. Dunstetter, G. Gasecki, M. Signes-Frehel, Tricalcium silicate Ca3SiO5 superstructure analysis: A route towards the structure of the M1 polymorph, Zeitschrift Fur Kristallographie. 227 (2012) 102–112. https://doi.org/10.1524/zkri.2012.1425.
[23] M. Palacios, H. Kazemi-Kamyab, S. Mantellato, P. Bowen, Laser diffraction and gas adsorption techniques, in: K. Scrivener, R. Snellings, B. Lothenbach (Eds.), A Practical Guide to Microstructural Analysis of Cementitious Materials, 1st ed., CRC Press, 2016: pp. 445–480.
[24] M. García-Maté, A.G. de La Torre, L. León-Reina, E.R. Losilla, M.A.G. Aranda, I. Santacruz, Effect of calcium sulfate source on the hydration of calcium sulfoaluminate eco-cement, Cement and Concrete Composites. 55 (2015) 53–61. https://doi.org/10.1016/j.cemconcomp.2014.08.003.
[25] L. Wadsö, Operational issues in isothermal calorimetry, Cement and Concrete Research. 40 (2010) 1129–1137. https://doi.org/10.1016/j.cemconres.2010.03.017.
[26] J.D. Zea-Garcia, A.G. de la Torre, M.A.G. Aranda, I. Santacruz, Processing and characterisation of standard and doped alite-belite-ye'elimite ecocement pastes and mortars, Cement and Concrete Research. 127 (2020). https://doi.org/10.1016/j.cemconres.2019.105911.
[27] B. Lothenbach, P.T. Durdziński, K. de Weerdt, Thermogravimetric analysis, in: K. Scrivener, R. Snellings, B. Lothenbach (Eds.), A Practical Guide to Microstructural Analysis of Cementitious Materials, 1st ed., CRC Press, 2016: pp. 177–212.
[28] A.G. de La Torre, S. Bruque, M.A.G. Aranda, Applied Crystallography Rietveld quantitative amorphous content analysis, J. Appl. Cryst. 34 (2001) 196–202.
[29] N.I. Golovastikov, R.G. Matveeva, N. v. Belov, Crystal structure of the tricalcium silicate 3CaO SiO2 = C3S, Soviet Physics - Crystallography. 20 (1975) 441–445.
[30] D.K. Smith, H.R. Leider, Low-temperature thermal expansion of LiH, MgO and CaO, Journal of Applied Crystallography. 1 (1968) 246–249. https://doi.org/10.1107/s0021889868005418.
[31] Á.G. de la Torre, M.-G. López-Olmo, C. Álvarez-Rua, S. García-Granda, Miguel.A.G. Aranda, Structure and microstructure of gypsum and its relevance to Rietveld quantitative phase analyses, Powder Diffraction. 19 (2004) 240–246. https://doi.org/10.1154/1.1725254.
[32] J.D. Jorgensen, Compression mechanisms in α-quartz structures - SiO2 and GeO2, Journal of Applied Physics. 49 (1978) 5473–5478. https://doi.org/10.1063/1.324517.
[33] F. Goetz-Neunhoeffer, J. Neubauer, Refined ettringite (Ca 6 Al 2 (SO 4) 3 (OH) 12 ·26H 2 O) structure for quantitative X-ray diffraction analysis , Powder Diffraction. 21 (2006) 4–11. https://doi.org/10.1154/1.2146207.
[34] H.E. Petch, The hydrogen positions in portlandite, Ca(OH)2, as indicated by the electron distribution, Acta Crystallographica. 14 (1961) 950–957. https://doi.org/10.1107/s0365110x61002771.
[35] R. Wartchow, Datensammlung nach der "learnt profile"-methode(LP) für calcit und vergleich mit der "background peak background"-methode (BPB), Zeitschrift Für Kristallographie. 186 (1989) 300–302.
[36] S. Joseph, J. Skibsted, Ö. Cizer, Hydration of polyphase Ca3SiO5-Ca3Al2O6 in the presence of gypsum and Na2SO4, Journal of the American Ceramic Society. 103 (2020) 1–30. https://doi.org/10.1111/jace.17321.
[37] D.A. Kulik, F. Winnefeld, A. Kulik, G.D. Miron, B. Lothenbach, CemGEMS – an easy-to-use web application for thermodynamic modeling of cementitious materials, RILEM Technical Letters. 6 (2021) 36–52. https://doi.org/10.21809/rilemtechlett.2021.140.
[38] B. Lothenbach, D.A. Kulik, T. Matschei, M. Balonis, L. Baquerizo, B. Dilnesa, G.D. Miron, R.J. Myers, Cemdata18: A chemical thermodynamic database for hydrated Portland cements and alkali-activated materials, Cement and Concrete Research. 115 (2019) 472–506. https://doi.org/10.1016/j.cemconres.2018.04.018.
[39] P.G. Gottschalk, J.R. Dunn, The five-parameter logistic: A characterization and comparison with the four-parameter logistic, Analytical Biochemistry. 343 (2005) 54–65. https://doi.org/10.1016/j.ab.2005.04.035.
[40] D. Stephan, S. Wistuba, Crystal structure refinement and hydration behaviour of 3CaO·SiO2 solid solutions with MgO, Al2 O3 and Fe2O3, Journal of the European Ceramic Society. 26 (2006) 141–148. https://doi.org/10.1016/j.jeurceramsoc.2004.10.031.
[41] F. Begarin, S. Garrault, A. Nonat, L. Nicoleau, Hydration of alite containing aluminium, Advances in Applied Ceramics. 110 (2011) 127–130. https://doi.org/10.1179/1743676110Y.0000000007.

[42] D. Wagner, F. Bellmann, J. Neubauer, Influence of aluminium on the hydration of triclinic C3S with addition of KOH solution, Cement and Concrete Research. 137 (2020) 106198. https://doi.org/10.1016/j.cemconres.2020.106198.
[43] R. Snellings, X-ray powder diffraction applied to cement, in: K. Scrivener, R. Snellings, B. Lothenbach (Eds.), A Practical Guide to Microstructural Analysis of Cementitious Materials, 1st ed., CRC Press, 2016: pp. 107–176.
[44] Y. He, X. Zhang, S. Liu, R.D. Hooton, T. Ji, Y. Kong, Impacts of sulphates on rheological property and hydration performance of cement paste in the function of polycarboxylate superplasticizer, Construction and Building Materials. 256 (2020) 119428. https://doi.org/10.1016/j.conbuildmat.2020.119428.
[45] B. Walkley, J.L. Provis, Solid-state nuclear magnetic resonance spectroscopy of cements, Materials Today Advances. 1 (2019) 100007. https://doi.org/10.1016/j.mtadv.2019.100007.
[46] M. Daugaard Andersen, H.J. Jakobsen, Jø. Skibsted, Incorporation of aluminum in the calcium silicate hydrate (C-S-H) of hydrated Portland cements: A high-field 27Al and 29Si MAS NMR investigation, Inorganic Chemistry. 42 (2003) 2280–2287. https://doi.org/10.1021/ic020607b.
[47] E. L'Hôpital, B. Lothenbach, D.A. Kulik, K. Scrivener, Influence of calcium to silica ratio on aluminium uptake in calcium silicate hydrate, Cement and Concrete Research. 85 (2016) 111–121. https://doi.org/10.1016/j.cemconres.2016.01.014.
[48] Y. Chiang, S.W. Chang, Bridging the gap between NMR measured mean silicate chain length and nano-scale silicate polymorphism of calcium silicate hydrates, Cement and Concrete Research. 140 (2021) 106268. https://doi.org/10.1016/j.cemconres.2020.106268.
[49] E. L'Hôpital, B. Lothenbach, G. le Saout, D. Kulik, K. Scrivener, Incorporation of aluminium in calcium-silicate-hydrates, Cement and Concrete Research. 75 (2015) 91–103. https://doi.org/10.1016/j.cemconres.2015.04.007.
[50] M.D. Andersen, H.J. Jakobsen, J. Skibsted, A new aluminium-hydrate species in hydrated Portland cements characterized by 27Al and 29Si MAS NMR spectroscopy, Cement and Concrete Research. 36 (2006) 3–17. https://doi.org/10.1016/j.cemconres.2005.04.010.
[51] A.S. Brykov, A.S. Vasil'ev, M. v. Mokeev, Hydration of portland cement in the presence of aluminum-containing setting accelerators, Russian Journal of Applied Chemistry. 86 (2013) 793–801. https://doi.org/10.1134/S1070427213060013.
[52] G. Deng, Y. He, L. Lu, S. Hu, Evolution of aluminate hydrate phases in fly ash-cement system under the sulfate conditions, Construction and Building Materials. 252 (2020) 119045. https://doi.org/10.1016/j.conbuildmat.2020.119045.
[53] T. Matschei, P. Kruspan, P. Sandberg, L. Wadso, Sulphate optimization of binders containing portland cement clinker using isothermal calorimetry, in: Proceedings of 15th International Congress on the Chemistry of Cement, Prague, 2019.
[54] F. Zunino, F. Martirena, K. Scrivener, Limestone calcined clay cements (LC3), ACI Materials Journal. 118 (2021) 49–60. https://doi.org/10.14359/51730422.
[55] F. Avet, K. Scrivener, Effect of temperature on the water content of C-A-S-H in plain Portland and blended cements, Cement and Concrete Research. 136 (2020) 106124. https://doi.org/10.1016/j.cemconres.2020.106124.
[56] F. Avet, E. Boehm-Courjault, K. Scrivener, Investigation of C-A-S-H composition, morphology and density in Limestone Calcined Clay Cement (LC3), Cement and Concrete Research. 115 (2019) 70–79. https://doi.org/10.1016/j.cemconres.2018.10.011.
[57] Z. Zhang, F. Han, P. Yan, Modelling the dissolution and precipitation process of the early hydration of C3S, Cement and Concrete Research. 136 (2020) 106174. https://doi.org/10.1016/j.cemconres.2020.106174.
[58] J.J. Thomas, A.J. Allen, H.M. Jennings, Hydration kinetics and microstructure development of normal and CaCl2-accelerated tricalcium silicate pastes, Journal of Physical Chemistry C. 113 (2009) 19836–19844. https://doi.org/10.1021/jp907078u.
[59] A. Ouzia, K. Scrivener, The needle model: A new model for the main hydration peak of alite, Cement and Concrete Research. 115 (2019) 339–360. https://doi.org/10.1016/j.cemconres.2018.08.005.
[60] L. Huang, Z. Yang, Early hydration of tricalcium silicate with potassium hydroxide and sulfate from pore solution and solid view, Construction and Building Materials. 230 (2020) 116988. https://doi.org/10.1016/j.conbuildmat.2019.116988.
[61] J. Fu, A.M. Jones, M.W. Bligh, C. Holt, L.M. Keyte, F. Moghaddam, S.J. Foster, T.D. Waite, Mechanisms of enhancement in early hydration by sodium sulfate in a slag-cement blend – Insights from pore solution chemistry, Cement and Concrete Research. 135 (2020) 106110. https://doi.org/10.1016/j.cemconres.2020.106110.

[62] A. Kumar, G. Sant, C. Patapy, C. Gianocca, K.L. Scrivener, The influence of sodium and potassium hydroxide on alite hydration: Experiments and simulations, Cement and Concrete Research. 42 (2012) 1513–1523. https://doi.org/10.1016/j.cemconres.2012.07.003.

Figure 1

Click here to access/download;Figure;Figure 1.jpg

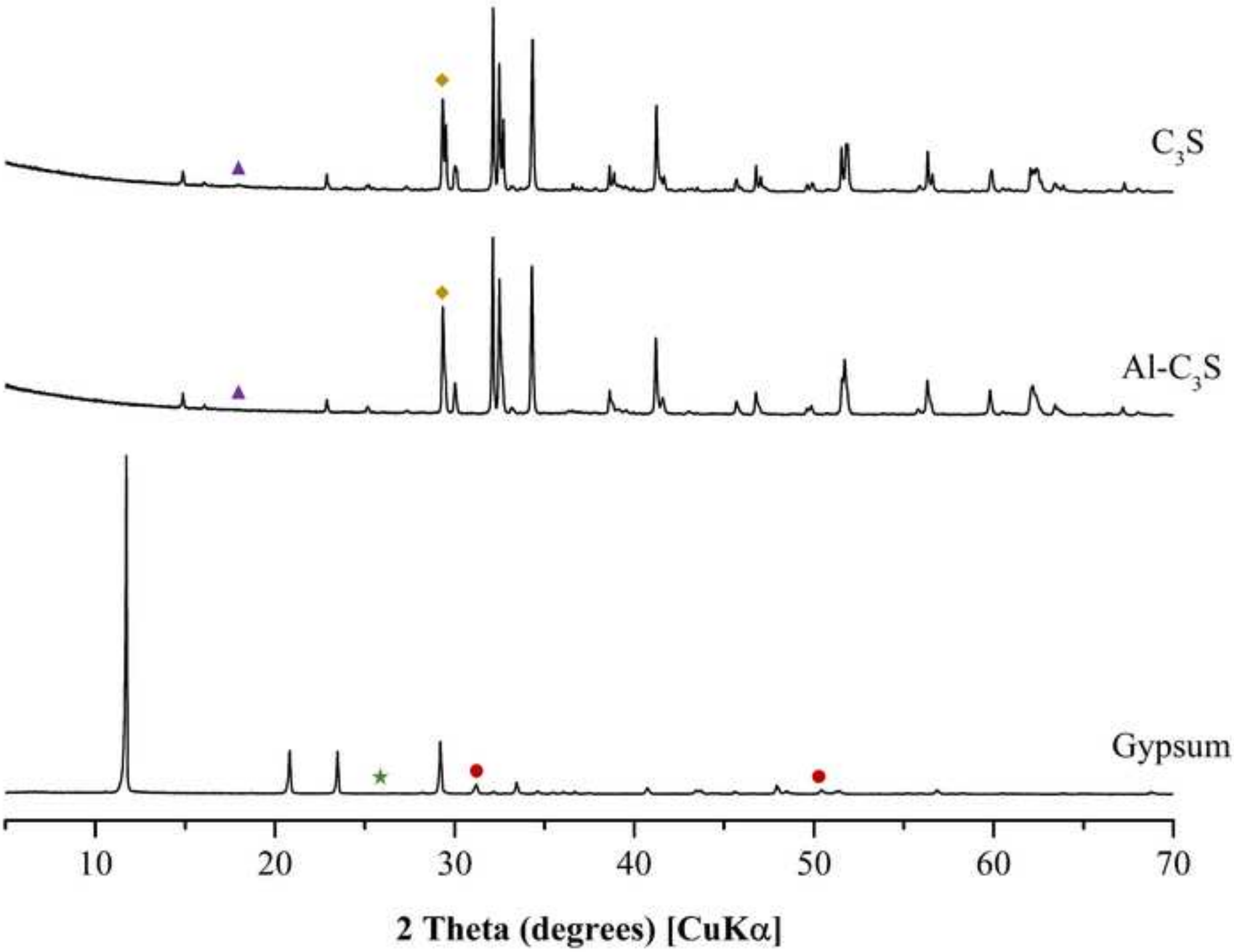

Figure 2

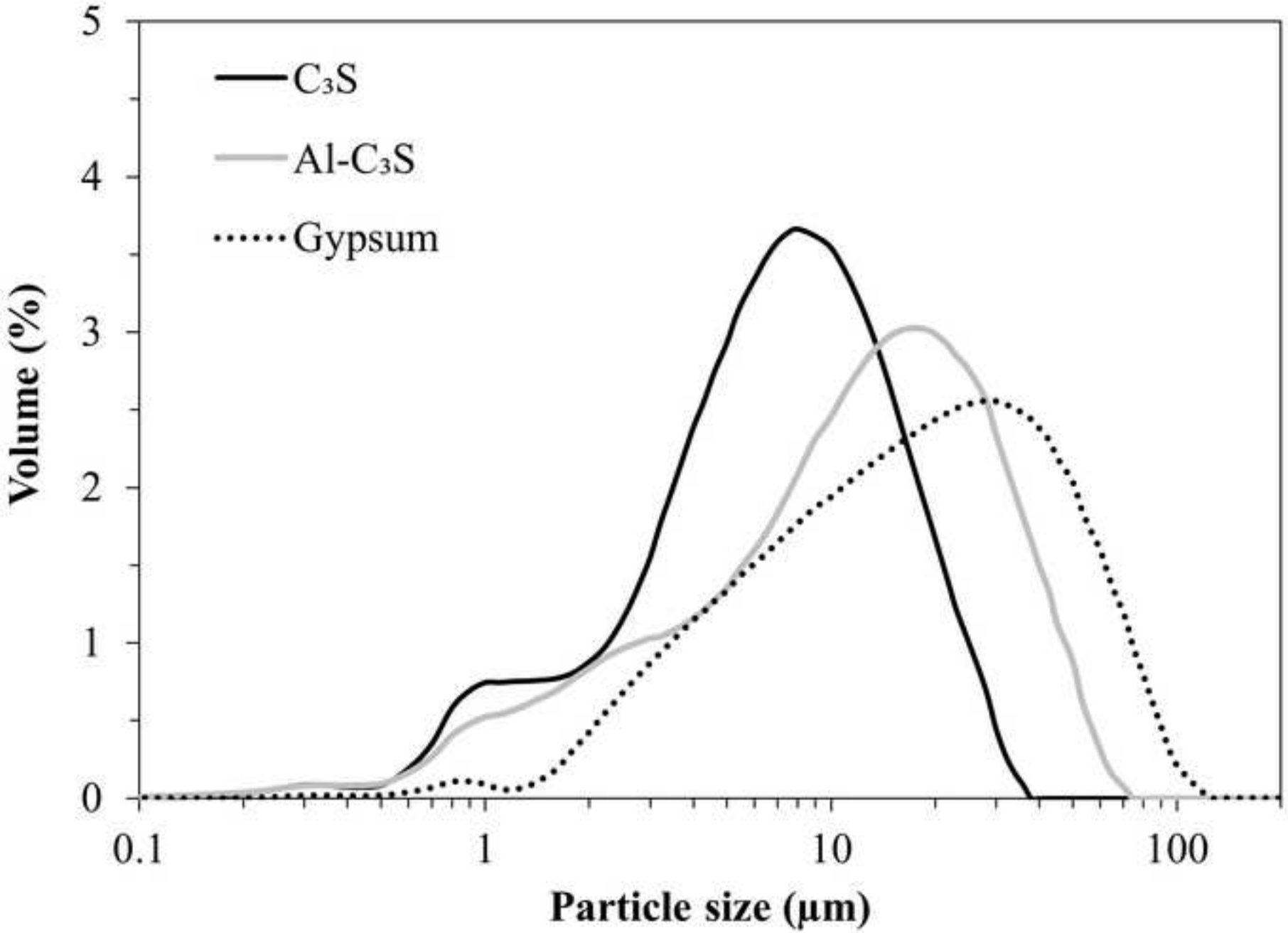

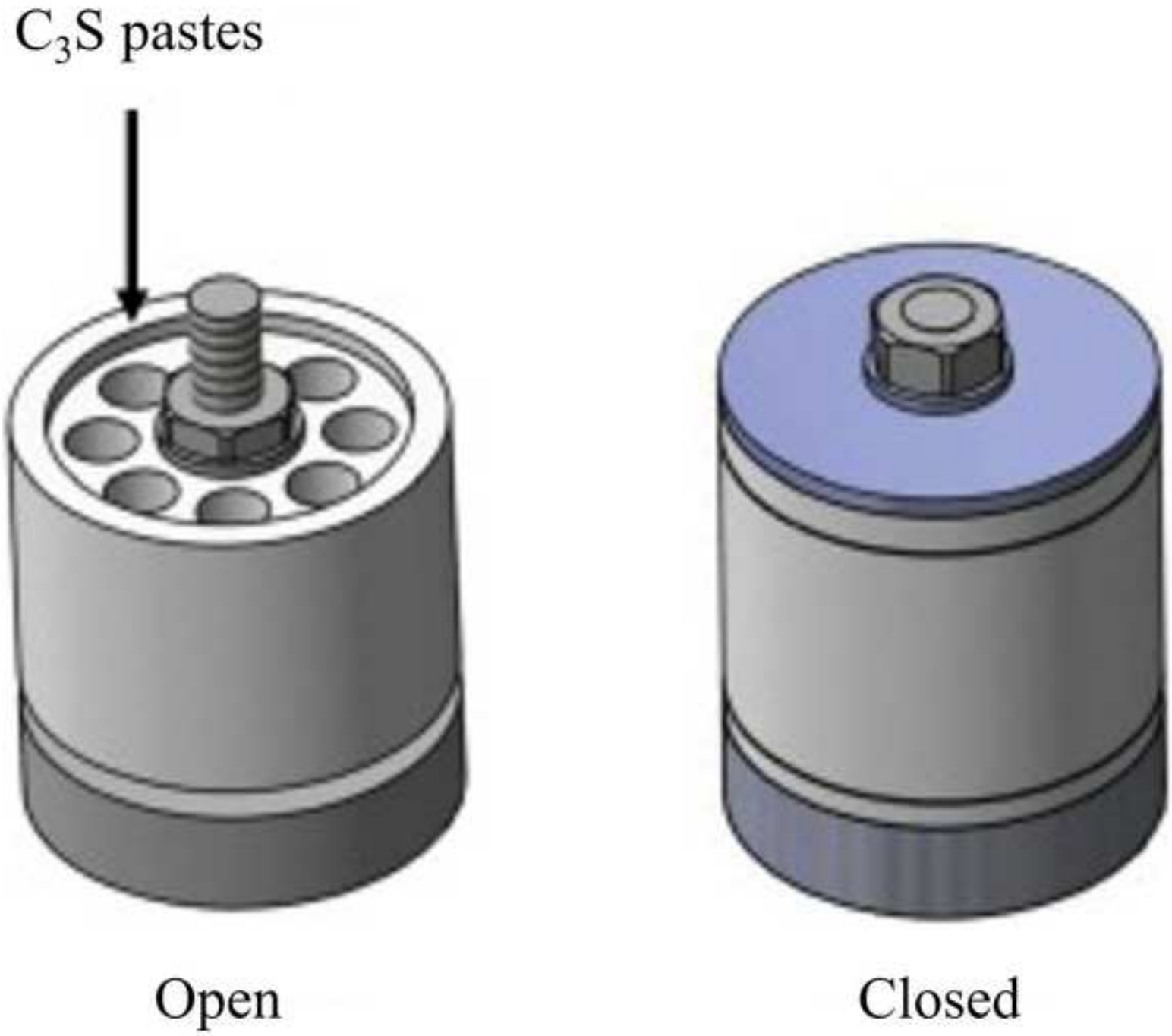

Figure 4A

Click here to access/download;Figure;Figure 4A.jpg

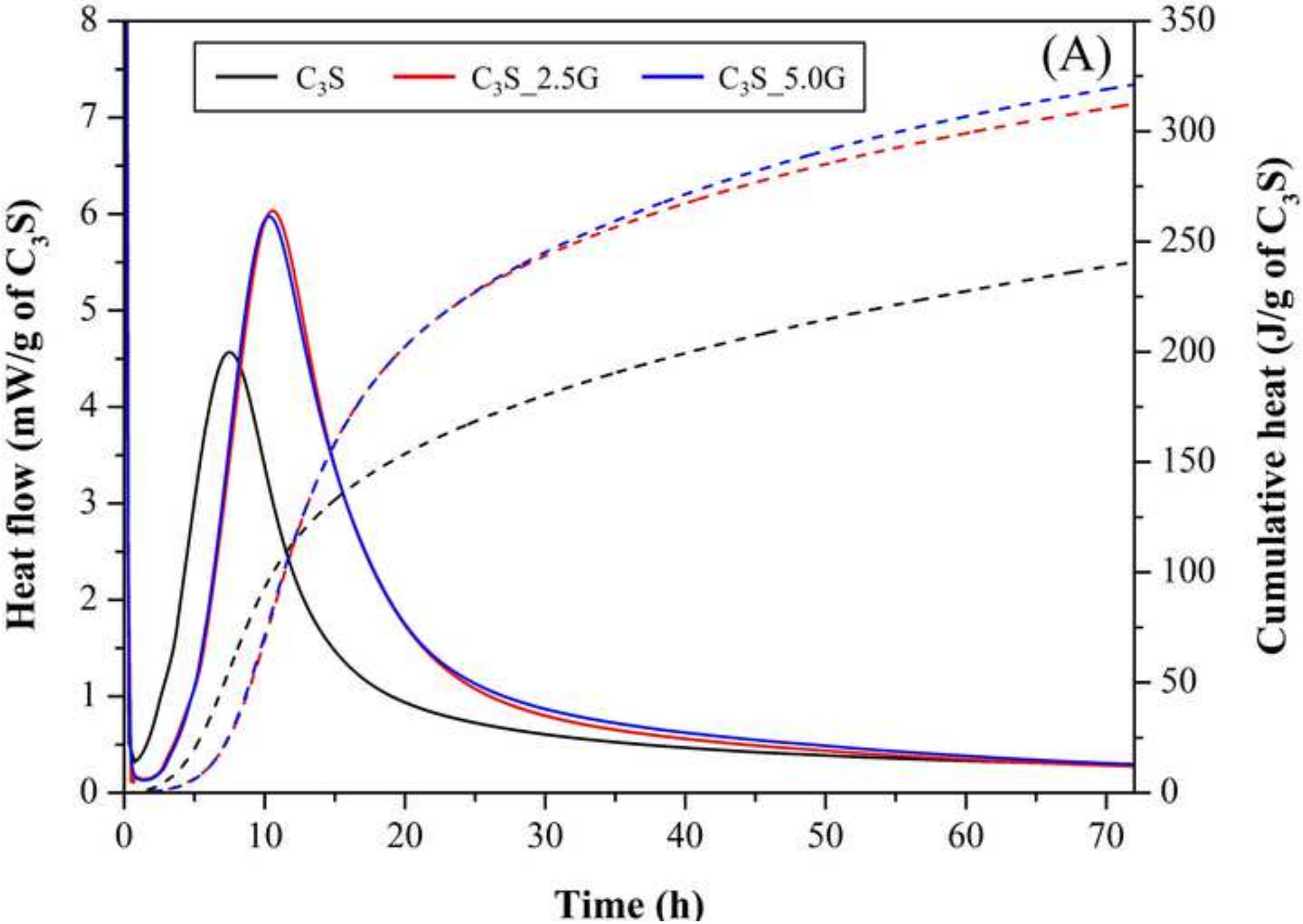

Figure 4B

Click here to access/download;Figure;Figure 4B.jpg

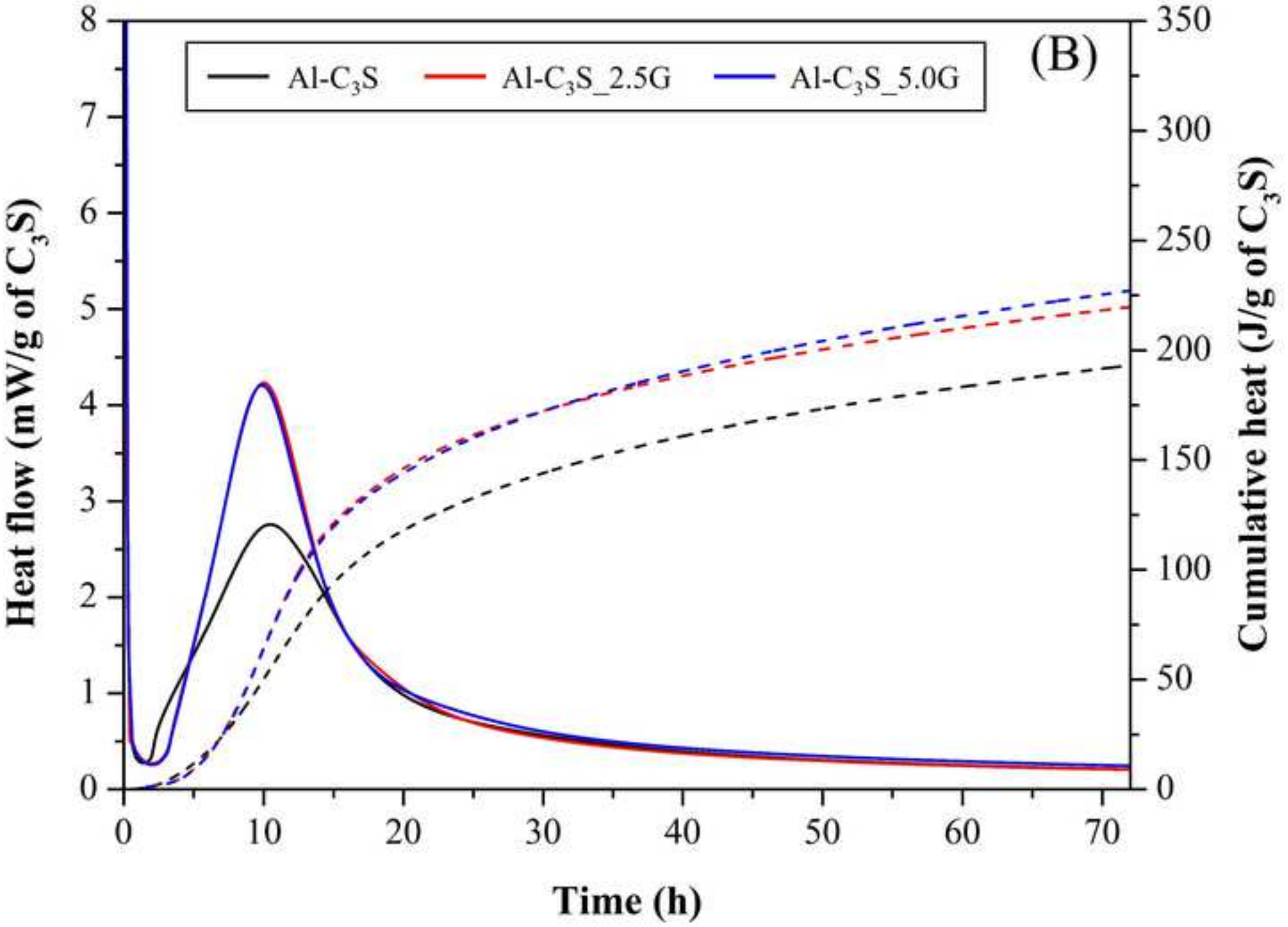

Figure 5A

Click here to access/download;Figure;Figure 5A.jpg

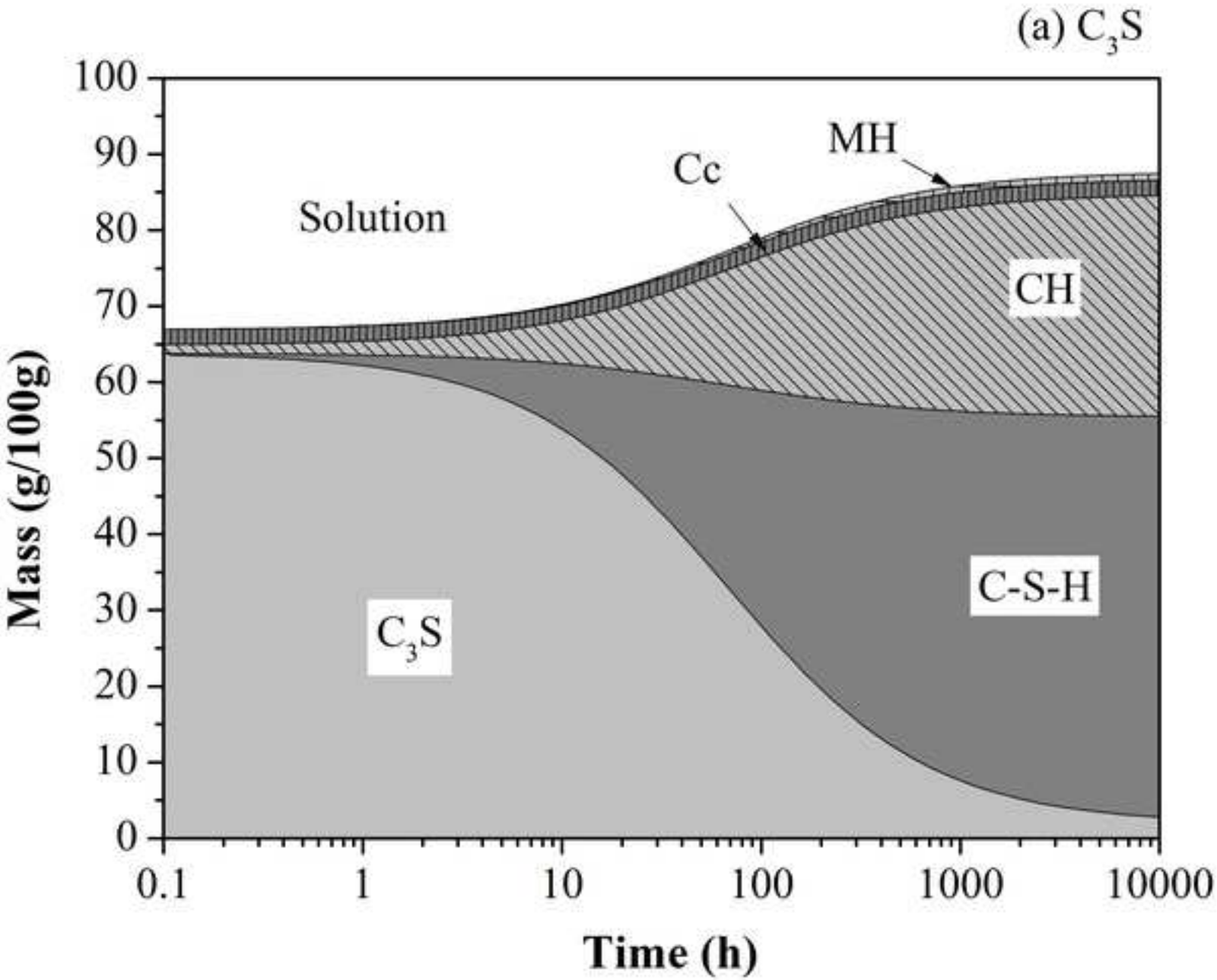

Figure 5B

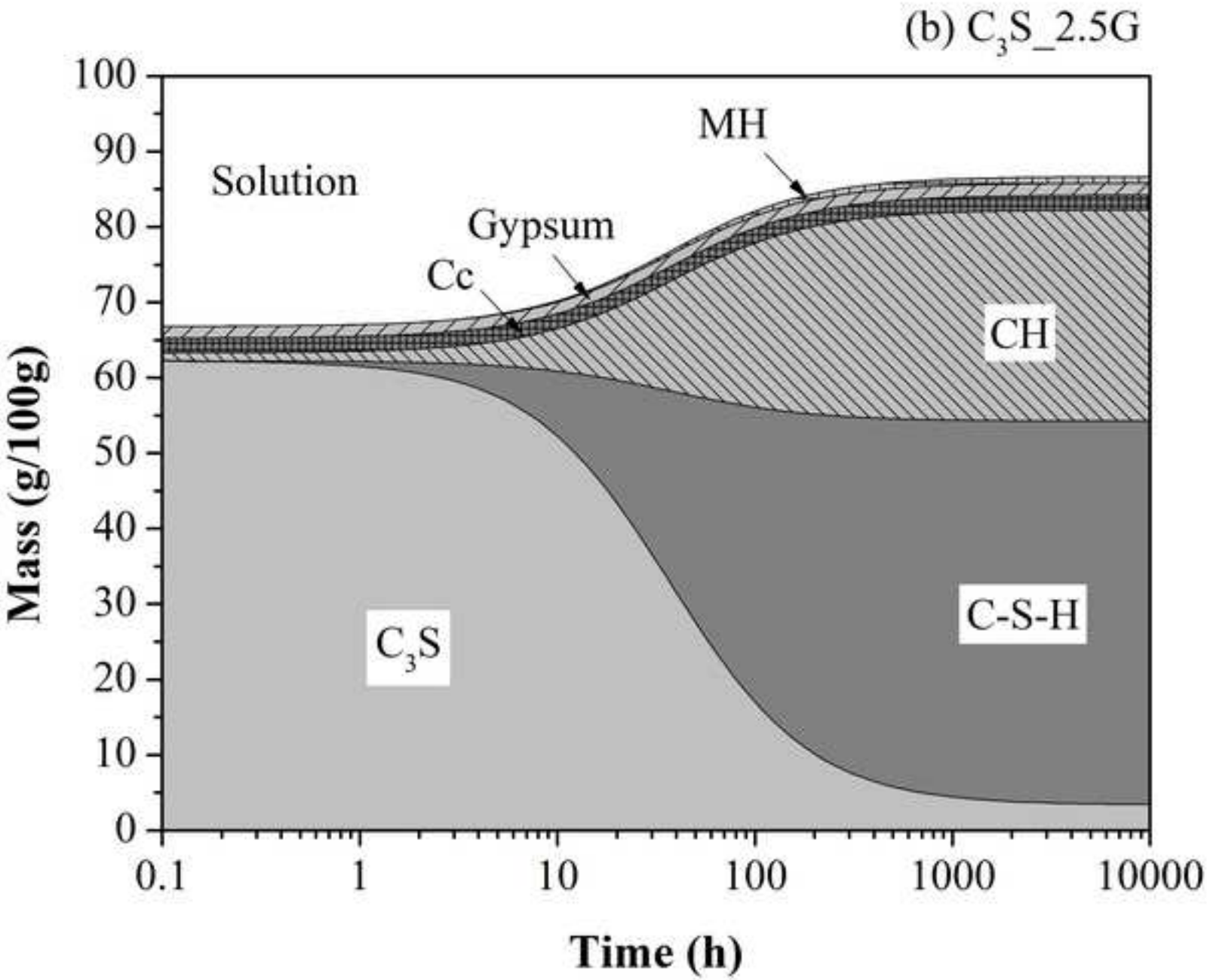

Figure 5C

Click here to access/download;Figure;Figure 5C.jpg

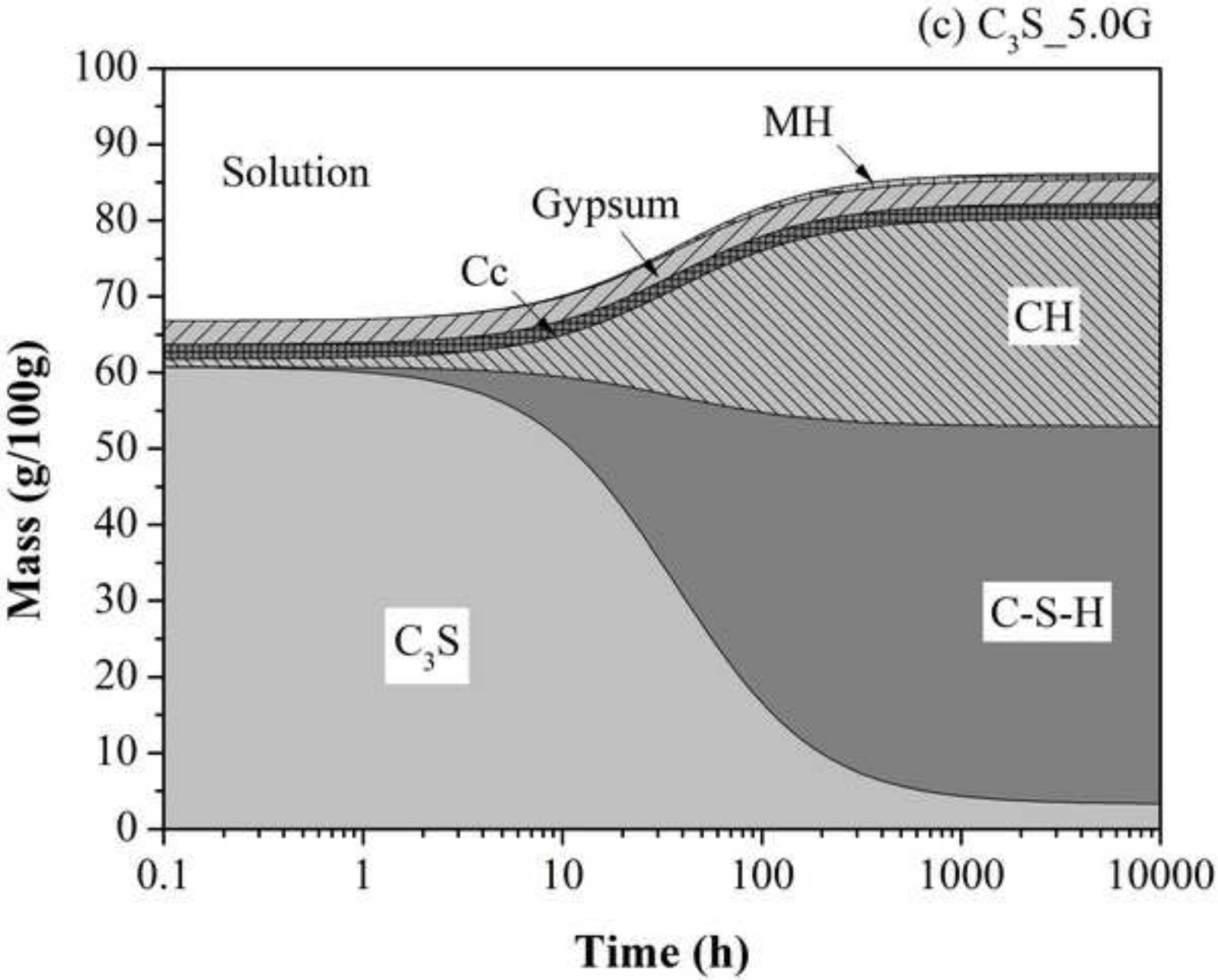

Figure 5D

Click here to access/download;Figure;Figure 5D.jpg

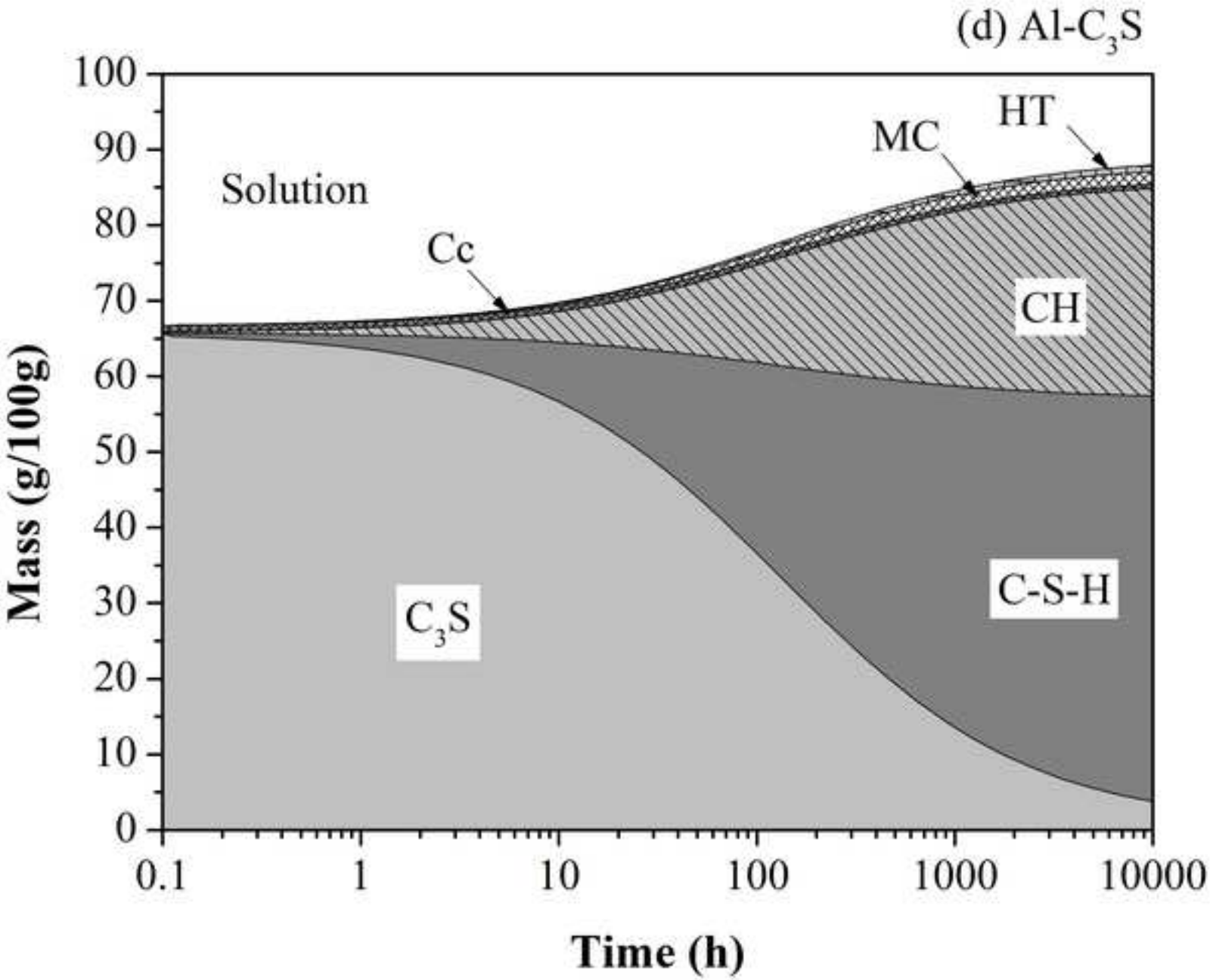

Figure 5E

Click here to access/download;Figure;Figure 5E.jpg

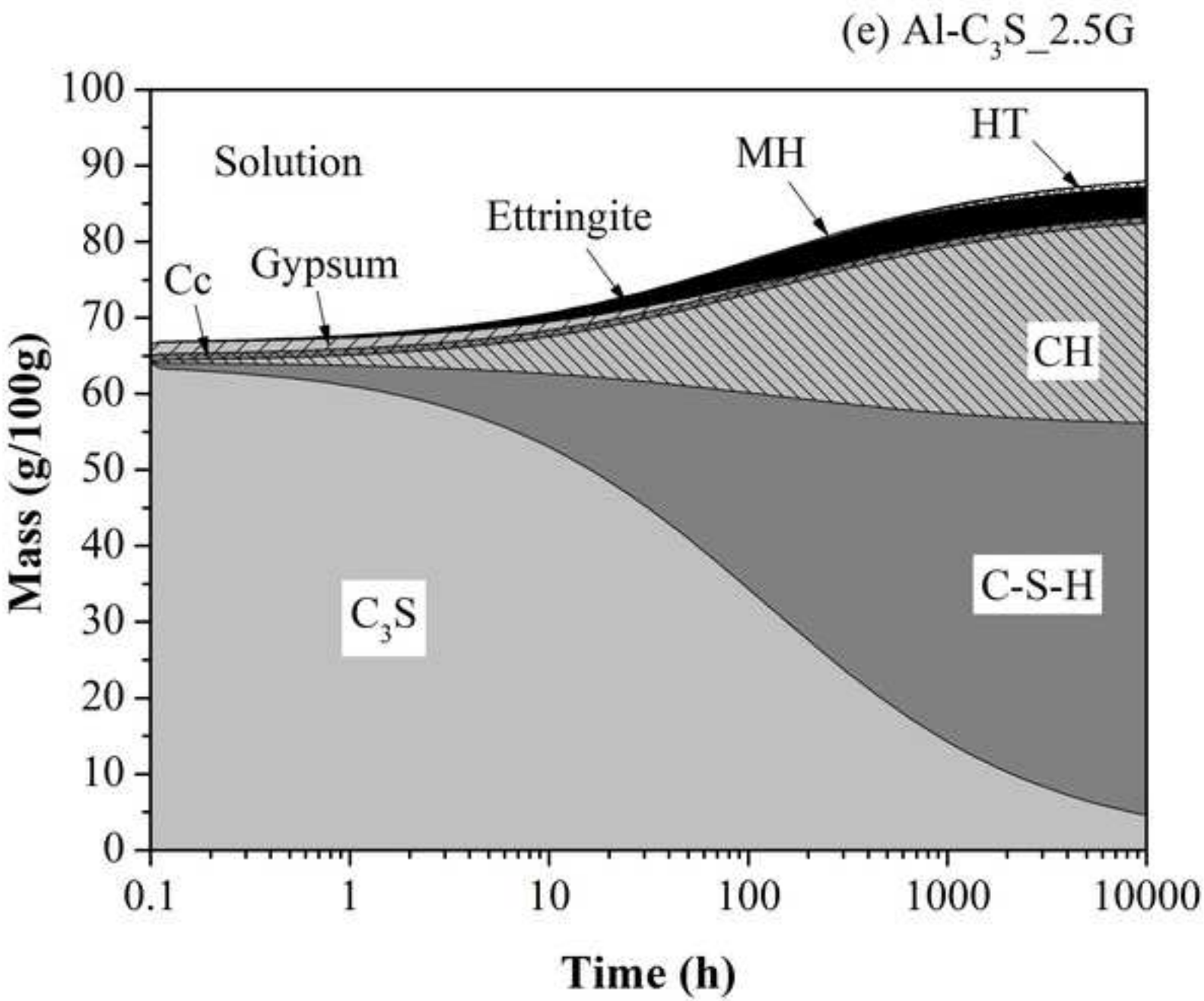

Figure 5F

Click here to access/download;Figure;Figure 5F.jpg

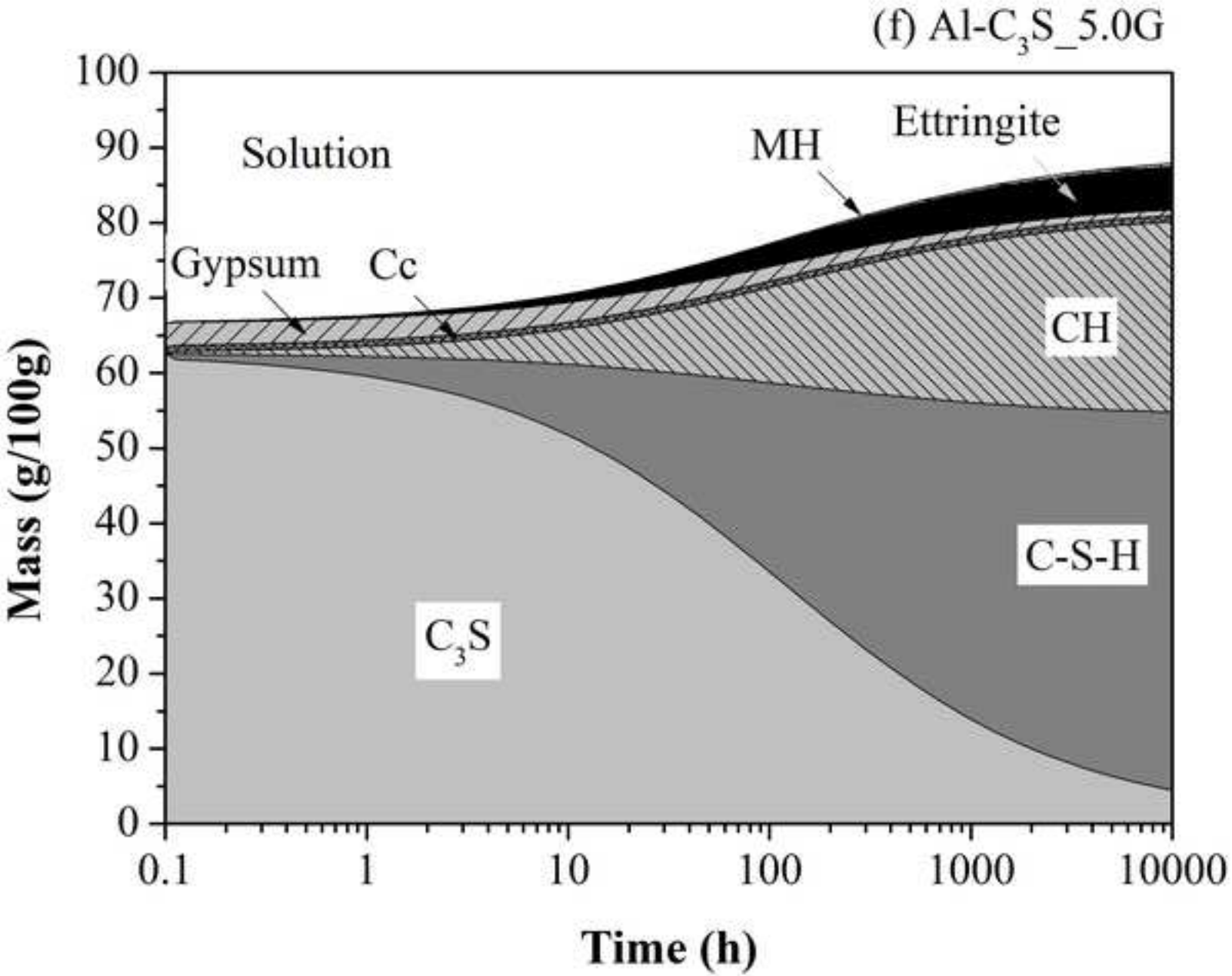

Figure 6A

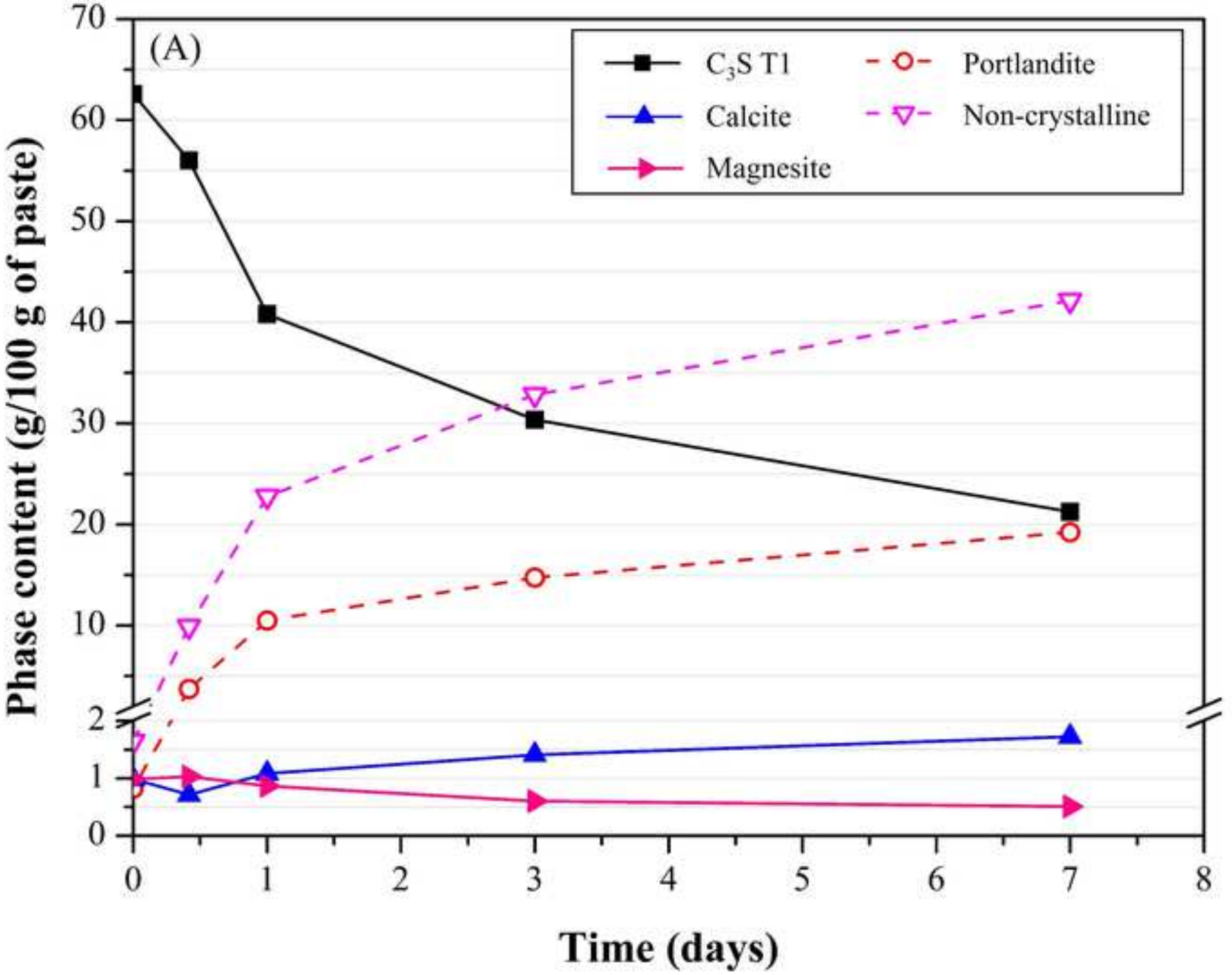

Figure 6B

Click here to access/download;Figure;Figure 6B.jpg

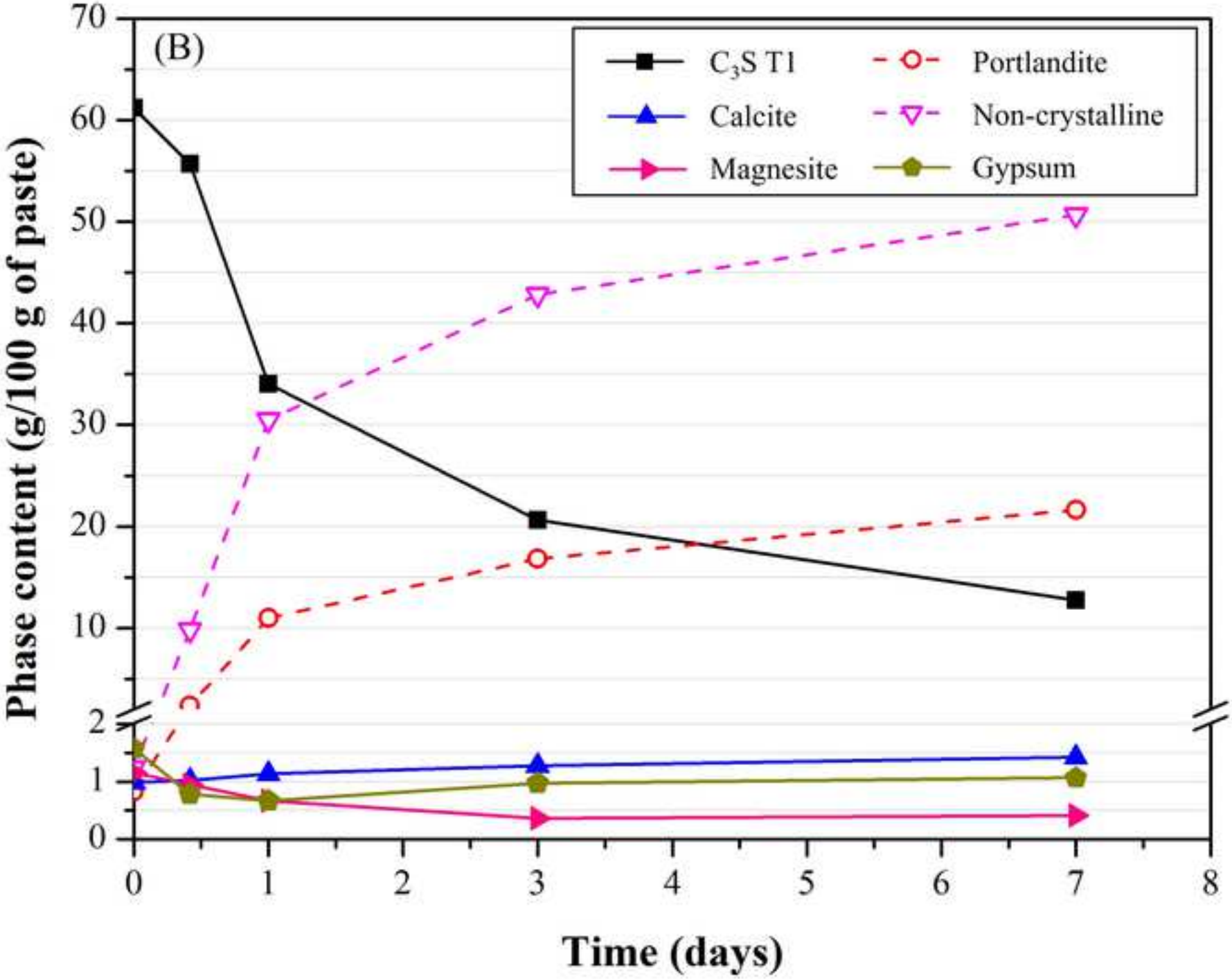

Figure 6C

Click here to access/download;Figure;Figure 6C.jpg

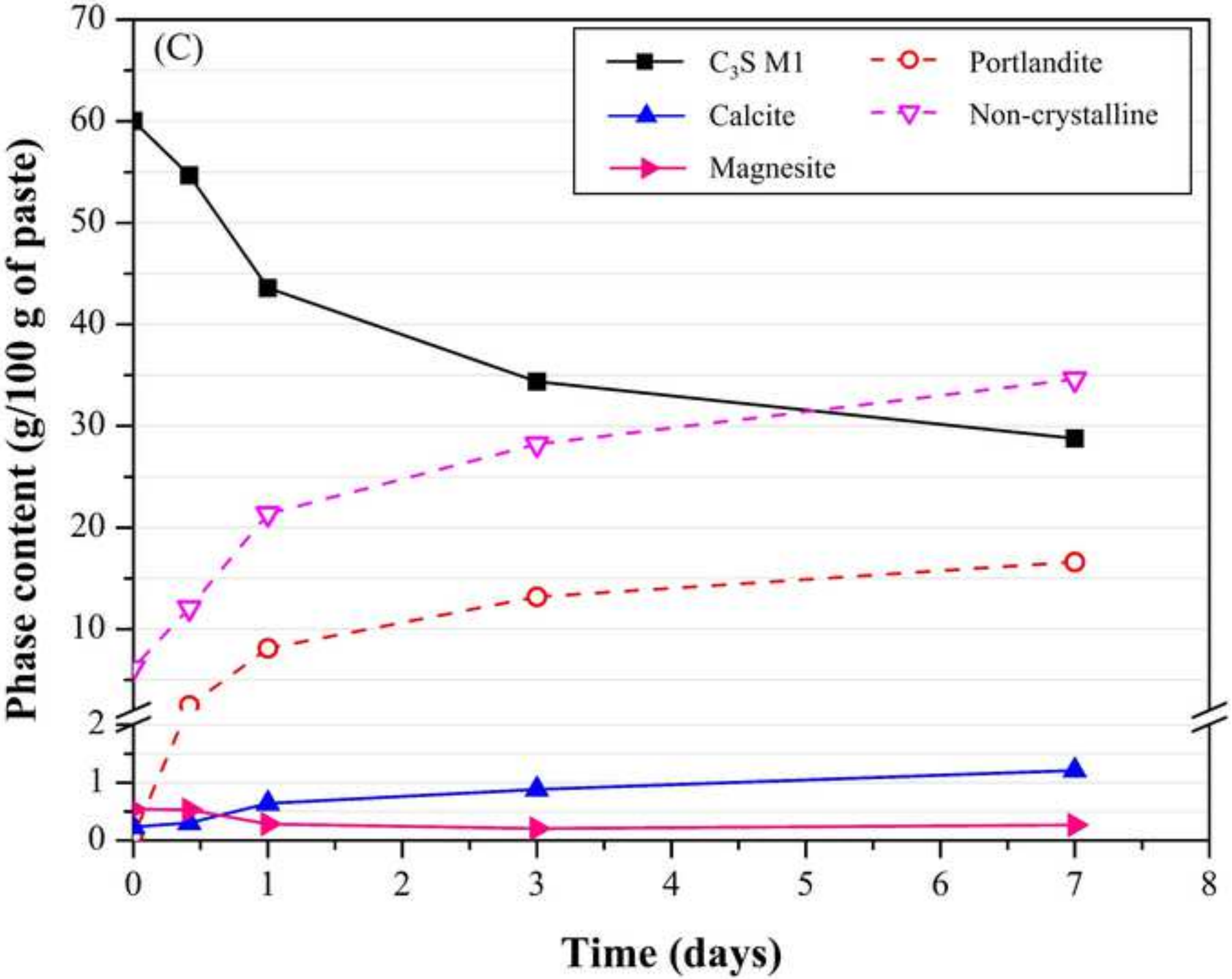

Figure 6D

Click here to access/download;Figure;Figure 6D.jpg

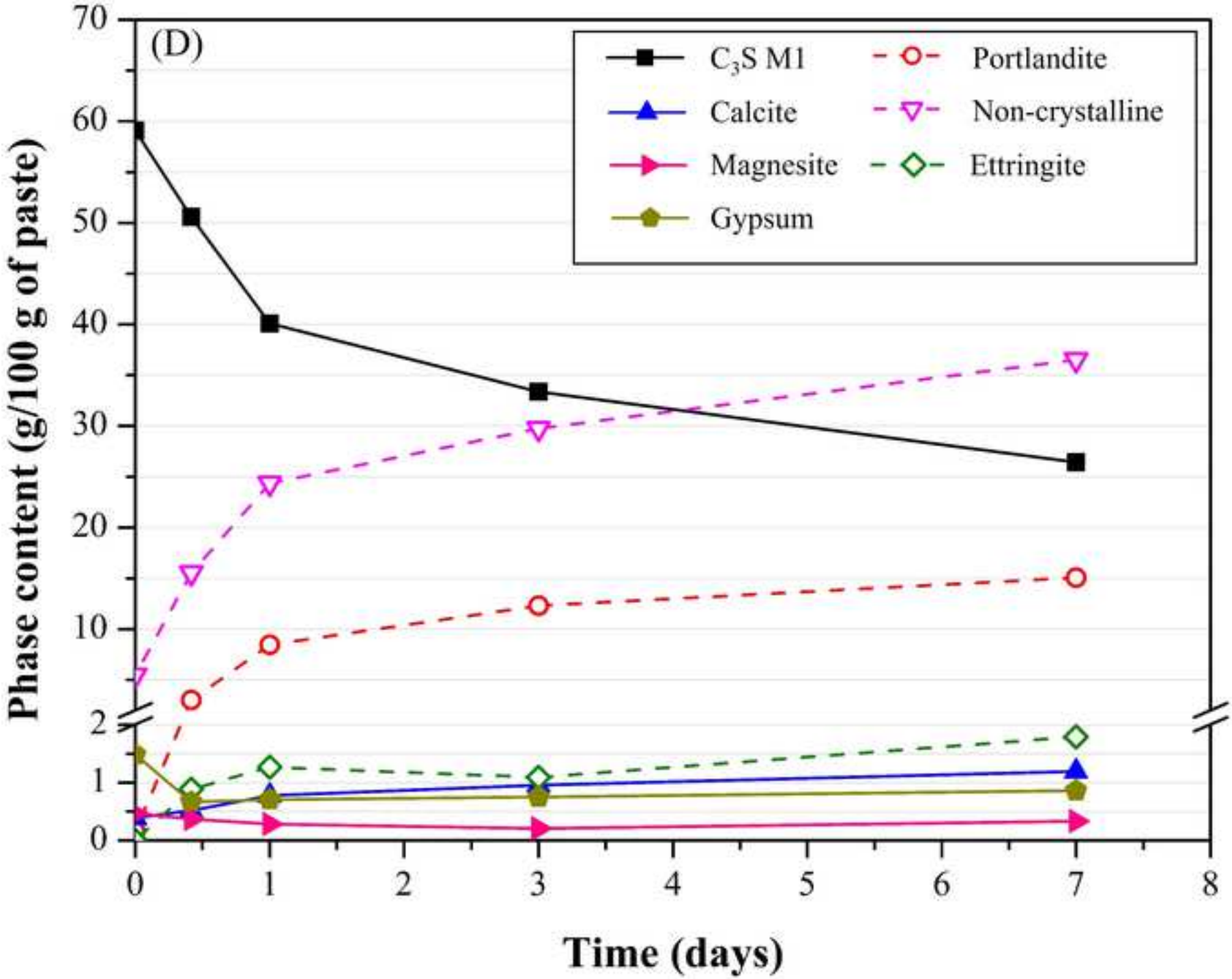

Figure 7

Click here to access/download;Figure;Figure 7.jpg

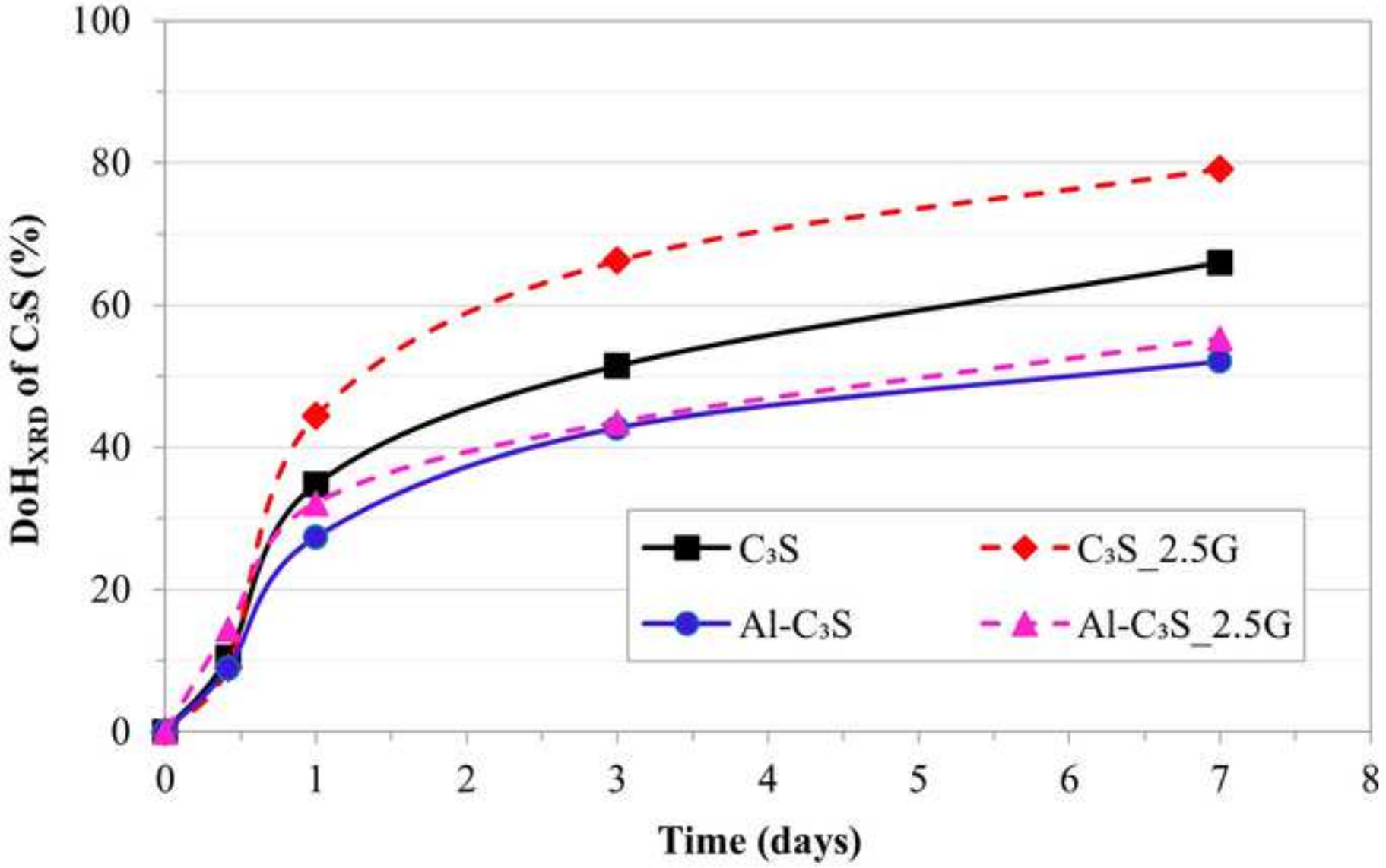

Figure 8A

Click here to access/download;Figure;Figure 8A.jpg

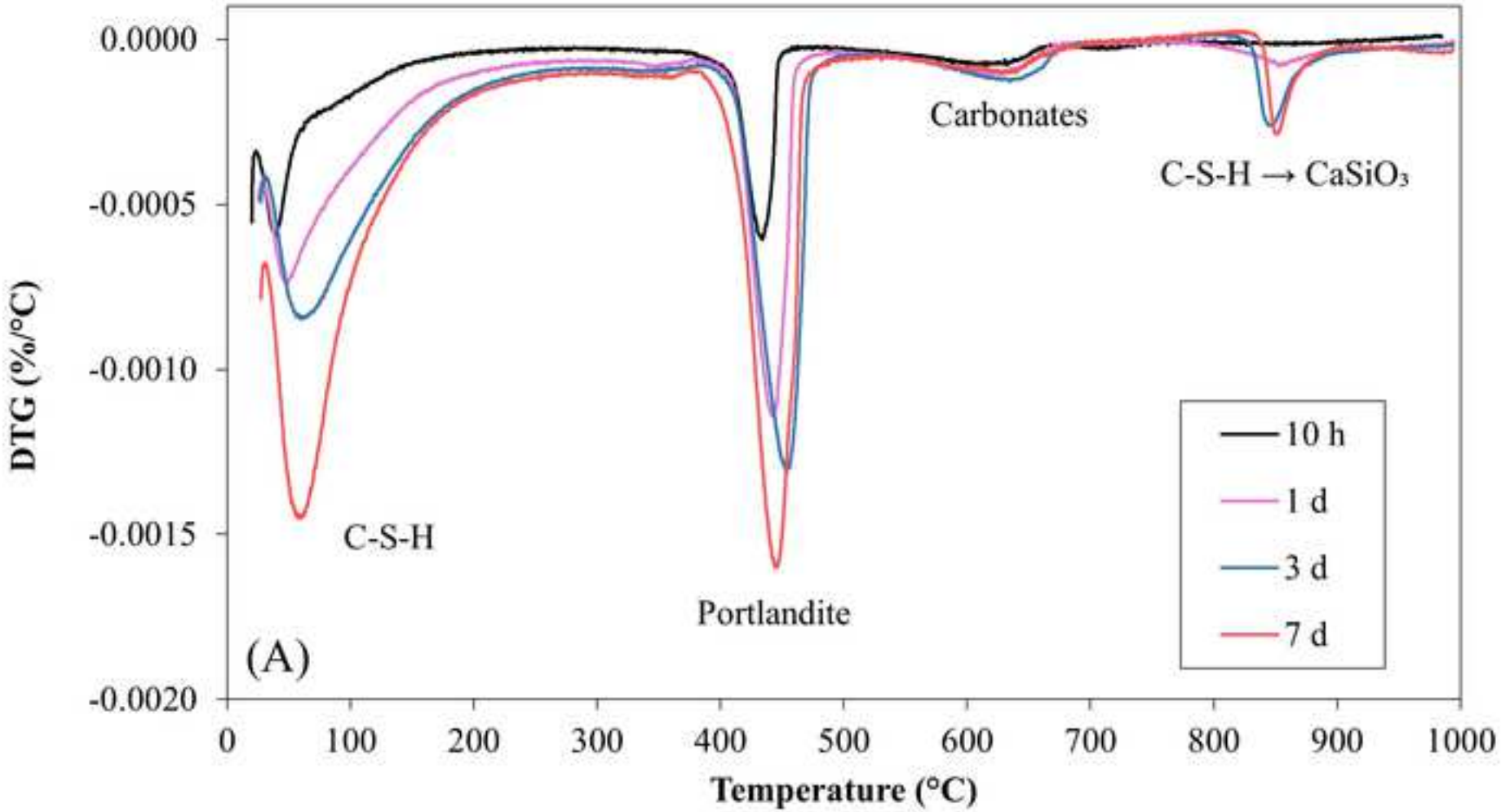

Figure 8B

Click here to access/download;Figure;Figure 8B.jpg

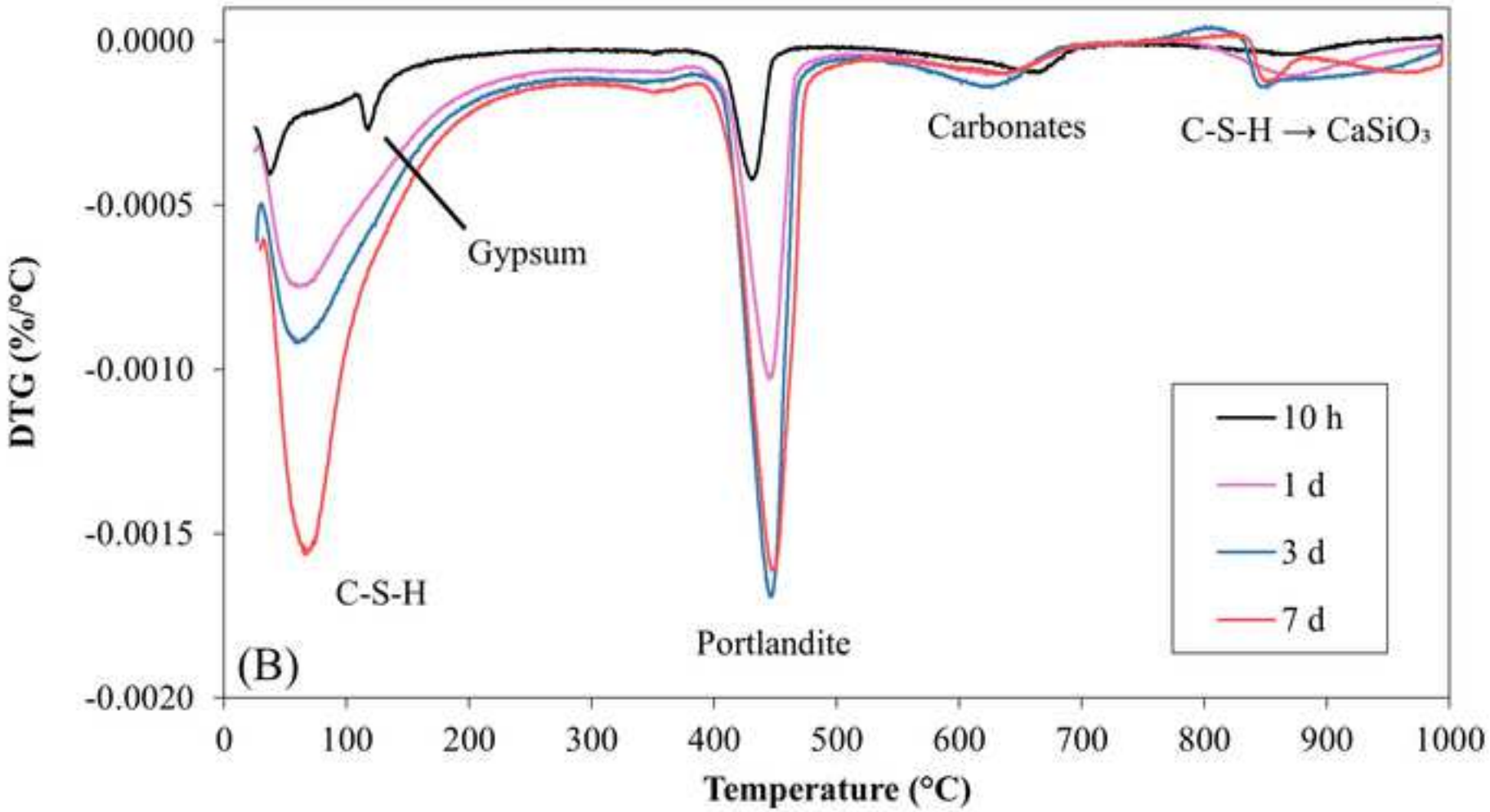

Figure 8C

Click here to access/download;Figure;Figure 8C.jpg

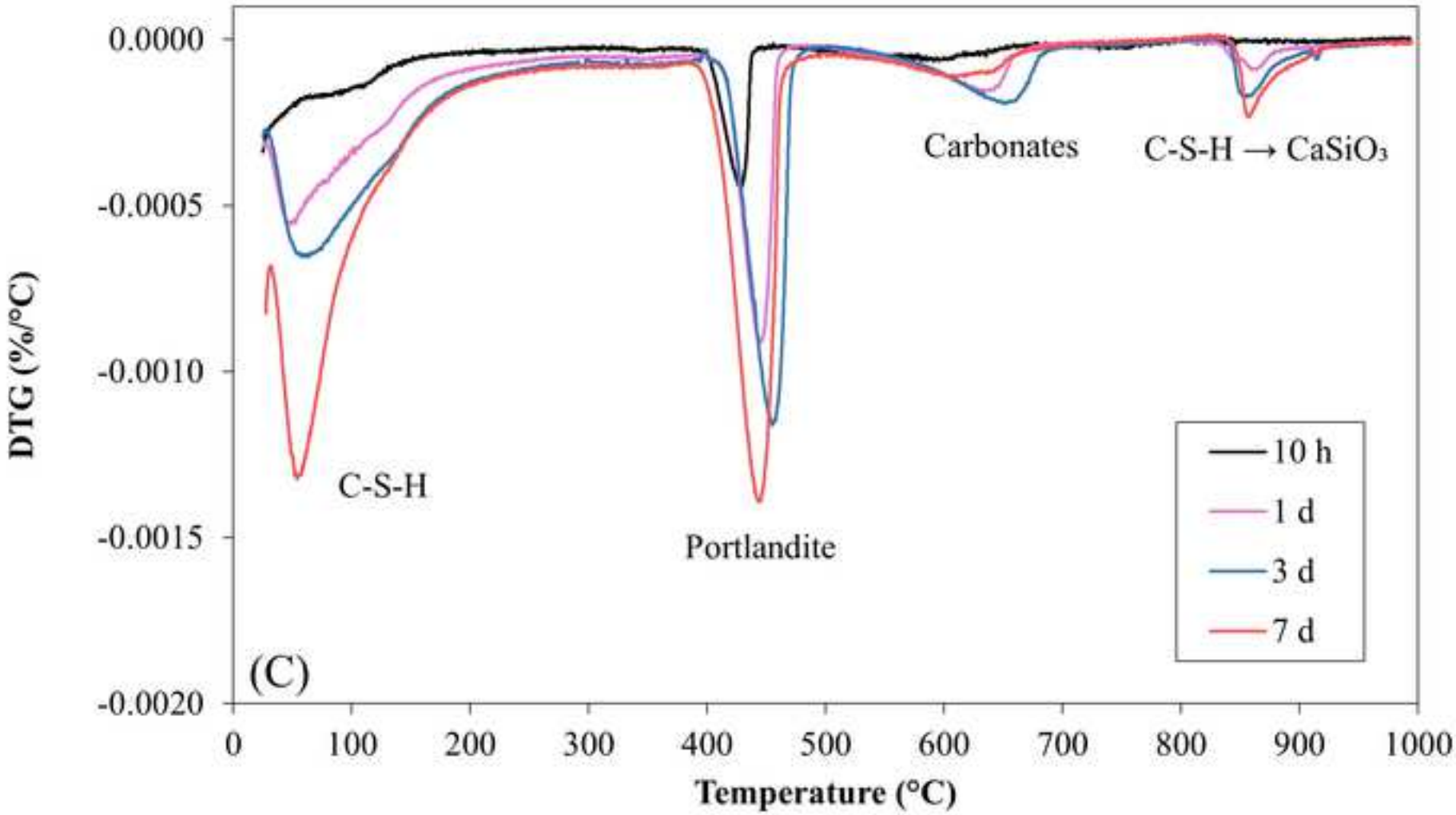

Figure 8D

Click here to access/download;Figure;Figure 8D.jpg

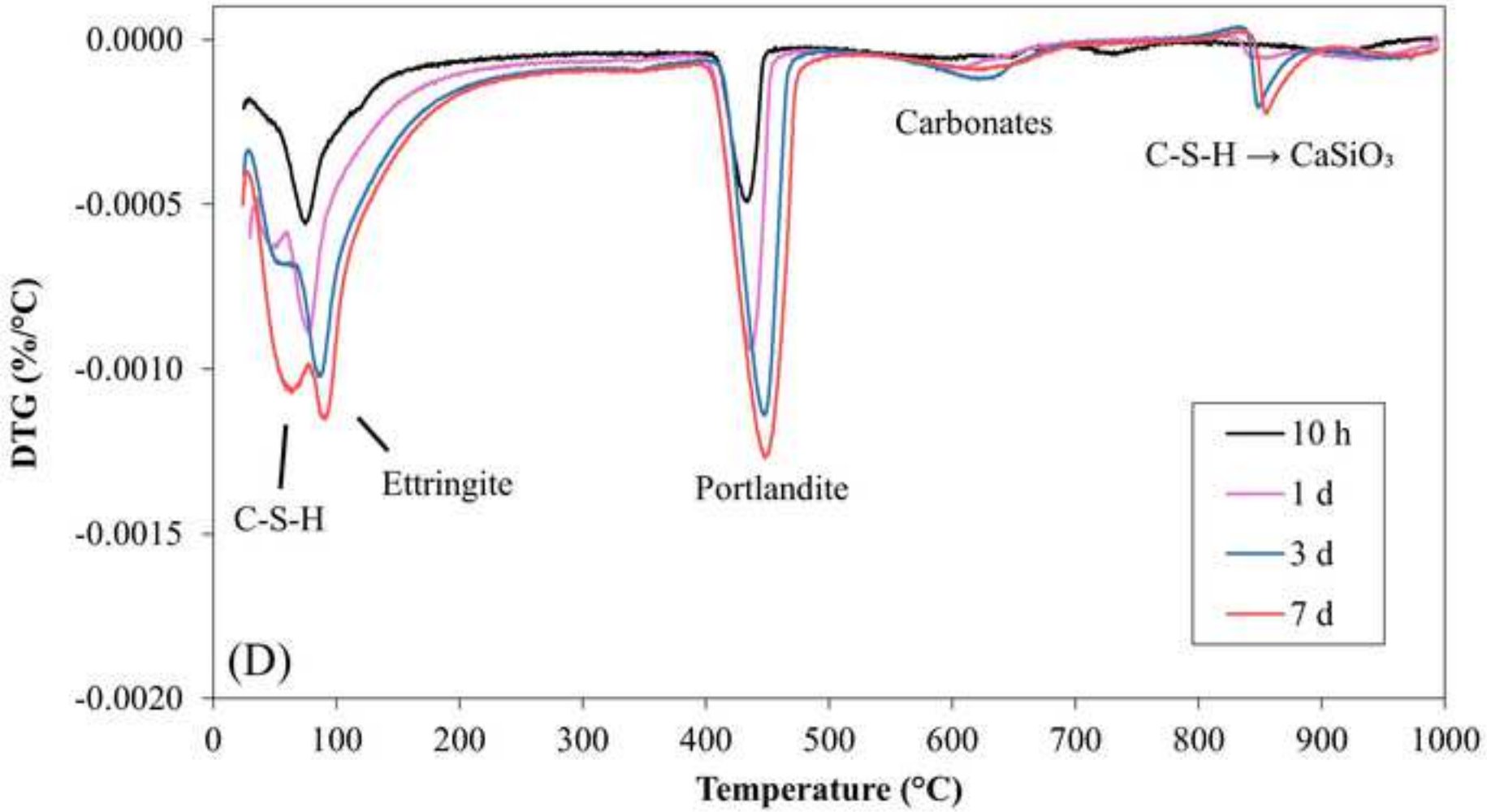

Figure 9

Click here to access/download;Figure;Figure 9.jpg

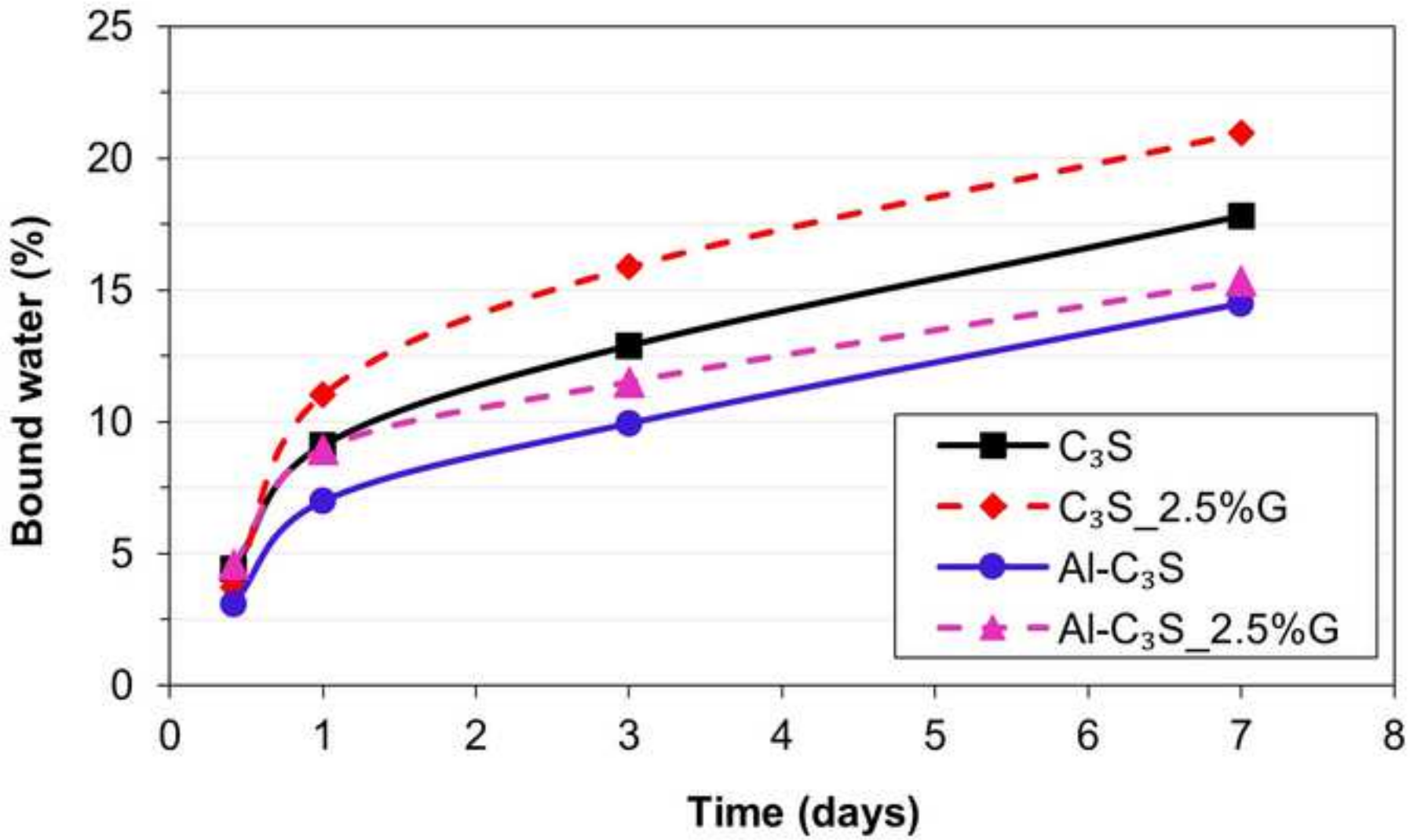

Figure 10

Click here to access/download;Figure;Figure 10.jpg

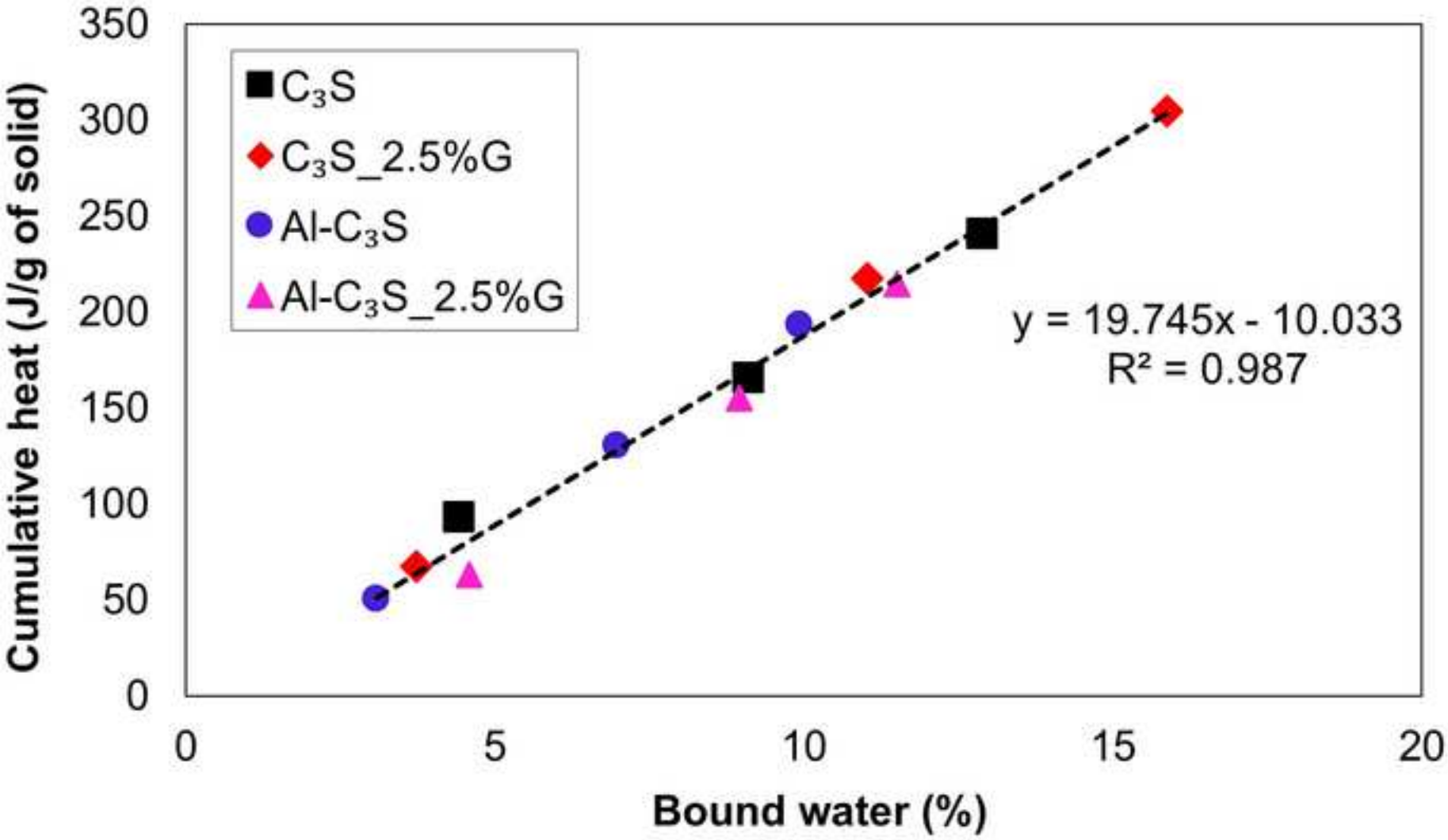

Figure 11

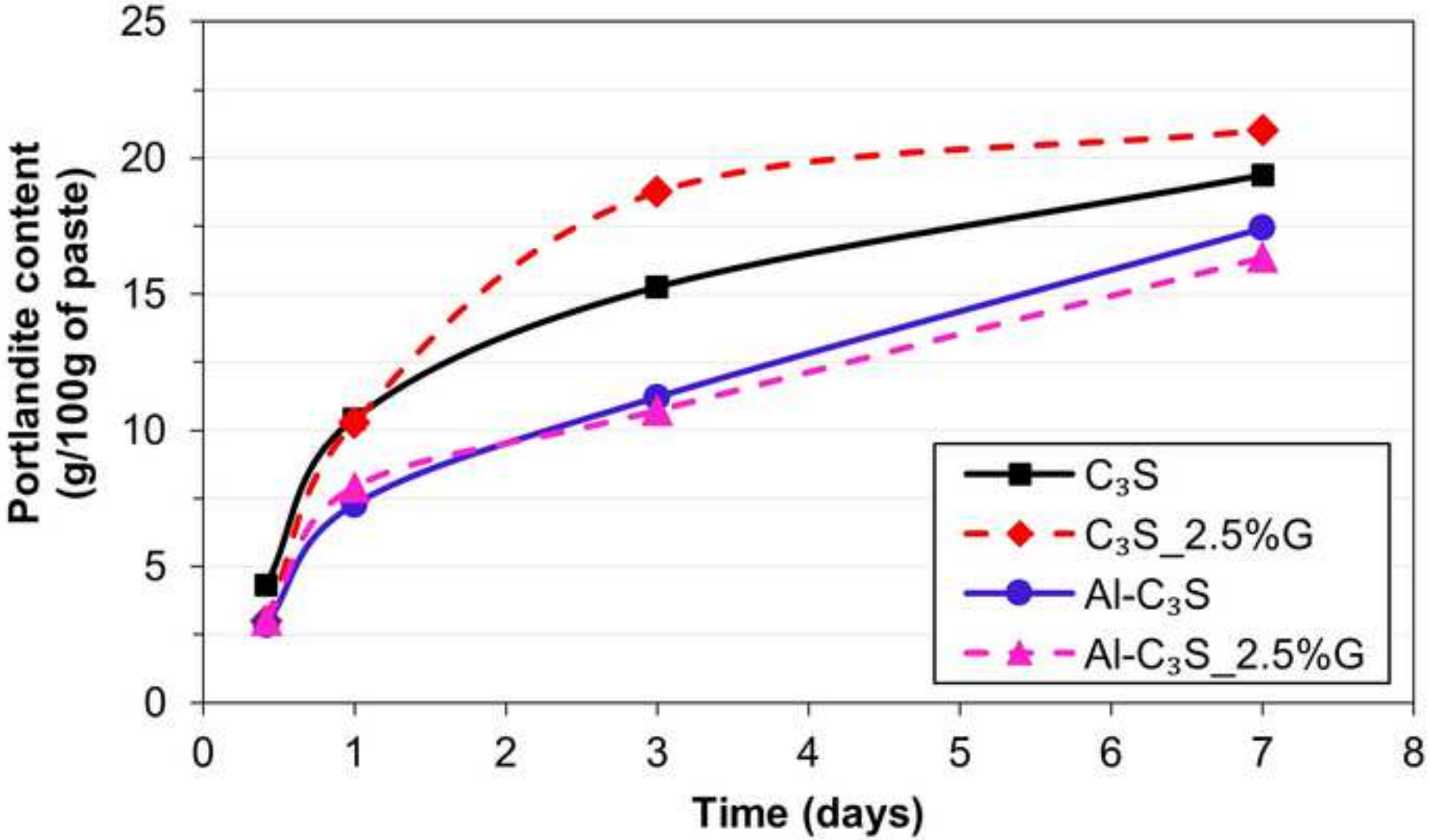

Figure 12

Click here to access/download;Figure;Figure 12.jpg

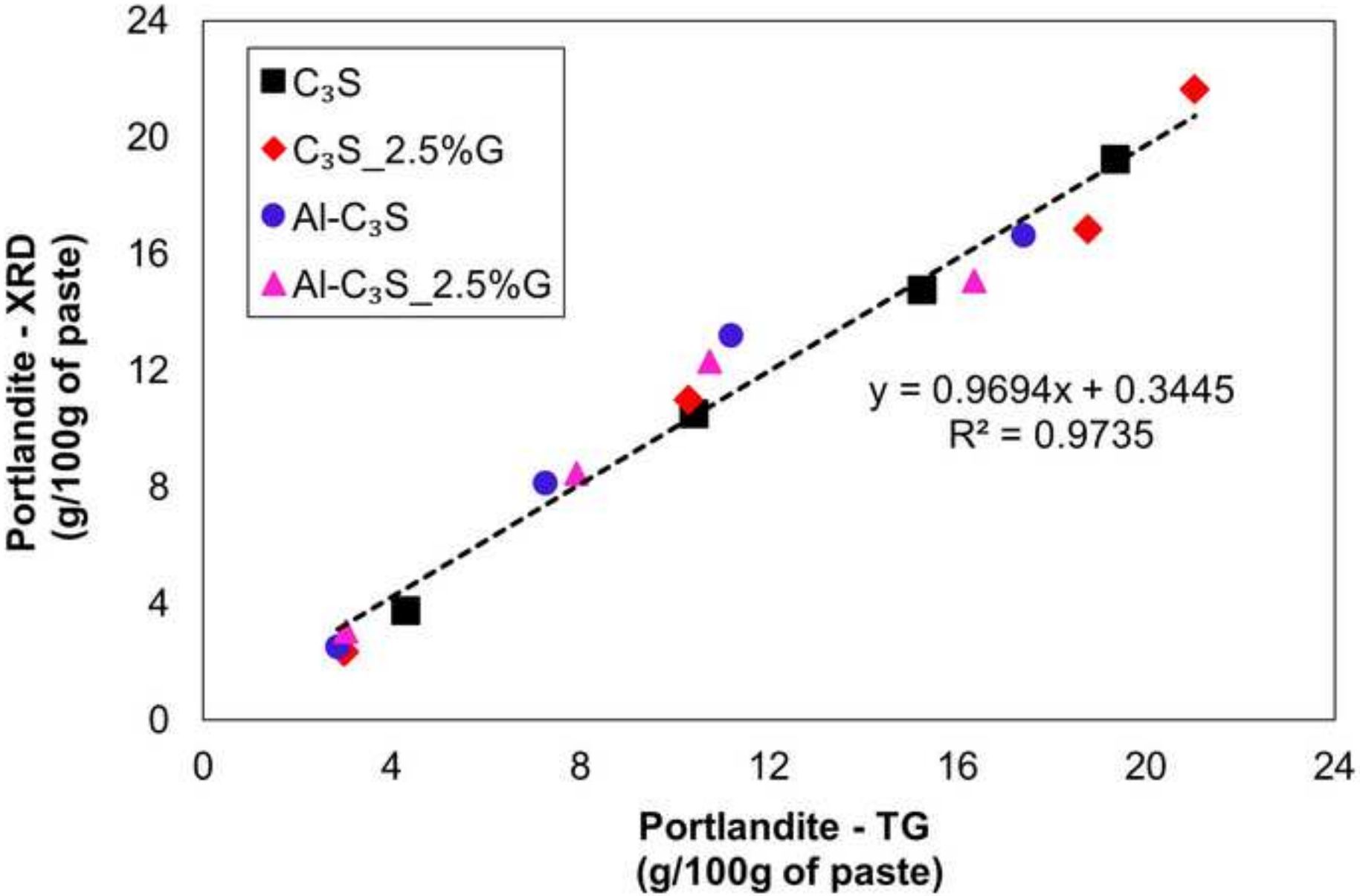

Figure 13

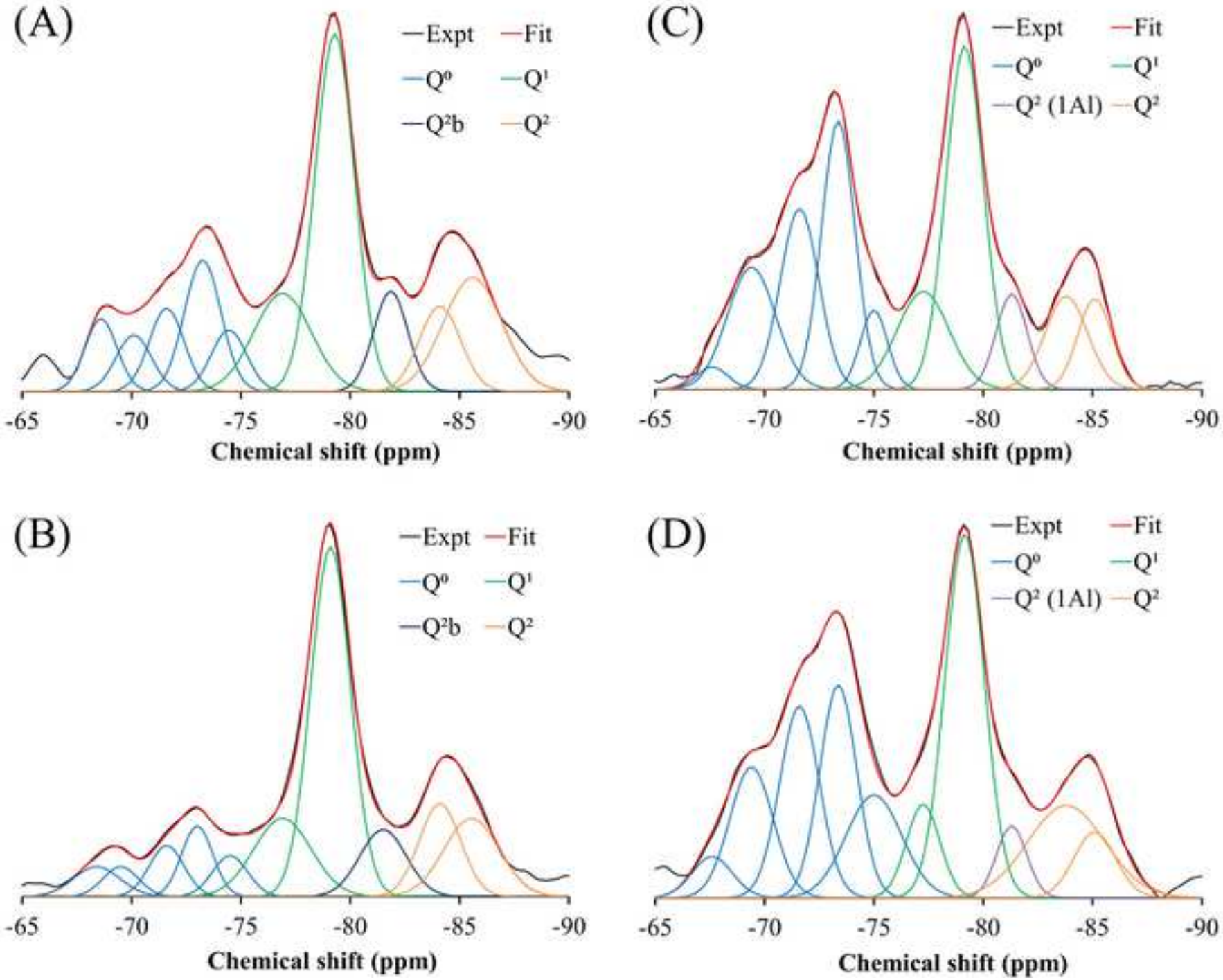

Figure 14

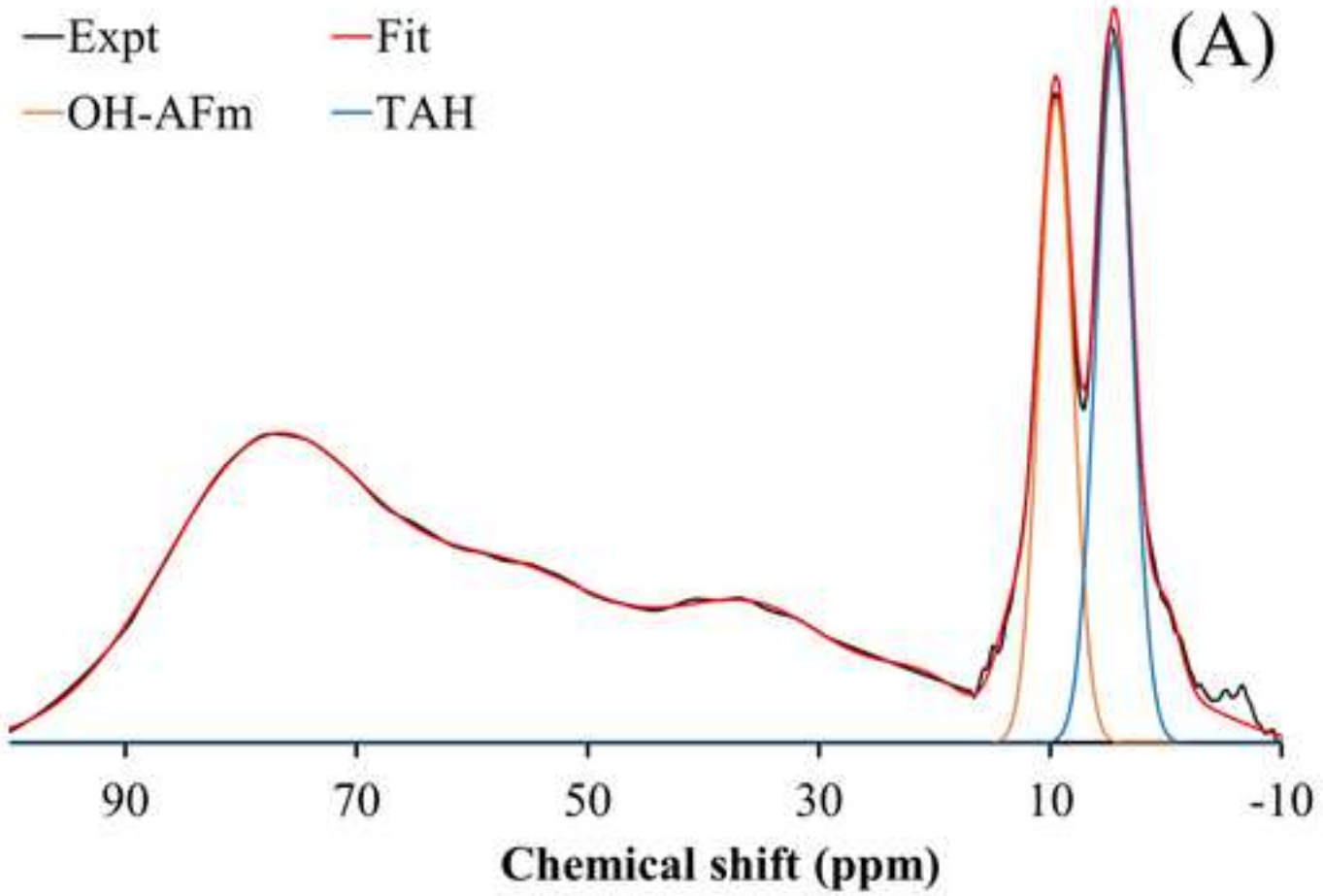

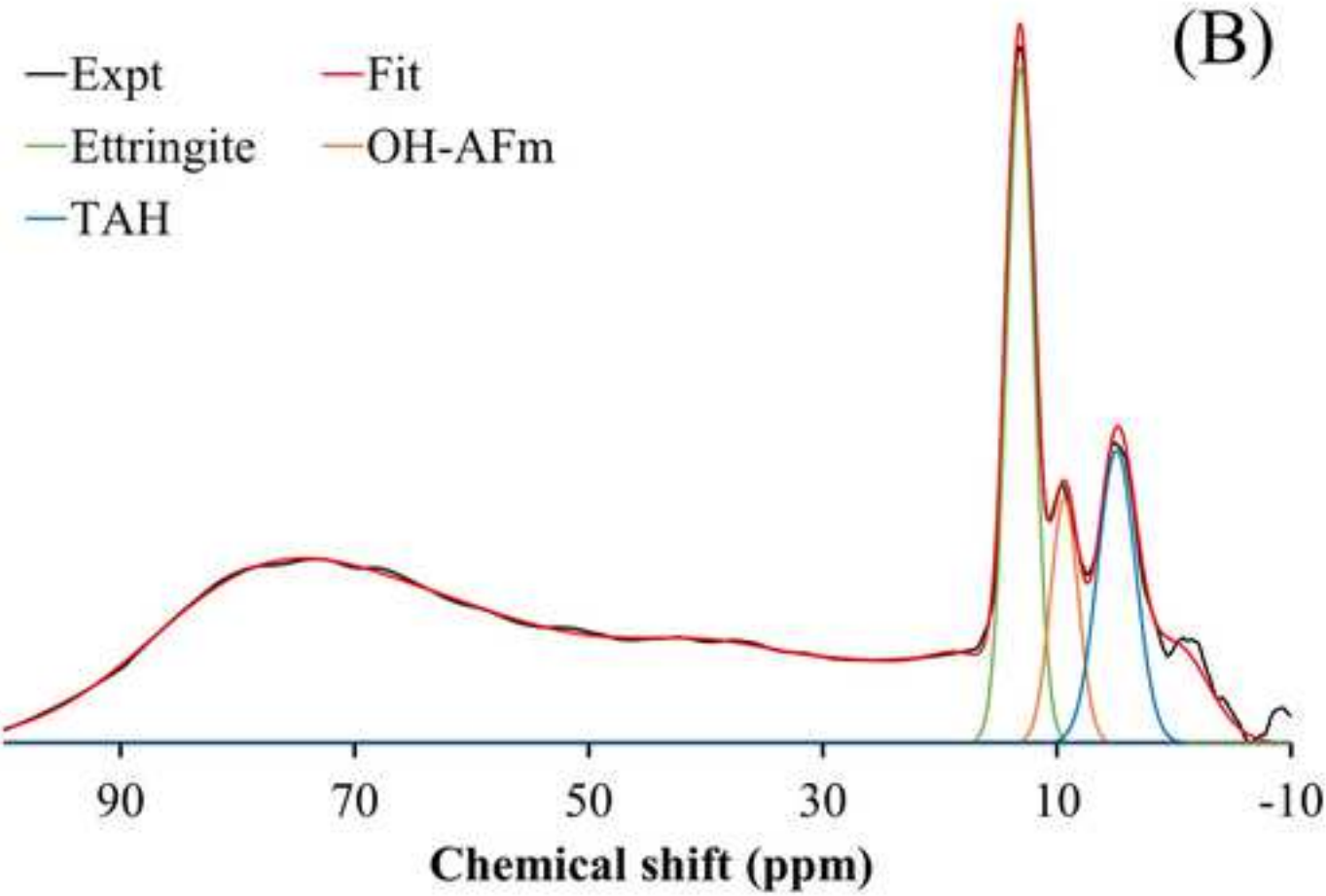

Figure 15

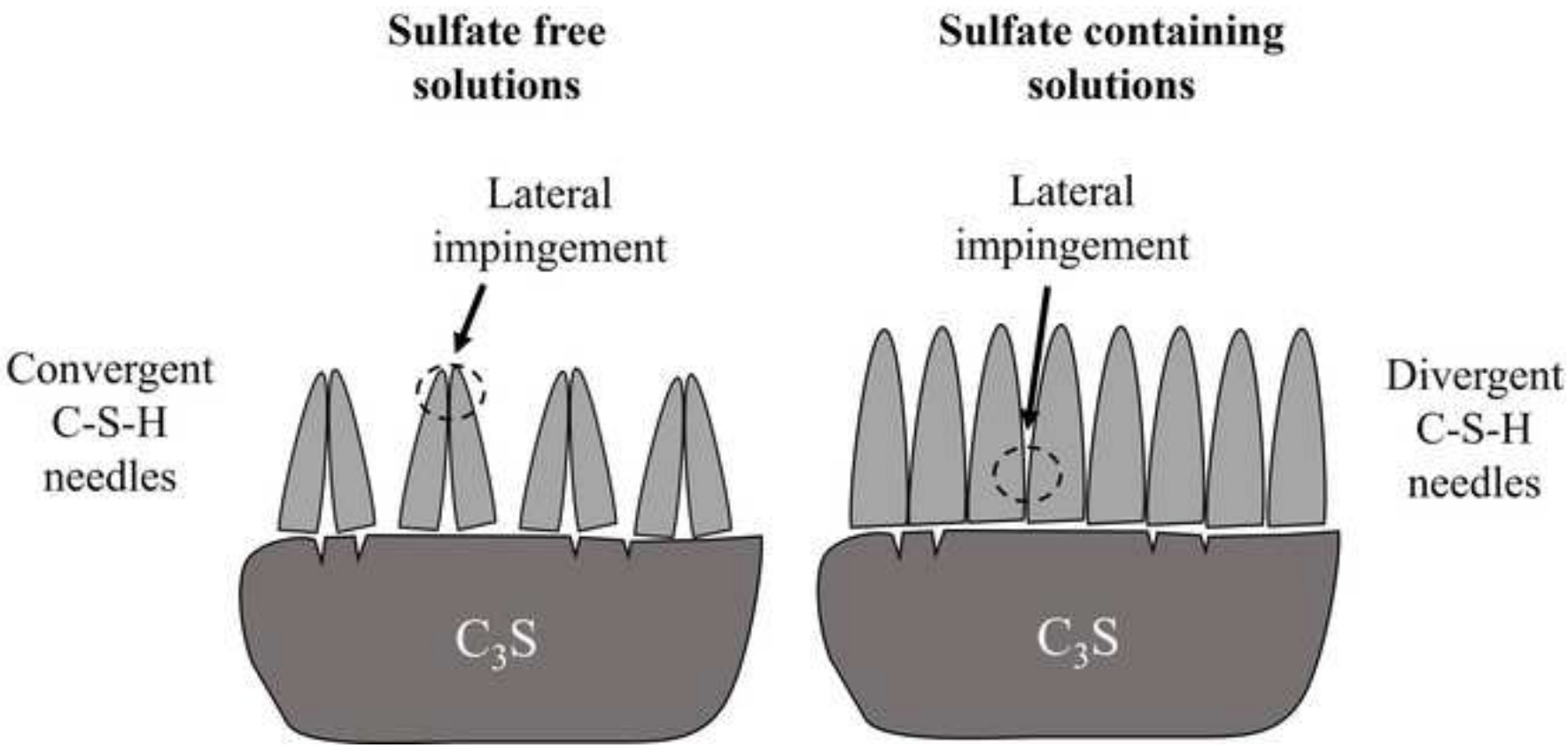

Declaration of interests

☒ The authors declare that they have no known competing financial interests or personal relationships that could have appeared to influence the work reported in this paper.

☐The authors declare the following financial interests/personal relationships which may be considered as potential competing interests:

J.S. Andrade Neto: Experimental and Formal analysis, Conceptualization, Investigation, Writing - original draft, review & editing. **E.D. Rodríguez:** Writing - review & editing. **P.J.M. Monteiro:** Writing - review & editing, Funding acquisition. **A.G. De la Torre:** Investigation and Supervision UMA research stage, Review & editing. **A.P. Kirchheim:** Advising and supervision. Review & editing. Funding acquisition, Project management.